Microfluidic vessels-on-chips for vascular disease modelling

Heleen Middelkamp

MICROFLUIDIC VESSELS-ON-CHIPS FOR VASCULAR DISEASE MODELLING

Heleen Hendrike Tijmentje Middelkamp

This dissertation has been approved by:

Supervisor
prof. dr. ir. A. van den Berg

Co-supervisor
prof. dr. A.D. van der Meer

Cover design: Artur Caneel, Heleen Middelkamp & Ridderprint
Printed by: Ridderprint | www.ridderprint.nl
Lay-out: Heleen Middelkamp
ISBN (print): 978-90-365-5723-8
ISBN (digital): 978-90-365-5724-5
DOI: 10.3990/1.9789036557245
URL: https://doi.org/10.3990/1.9789036557245

MICROFLUIDIC VESSELS-ON-CHIPS FOR VASCULAR DISEASE MODELLING

DISSERTATION

to obtain
the degree of doctor at the University of Twente,
on the authority of the rector magnificus,
prof. dr. ir. A. Veldkamp,
on account of the decision of the Doctorate Board
to be publicly defended
on Friday 8 September 2023 at 14.45 hours

by

Heleen Hendrike Tijmentje Middelkamp

born on the 18th of August, 1985
in Enschede, The Netherlands

Graduation Committee:

Chair / secretary:

prof.dr. J.N. Kok

Supervisor:

prof. dr. ir. A. van den Berg
University of Twente, EEMCS, Biomedical and Environmental Sensorsystems

Co-supervisor:

prof. dr. A.D. van der Meer
University of Twente, TNW, Applied Stem Cell Technologies

Committee Members:

prof. dr. A. Maassen van den Brink
Erasmus MC, Internal medicine

prof. dr. A.M.J.M. van den Maagdenberg
Leiden University Medical Centre, Human Genetics and Neurology

prof. dr. ir. N. Bosschaart
University of Twente, TNW, Biomedical Photonic Imaging

dr. R. Bansal
University of Twente, TNW, Medical Cell BioPhysics

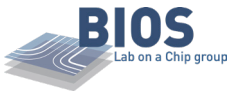

UNIVERSITY OF TWENTE. | MESA+ INSTITUTE | TECHMED CENTRE | Organ-on-Chip Center Twente

The research presented in this thesis was performed at the BIOS lab on a chip group at the MESA+ institute, TECHMED centre and Organ-on-chip center Twente of the University of Twente, Enschede, The Netherlands. This work was supported by the Netherlands Organ-on-Chip Initiative, an NWO Gravitation project (024.003.001) funded by the Ministry of Education, Culture and Science of the government of the Netherlands.

Table of Contents

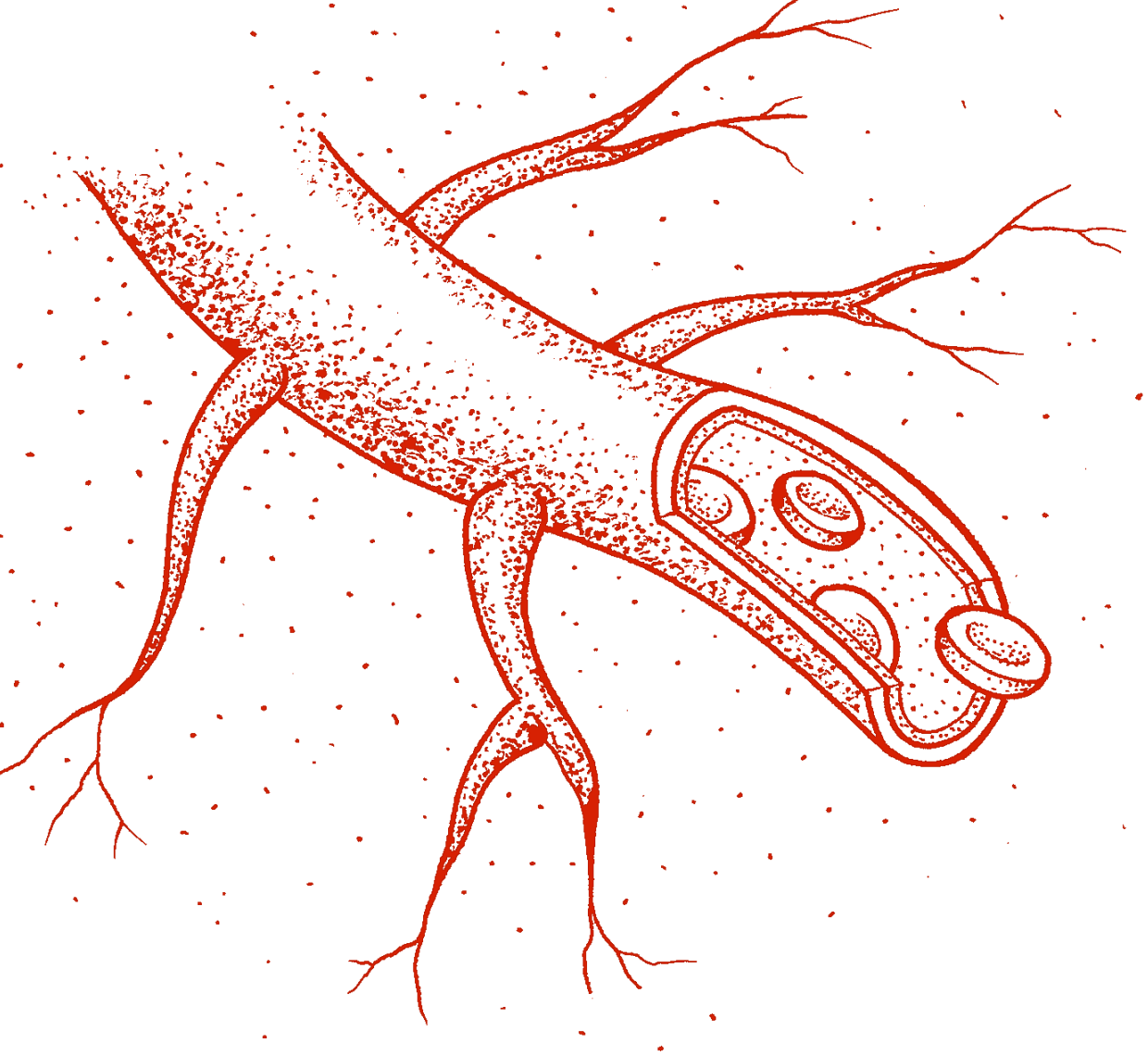

1

General introduction

H.H.T. Middelkamp

1.1 Blood vessels

Blood vessels are one of the main components of the circulatory system (figure 1b) with approximately 100.000 km of blood vessels in the human body[1]. There are multiple types of vessels, ranging from arteries, which transport oxygen and nutrients to the organs and tissues of the body, to the veins, which transport the deoxygenated blood back to the heart. Because of the different purposes of the different types of vessels, their sizes can vary, from only 5-10 µm in capillaries to 25-60 mm in arteries[2–4]. The structural variances between the different types of vessels is mainly due to different directions and pressures of flow. Blood flow and pressure in the veins is low, and unidirectional blood flow is facilitated by the presence of venous valves (figure 1a). Blood flow in arteries is much higher than in veins; this means that arteries experience a higher shear stress than veins[5,6]. The larger blood vessels, such as the veins and arteries, consist of three different layers of cells: the *tunica intima*, the innermost layer which provides a smooth pathway for the blood; the *tunica media*, the middle layer to regulate the inner diameter; and the *tunica adventitia*, the outer layer to provide structural support[2]. The *tunica intima* consists of a single layer of endothelial cells; the *tunica media*, which is the thickest in arteries, consists mainly of smooth muscle cells; and the *tunica adventitia*, which is the thickest in veins, consists of connective tissues (figure 1a)[7]. Although the *tunica intima* consists of only one layer of endothelial cells, this layer is imperative in maintaining vascular hemostasis[8–10]. By secreting cytokines, the endothelial cells communicate with other cells in the blood stream such as first responder white blood cells (e.g. monocytes) and blood platelets[11–13]. Furthermore, the endothelial cells form a barrier, preventing the blood from leaking out of the blood vessels and therefore prevent internal bleeding[14,15]. This endothelial cell layer is therefore very important for proper vascular function.

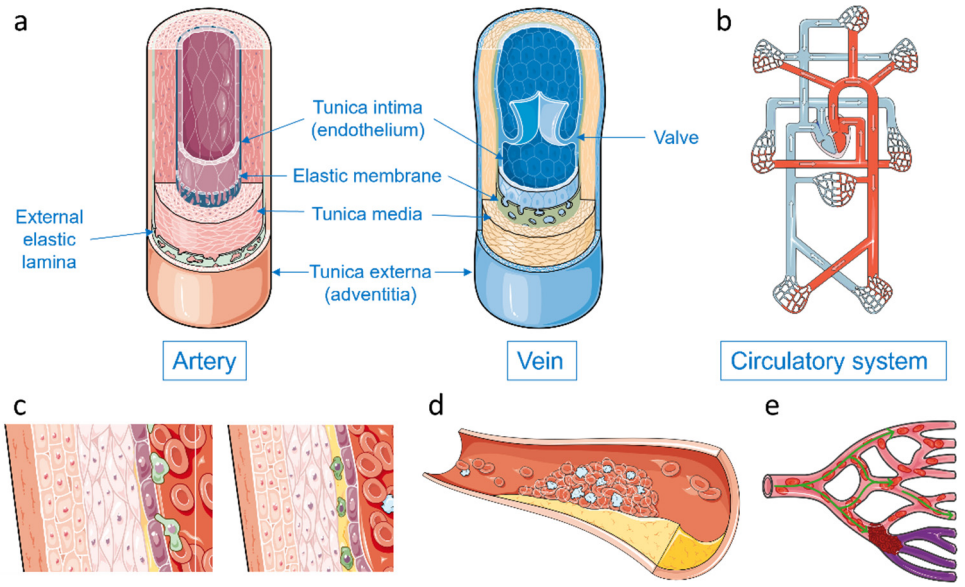

Figure 1-1: Blood vessel pathology. a) Different vessel types such as veins and arteries have different cell layers, to maintain the required functionality. b) Our body's circulatory system consists of arteries (red) and veins (blue) to provide all organs and tissues with oxygen and nutrients. Blood is pumped through the arteries by the heart, moves to the veins via capillaries and is pumped back to the heart using venous valves. c) When the endothelium inflames, monocytes (green) are transported to the inflammatory site; once at the inflammatory site the monocytes will attach to and migrate through the endothelium. d) Dead monocytes form an atherosclerotic plaque in an artery. A thrombus consisting of red blood cells, fibrin and platelets forms due to the cytokines excreted by the inflamed endothelium or due to plaque rupture. e) The thrombus can block blood flow towards essential regions of tissues such as the heart or brain. This figure was partly generated using Servier Medical Art, provided by Servier, licensed under a Creative Commons Attribution 3.0 unported license.

1.2 Vascular disease

Cardiovascular diseases are the leading cause of death worldwide, with >30 % of all deaths being caused by circulatory system (figure 1b) diseases such as stroke and ischemic heart disease[16]. These diseases are of vascular origin and are caused by reduced flow to either the heart or the brain. This reduced flow is usually caused by an atherosclerotic plaque which either disrupts the flow or can rupture causing a blood clot to form and completely block the flow towards the desired area in the body (figure 1d, 1e), thus depriving the organ of nutrients and oxygen, leading to tissue death[17–20]. These atherosclerotic plaques take years to develop and have other underlying causes, such as long-time exposure to inflammatory factors such as smoking, cholesterol, and stress[21–23].

Before vascular disease reaches the severity of an atherosclerotic plaque rupture, resulting in thrombus formation, several other disease processes can induce vascular dysfunction and immune responses, which include many of the same factors prominent in severe cardiovascular diseases. White blood cells such as monocytes and macrophages are first responder cells when it comes to vascular inflammation, but also wound healing. When endothelial cells become activated by for example stress, or even ageing, they signal other players of the immune system by cytokine excretion[10]. Moreover, the endothelial cells will express more vascular adhesion markers such as vascular cell adhesion molecule-1 (VCAM-1) and intercellular adhesion molecule-1 (ICAM-1), which leads to adhesion of the monocytes[24,25]. The monocytes will infiltrate the blood vessel wall and help to dispose of pathogens by phagocytosis (figure 1c)[26–29].

The cytokines excreted by the endothelial cell layer can help getting rid of pathogens, but they can also activate other processes in the blood such as blood clotting, which is also called thromboinflammation[30]. Virchow's triad describes the three components involved in the thrombus formation, specifically: hypercoagulability of blood, alteration of blood flow and vessel wall injury[31]. These three factors are intertwined, and one usually causes the other. Healthy endothelium presents an anticoagulant surface and endothelial damage can therefore cause the clotting process to start. Atherosclerotic plaque can cause a disturbance in flow, resulting in turbulent flow, which can activate endothelial cells and with that blood clotting. Platelets in blood, which get activated in wound healing, can also be activated by inflamed endothelium, resulting in the commencement of the blood clotting process, and therefore lead to undesired thrombus formation.

1.3 Blood vessels-on-chips

A new method for investigating blood vessels and blood vessel diseases are organs-on-chips (OoCs), and specifically blood vessels-on-chips (BVoC). OoCs are microphysiological devices that recapitulate organs or organ-specific functions[32–34]. They usually consist of one, or multiple channels moulded in poly(dimethylsiloxane) (PDMS), which is a flexible and gas-permeable substrate. Multiple channels can be separated by a (semi-)permeable membrane, to enable nutrients and cell type-specific cytokines to be transported between the microchannels. BVoCs have been used extensively for the study of vasculature and vascular diseases (see chapter 2 for a full overview) and multiple advances have already been made towards more

physiologically relevant models, for example by culturing endothelial cells in a three-dimensional (3D) hydrogel-based lumen.

An important aspect of modelling BVoCs can be the incorporation of multiple cell types. The type of cell to incorporate is dependent on the research question. If a more complex vascular model is required, the incorporation of other vascular cell types such as smooth muscle cells and fibroblasts can be beneficial. However, when specific organs or organ functions need to be addressed, the incorporation of these organ specific cells, such as cardiomyocytes (heart) or neurons (brain) may be required. For example, the blood-brain-barrier (BBB) is an important and exceptionally tight blood vessel barrier to prevent undesired molecules from entering the brain. Multiple cell types are required to model this intricate system, however, often a conventional two-dimensional (2D) well plate is used to culture these cells in monoculture, or co-cultures are performed in transwell systems[35–38]. While these models have the advantages of being less costly and are easier to standardize than a more complex system, the lack of endothelial shear stress and cell-cell interaction will affect the results[35–37,39]. There is still a lack in standardized 3D systems in which multiple cell types can be cultured[40–42]. Furthermore, the effects of culturing these cells on a different substrate and in a 3D-system compared to the conventional 2D systems on gene expression levels needs to be properly assessed[43,44]. An added benefit is the interaction these different types of cell experience. The interaction of these organ-specific and vascular cells will not only make the model be more relevant for the research question; these cells have the ability to affect each other on molecular and functional levels and can therefore be imperative to incorporate to achieve a more realistic and predictive model[43,45,46].

The interaction of multiple cell types is not only imperative when modelling organ specific vasculature as it is also of great importance for modelling the vascular system and vascular diseases such as early atherosclerosis and other vascular immune responses[13,47–50]. Early atherosclerosis is still incompletely understood, with important questions why some patients are at higher risk for cardiovascular diseases and respond to specific target therapeutics while others do not[4,51,52]. Vascular senescence and long term vascular inflammation are often identified to initiate early atherosclerotic plaque development[53,54]. Vascular inflammation and damage lead to immune cell recruitment, such as the first responder monocytes, which eventually form an early atherosclerotic plaque[23,27,50,55,56]. The interaction of endothelial cells with monocytes is therefore imperative in modelling vascular inflammation or

endothelial cell damage[27,29,47,57]. When modelling endothelial cell damage or inflammatory responses, standard read-outs are fluorescent staining of endothelial cell markers. However, this does not show the functional differences in the blood vessel such as monocyte adhesion and thrombus formation which will make them more physiologically relevant and can assist in assessing patient specific responses. Furthermore, the demand for standardized quantifiable read-outs is rising[58]. Some BVoC models with blood perfusion assays and monocyte adhesion assays are already in existence[59–64], however standardization, quantification of read-outs, and systematically setting up co-cultures in these models needs to be optimized, making the models and measurements translatable and comparable[58,65–67].

Current blood perfusion models often use fluorescently labelled markers with an end-point fluorescent microscopic measurement of thrombus formation[62,68,69]. Thrombus formation and development in BVoCs are difficult to observe in real time using these assays, furthermore, these fluorescent images give a 2D view of a thrombus. Therefore a non-invasive method of measuring blood clot formation over time, in multiple dimensions, will be an addition in understanding clotting mechanisms[70,71].

Many challenges remain in creating physiologically relevant BVoC models, such as creating BVoC models for vascular disease modelling, which include multiple relevant cell types and with the possibility of relevant and quantifiable read-outs. This thesis aims to contribute to the field of BVoC development by presenting new chip designs, methods for co-culturing cells, and quantifyable read-outs.

1.4 Thesis outline

This thesis presents the research towards BVoCs for vascular disease modelling. Using different chip designs and different cell types, we show the ability to create several vessel-on-chip (VoC) models, for different disease types and/or organs with different quantifiable read-outs.

Chapter 2 consists of two parts. The first part describes the importance of early involvement of stakeholders in the development of OoCs. It shows the differences in stakeholder opinions, which can be overcome by involvement early in the development process. The next part summarizes the VoC models currently used. Next to that we discuss which quantification possibilities are currently in use *in vivo* and *in vitro* and where VoCs are still lacking.

In **chapter 3** we have designed a 3D BVoC monocyte adhesion assay to show donor-specific trained immunity for endothelial cells. Using donor-specific human umbilical vein endothelial cells (HUVECs) which were seeded in a 3D rat tail type-1 collagen lumen, we have used tissue necrosis factor-α (TNF-α) to achieve HUVEC training and show a donor specific training response on a functional level. For **chapter 4** the same 3D BVoC model was used to show the effect of embedded lipid-laden macrophages in the endothelial cell layer in the context of thromboinflammation. Thus, we aim to show the difference in thrombus formation in chips, which have macrophages embedded in the endothelial cell layer. We have systematically set up the model using human induced pluripotent stem cell derived endothelial cells (hiPSC-ECs) and THP-1-derived macrophages by optimizing several processes such as obtaining and maintaining lipid-laden macrophages and medium composition. After the model was established, we have set up a blood perfusion assay to observe differences in endothelial thromboinflammatory response.

Chapter 5 shows a design for a BBB-on-chip. This was the first time ever a complete differentiation of hiPSC to neurons was performed on a microfluidic chip. We designed an open-top microfluidic chip, consisting of 2 channels separated by a porous membrane. Using Neurogenin-2 (Ngn2) overexpressing hiPSCs, we could differentiate towards cortical upper-layer II/III excitatory neurons. After successful differentiation, the next step was to seed HUVECs in the bottom channel and observe the transcriptomic changes the 2 different cell types undergo when cultured in a microfluidic chip design with and without other cells present. RNA-sequencing was performed to show these transcriptomic differences.

Chapter 6 shows the ability to non-invasively, without fluorescent labelling, image thrombus formation over time in a straight microfluidic channel. Squared 300 x 50 µm PDMS channels lined with HUVECs were used in this preliminary research project. Optical coherence tomography (OCT) was used to track thrombosis during a blood perfusion assays.

Finally, in **chapter 7** we summarize the work in this thesis and give an outlook for future research with regards to BVoCs.

References

1. Cleveland Clinics. Blood vessels. https://my.clevelandclinic.org/health/body/21640-blood-vessels (2021).
2. Tucker, W. D., Arora, Y. & Mahajan, K. *Anatomy, Blood Vessels*. (StatPearls Publishing, Treasure Island (FL), 2022).
3. Pollet, A. M. A. O. & den Toonder, J. M. J. Recapitulating the vasculature using Organ-on-Chip technology. *Bioengineering* **7**, 1–18 (2020).
4. Fleischer, S., Tavakol, D. N. & Vunjak-Novakovic, G. From Arteries to Capillaries: Approaches to Engineering Human Vasculature. *Adv. Funct. Mater.* **1910811**, 1–23 (2020).
5. Torres-Vázquez, J., Kamei, M. & Weinstein, B. M. Molecular distinction between arteries and veins. *Cell Tissue Res.* **314**, 43–59 (2003).
6. Corada, M., Morini, M. F. & Dejana, E. Signaling pathways in the specification of arteries and veins. *Arterioscler. Thromb. Vasc. Biol.* **34**, 2372–2377 (2014).
7. Townsley, M. I. Structure and composition of pulmonary arteries, capillaries and veins. *Compr Physiol.* 675–709 (2013) doi:10.1002/cphy.c100081.Structure.
8. Jia, G., Aroor, A. R., Jia, C. & Sowers, J. R. Endothelial cell senescence in aging-related vascular dysfunction. *Biochim. Biophys. Acta - Mol. Basis Dis.* 0–1 (2018) doi:10.1016/j.bbadis.2018.08.008.
9. Fernández-Hernando, C. & Suárez, Y. MicroRNAs in endothelial cell homeostasis and vascular disease. *Curr Opin Hematol* 227–236 (2018) doi:10.1097/MOH.0000000000000424.MicroRNAs.
10. Mameli, E., Martello, A. & Caporali, A. Autophagy at the interface of endothelial cell homeostasis and vascular disease. *FEBS J.* **289**, 2976–2991 (2022).
11. Shirai, T., Hilhorst, M., Harrison, D. G. & Weyand, Cornelia, M. Macrophages in Vascular Inflammation – From Atherosclerosis to Vasculitis. *Autoimmunity* **48**, 139–151 (2015).
12. Muthard, R. W. & Diamond, S. L. Side view thrombosis microfluidic device with controllable wall shear rate and transthrombus pressure gradient. *Lab Chip* **13**, 1883–91 (2013).
13. Chen, Z. *et al.* Real-time observation of leukocyte-endothelium interactions in tissue-engineered blood vessel. *Lab Chip* **18**, 2047–2054 (2018).
14. Stevens, T., Garcia, J. G. N., Shasby, D. M., Bhattacharya, J. & Malik, B. EB2000 symposium report Mechanisms regulating endothelial cell barrier function. *Exp. Biol.* **279**, 419–422 (2011).
15. Keep, R. F. *et al.* Blood-brain barrier function in intracerebral hemorrhage. *Acta Neurochir. Suppl.* 73–77 (2008) doi:10.1007/978-3-211-09469-3_15.
16. World Health Organization. Leading causes of death worldwide in 2016 (in millions). Statista. https://www.statista.com/statistics/288839/leading-causes-of-death-worldwide/ (2019).
17. Thygesen, K., Alpert, J. S. & White, H. D. Universal definition of myocardial infarction. *Circulation* **116**, 2634–2653 (2007).
18. Johnson, W., Onuma, O., Owolabi, M. & Sachdev, S. Stroke: A global response is needed. *Bull. World Health Organ.* **94**, 634A-635A (2016).
19. Coupland, A. P., Thapar, A., Qureshi, M. I., Jenkins, H. & Davies, A. H. The definition of stroke. *J. R. Soc. Med.* **110**, 9–12 (2017).
20. Reed, G. W., Rossi, J. E. & Cannon, C. P. Acute myocardial infarction. *Lancet* **389**, 197–210 (2017).
21. Allard C. van der Wal, A. E. B. Atherosclerotic plaque rupture – pathologic basis of plaque stability and instability, Cardiovasc Res. *Cardiovasc Res* **41**, 334–344 (1999).
22. Katsuumi, G., Shimizu, I., Yoshida, Y. & Minamino, T. Vascular Senescence in Cardiovascular and Metabolic Diseases. *Front. Cardiovasc. Med.* **5**, 1–13 (2018).
23. Bentzon, J. F., Otsuka, F., Virmani, R. & Falk, E. Mechanisms of plaque formation and rupture. *Circ. Res.* **114**, 1852–1866 (2014).
24. Kaukoranta-Tolvanen, S. S. E., Ronni, T., Leinonen, M., Saikku, P. & Laitinen, K. Expression of

adhesion molecules on endothelial cell stimulated by Chlamydia pneumoniae. *Microb. Pathog.* **21**, 407–411 (1996).
25. Khan, O. F. & Sefton, M. V. Perfusion and characterization of an endothelial cell-seeded modular tissue engineered construct formed in a microfluidic remodeling chamber. *Biomaterials* **31**, 8254–8261 (2010).
26. Dale, D. C., Boxer, L. & Conrad Liles, W. The phagocytes: Neutrophils and monocytes. *Blood* **112**, 935–945 (2008).
27. Mestas, J. & Ley, K. Monocyte-Endothelial Cell Interactions in the Development of Atherosclerosis. *Trends Cardiovasc. Med.* **18**, 228–232 (2008).
28. Chistiakov, D. A., Melnichenko, A. A., Myasoedova, V. A., Grechko, A. V. & Orekhov, A. N. Mechanisms of foam cell formation in atherosclerosis. *J. Mol. Med.* **95**, 1153–1165 (2017).
29. Delavary, B. M., van der Veer, W. M., van Egmond, M., Niessen, F. B. & Beelen, R. H. J. Macrophages in skin injury and repair. *Immunobiology* **216**, 753–762 (2011).
30. Li, J., Han, X., Knauss, E. A., Woulfe, D. S. & Nieman, M. T. *GPCRs in thromboinflammation and hemostasis*. *GPCRs: Structure, Function, and Drug Discovery* (Elsevier Inc., 2019). doi:10.1016/B978-0-12-816228-6.00019-2.
31. Kushner, A., West, W. P., Khan Suheb, M. Z. & Pillarisetty, L. S. *Virchow Triad*. (StatPearls Publishing, Treasure Island (FL), 2022).
32. Polini, A. *et al.* Organs-on-a-chip: a new tool for drug discovery. *Expert Opin. Drug Discov.* **9**, 335–52 (2014).
33. Ingber, D. E. Human organs-on-chips for disease modelling, drug development and personalized medicine. *Nat. Rev. Genet.* **23**, 467–491 (2022).
34. Van Den Berg, A., Mummery, C. L., Passier, R. & Van der Meer, A. D. Personalised organs-on-chips: functional testing for precision medicine. *Lab Chip* **19**, 198–205 (2019).
35. Jagtiani, E., Yeolekar, M., Naik, S. & Patravale, V. In vitro blood brain barrier models: An overview. *J. Control. Release* **343**, 13–30 (2022).
36. Abizanda-campo, S., Ayuso, J. M., Ochoa, I. & Oliv, S. Towards Novel Biomimetic In Vitro Models of the Blood – Brain Barrier for Drug Permeability Evaluation. (2023).
37. Sivandzade, F. & Cucullo, L. In-vitro blood–brain barrier modeling: A review of modern and fast-advancing technologies. *J. Cereb. Blood Flow Metab.* **38**, 1667–1681 (2018).
38. Hajal, C., Roi, B. Le, Kamm, R. D. & Maoz, B. M. Biology and Models of the Blood-Brain barrier. *Annu Rev Biomed Eng* (2021).
39. Ruck, T., Bittner, S. & Meuth, S. G. Blood-brain barrier modeling: Challenges and perspectives. *Neural Regen. Res.* **10**, 889–891 (2015).
40. Appelt-Menzel, A. *et al.* Human iPSC-Derived Blood-Brain Barrier Models: Valuable Tools for Preclinical Drug Discovery and Development? *Curr. Protoc. Stem Cell Biol.* **55**, (2020).
41. Shin, Y. *et al.* Blood–Brain Barrier Dysfunction in a 3D In Vitro Model of Alzheimer's Disease. *Adv. Sci.* **6**, (2019).
42. Nikolakopoulou, P. *et al.* Recent progress in translational engineered in vitro models of the central nervous system. *Brain* **143**, 3181–3213 (2021).
43. Middelkamp, H. H. T. *et al.* Cell type-specific changes in transcriptomic profiles of endothelial cells, iPSC-derived neurons and astrocytes cultured on microfluidic chips. *Sci. Rep.* **11**, 1–12 (2021).
44. Delsing, L. *et al.* Barrier Properties and Transcriptome Expression in Human iPSC-Derived Models of the Blood–Brain Barrier. *Stem Cells* 1–12 (2018) doi:10.1002/stem.2908.
45. Delsing, L. *et al.* Barrier properties and transcriptome expression in human iPSC-derived models of the blood-brain barrier. *Sumbitted* (2018) doi:10.1002/stem.2908.
46. Sances, S. *et al.* Human iPSC-Derived Endothelial Cells and Microengineered Organ-Chip Enhance Neuronal Development. *Stem Cell Reports* **10**, 1222–1236 (2018).
47. Drummer, C. *et al.* Trained Immunity and Reactivity of Macrophages and Endothelial Cells. *Arterioscler. Thromb. Vasc. Biol.* **41**, 1032–1046 (2021).

48. Hong, H. & Tian, X. Y. The Role of Macrophages in Vascular Repair and Regeneration after Ischemic Injury. *Int. J. Mol. Sci.* (2020) doi:https://doi.org/10.3390/ijms21176328.
49. Teague, H. L. *et al.* Unraveling Vascular Inflammation: From Immunology to Imaging. *J. Am. Coll. Cardiol.* **70**, 1403–1412 (2017).
50. Islam, K., Nasser, R., Gater, D. & Pearson, Y. E. Co-culture Methods Used to Model Atherosclerosis In Vitro Using Endothelial , Smooth Muscle and Monocyte Cells. *J. Biomed. Eng.* (2016).
51. Phillippe, H. M. Overview of venous thromboembolism. *Am. J. Manag. Care* **23**, S376–S382 (2017).
52. Shen, M., Quertermous, T., Fischbein, M. P. & Wu, J. C. Generation of Vascular Smooth Muscle Cells from Induced Pluripotent Stem Cells: Methods, Applications, and Considerations. *Circ. Res.* 670–686 (2021) doi:10.1161/CIRCRESAHA.120.318049.
53. Grootaert, M. O. J. *et al.* Vascular smooth muscle cell death, autophagy and senescence in atherosclerosis. *Cardiovasc. Res.* **114**, 622–634 (2018).
54. Basatemur, G. L., Jørgensen, H. F., Clarke, M. C. H., Bennett, M. R. & Mallat, Z. Vascular smooth muscle cells in atherosclerosis. *Nat. Rev. Cardiol.* **16**, 727–744 (2019).
55. Westhorpe, C. L. V. *et al.* Endothelial cell activation promotes foam cell formation by monocytes following transendothelial migration in an in vitro model. *Exp. Mol. Pathol.* **93**, 220–226 (2012).
56. Chen, C. N. *et al.* Neutrophils, lymphocytes, and monocytes exhibit diverse behaviors in transendothelial and subendothelial migrations under coculture with smooth muscle cells in disturbed flow. *Blood* **107**, 1933–1942 (2006).
57. Martin, J., Mcgregor, L. & Mcgregor, J. L. The Dialogue Between Endothelial Cells and Monocytes / Macrophages in Vascular Syndromes. 1751–1759 (2007).
58. Low, L. A., Mummery, C., Berridge, B. R., Austin, C. P. & Tagle, D. A. Organs-on-chips: into the next decade. *Nat. Rev. Drug Discov.* **20**, 345–361 (2021).
59. Westein, E. *et al.* Atherosclerotic geometries exacerbate pathological thrombus formation poststenosis in a von Willebrand factor-dependent manner. *Proc. Natl. Acad. Sci.* **110**, 1357–1362 (2013).
60. Albers, H. J., Passier, R., van den Berg, A. & van der Meer, A. D. Automated analysis of platelet aggregation on cultured endothelium in a microfluidic chip perfused with human whole blood. *Micromachines* **10**, (2019).
61. Halaidych, O. V., van den Hil, F., Mummery, C. L. & Orlova, V. V. Microfluidic assay for the assessment of leukocyte adhesion to human induced pluripotent stem cell-derived endothelial cells (HiPSC-ECs). *J. Vis. Exp.* **2018**, 1–8 (2018).
62. Tovar-Lopez, F. J. *et al.* A microfluidics device to monitor platelet aggregation dynamics in response to strain rate micro-gradients in flowing blood. *Lab Chip* **10**, 291–302 (2010).
63. Colace, T. V., Muthard, R. W. & Diamond, S. L. Thrombus growth and embolism on tissue factor-bearing collagen surfaces under flow: Role of thrombin with and without fibrin. *Arterioscler. Thromb. Vasc. Biol.* **32**, 1466–1476 (2012).
64. Schneider, S. *et al.* Peristaltic on-chip pump for tunable media circulation and whole blood perfusion in PDMS-free organ-on-chip and Organ-Disc systems. *Lab Chip* **21**, 3963–3978 (2021).
65. Feng, J. J. & Hedtrich, S. A similarity scaling approach for organ-on-chip devices. *Lab Chip* **22**, 3663–3667 (2022).
66. Esch, E. W., Bahinski, A. & Huh, D. Organs-on-chips at the frontiers of drug discovery. *Nat. Rev. Drug Discov.* **14**, 248–260 (2015).
67. Mastrangeli, M., Millet, S. & van den Eijnden-Van Raaij, J. Organ-on-chip in development: Towards a roadmap for organs-on-chip. *ALTEX* **36**, 650–668 (2019).
68. van Dijk, C. G. M. *et al.* A new microfluidic model that allows monitoring of complex vascular structures and cell interactions in a 3D biological matrix. *Lab Chip* **20**, 1827–1844 (2020).

69. Jackson, S. P., Nesbitt, W. S. & Westein, E. Dynamics of platelet thrombus formation. *J. Thromb. Haemost.* **7**, 17–20 (2009).
70. Morita, N. *et al.* Real-time, non-invasive thrombus detection in an extracorporeal circuit using micro-optical thrombus sensors. *Int. J. Artif. Organs* **44**, 565–573 (2021).
71. Zhuo, S., Li, M., Lu, Z. & Chen, K. High-resolution characterization of the coagulation and drying processes of whole blood based on optical coherence tomography. 1–9 (2023) doi:10.3389/fphy.2023.1159504.

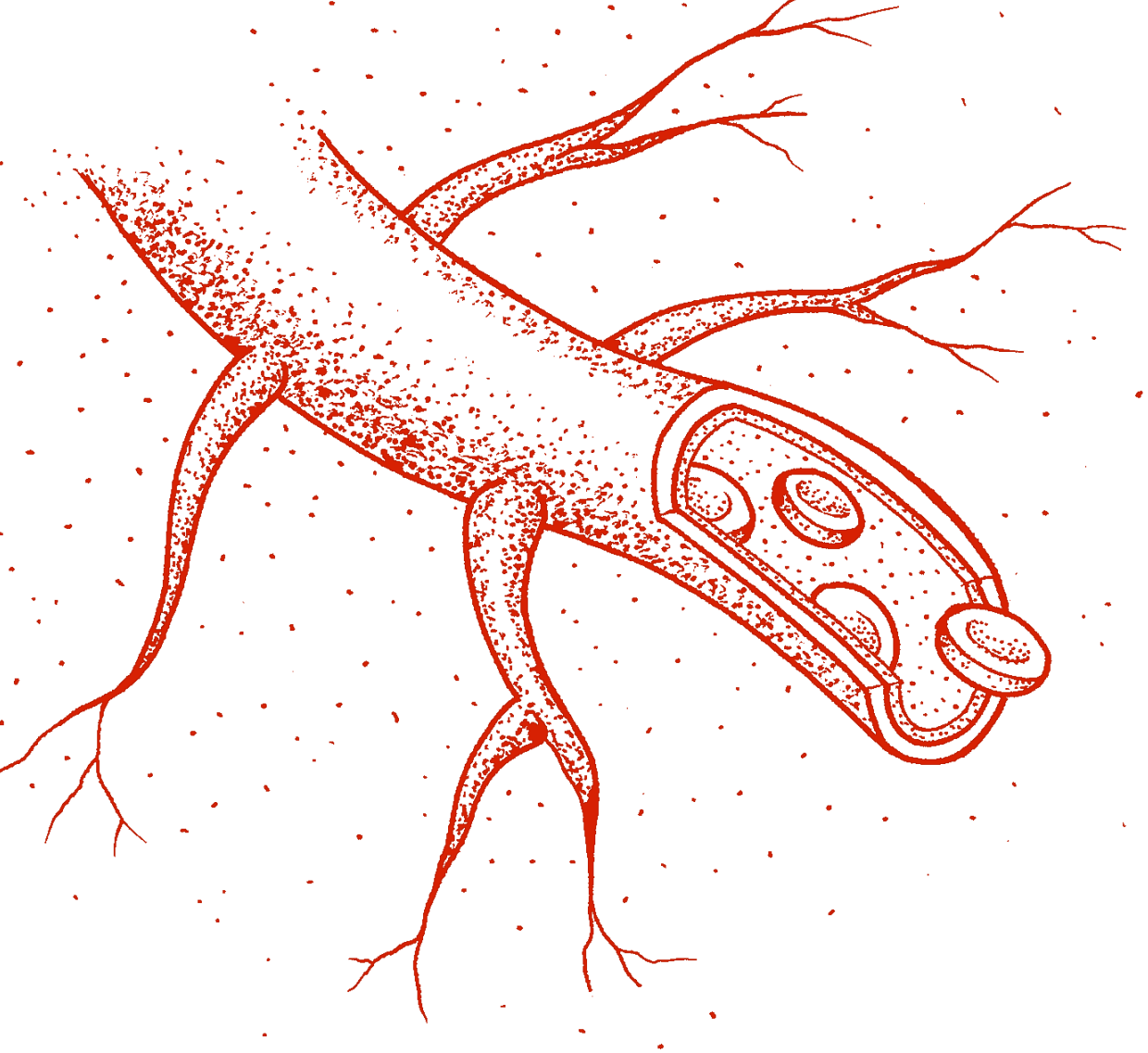

2

Organs-on-chips for vascular disease modelling and drug development

Based on:
H.H.T. Middelkamp
A.D. van der Meer
et. al.
Appl. in vitro tox. 2 (2), 74-81 (2016)

V. Paloschi
M. Sabater-Lleal
H.H.T. Middelkamp
et. al
Cardiovasc. res. 117 (14), 2742-2754 (2022)

D.M. Nahon
R. Moerkens
H.H.T. Middelkamp
et.al.
Manuscript accepted

Abstract

Organs-on-chips are three-dimensional microfluidic cell culture systems that simulate the function of tissues and organ subunits. Organ-on-chip systems are expected to contribute to drug candidate screening and the reduction of animal tests in preclinical drug development and may increase efficiency of these processes. To maximize the future impact of the technology on drug development, it is important to make informed decisions regarding the attributes and features of organs-on-chips even though the technology is still in a stage of early development. It is likely that different stakeholders in organ-on-chip development, like engineers, biologists, regulatory scientists, and pharmaceutical researchers, will have different perspectives on how to maximize the future impact of the technology. Various aspects of organ-on-chip development, like costs, materials, features, cell source, read-out technology, types of data and compatibility with existing technology, will likely be judged differently by different stakeholders. Early health technology assessment is needed in order to facilitate the essential integration of such potentially conflicting views in the process of technology development. We discuss the potential impact of organs-on-chips on the drug development process, and we use a pilot study to give examples of how different stakeholders have different perspectives on attributes of organ-on-chip technology. As a future tool in early health technology assessment of organs-on-chips, we suggest the use of multi-criteria decision analysis, which is a formal method to deal with multiple and conflicting criteria in technology development. We argue that it is essential to design and perform a comprehensive multi-criteria decision analysis for organ-on-chip development, so the future impact of this technology in the pharmaceutical industry can be maximized.

The development of organs-on-chip has revolutionized *in vitro* cell-culture experiments by allowing a better mimicry of human physiology and pathophysiology that has consequently led researchers to gain more meaningful insights into disease mechanisms. Several vessel-on-chip models have been demonstrated to recapitulate fundamental aspects of the human cardiovascular system in the recent past. These two-dimensional, and three-dimensional systems include vessels-on-chips with layer-based structures and the inclusion of physiological and pathological shear stress conditions. The opportunities to discover novel targets and to perform drug testing with chip-based platforms have substantially enhanced, thanks to the utilization of patient-derived cells and precise control of their microenvironment.

These organ models will provide an important asset for future approaches to personalized vascular medicine and improved patient care. However, certain technical and biological challenges remain, making the global utilization of organs-on-chips to tackle unanswered questions in vascular science still rather challenging. This review chapter aims to introduce health technology assessment and multi-criteria decision analysis in the context of organs-on-chips in the drug development process, and summarize published work on vessels-on-chips, it gives an overview of the current quantification methods already existent for healthy and disease models of vessels-on-chip, but also provides an outlook and perspective on how these advanced in vitro systems can be used to tailor disease models with patient-specific characteristics.

2.1 Introduction

Drug development is an expensive and lengthy process. A study published in 2012 indicates drug development costs $1.2 billion per successfully developed drug[1]. Moreover, it takes – on average – 10-15 years of preclinical and clinical testing before a new drug reaches the market. Only 27% of drugs that enter the clinical trial phase of the drug development process are approved for market[2]. Main reasons for drugs to fail in clinical trials are lack of efficacy (43%) and toxicity (33%)[3]. Most prominent in drug toxicity is cardiac toxicity; therefore, it can be imperative to develop a cardiovascular model for the drug development process.

Cardiovascular diseases (CVDs) are a group of disorders affecting the heart and the vasculature that represent the number one cause of mortality globally[4]. Only in Europe, CVDs causes over 4 million deaths each year[5], accounting for 47% of all deaths in Europe. The most common underlying pathology in CVDs is atherosclerosis, which causes an ischemia in the heart and in peripheral arteries. Atherosclerosis is defined as a chronic disease of the vasculature, whose architecture is slowly remodeled over time. This disease and remodeling process involves the interplay of numerous cell subtypes, including endothelial cells (ECs) (becoming dysfunctional), leukocytes, monocytes, and macrophages (triggering inflammation), and smooth muscle cells (which dedifferentiate or undergo apoptosis)[6,7].

Unstable atherosclerotic plaques can rupture, which results in arterial thrombosis. Thrombosis, the formation of blood clots, prevents blood flow, and triggers life-threatening clinical conditions in the arterial system, such as myocardial infarction (MI) and ischemic forms of stroke (IS). Although MI and IS are usually acute events resulting from chronic atherosclerotic processes affecting coronary and carotid arteries, respectively, venous thromboembolism (VTE) is mainly caused by hemostatic or coagulation abnormalities[8].

A new promising technology for early validation of CVD drug efficacy and detection of toxicity are organs-on-chips (OoCs)[9]. In recent years, OoCs have emerged as powerful new tools to fill the translational gap from animal models to human disease, with a particular potential to even replace animal testing in the future[10]. OoC technology will improve the modelling of organs or organ systems for healthcare research while immensely impacting the precision medicine approach[10].

In this chapter, we introduce the general concept and scientific potential of OoC systems in drug development. We discuss the importance of involving stakeholders early in the drug development process. Furthermore, we illustrate the fabrication of blood vessels-on-chip (BVoC), the current quantification methods and the opportunities and challenges of utilizing OoCs in preclinical drug testing and target discovery.

2.1.1 Organs-on-Chips

OoCs are engineered devices, which combine cells, biomaterials, and microfabrication to simulate the activity and function of tissues and organ subunits. They are often in multi-channel three-dimensional (3D) microfluidic formats that mimic cell responses more accurately than regular *in vitro* cell cultures in two-dimensions (2D)[11–15]. The devices integrate micro-engineered 3D tissues with microfluidic network systems[16], allowing living cells to be cultured in micrometer-sized chambers which are continuously perfused, thereby modelling essential functions of living organs or tissues at a small scale[12,17–19]. The microenvironment of the cell culture can be tailored to mimic an organ very realistically; for example biophysical constraints such as mechanical strain associated with breathing in the lung can be included, or perfusion with blood or blood substitutes at rates equivalent to the true shear stress on blood vessel walls (figure 1, figure 5)[9,20]. Cells can be grown as monocultures using just one cell type or as co-cultures of two or more cell types in 2D on for example a permeable membrane, or in 3D (figure 4)[12,21,22].

The high level of control, enabling customized cell-culture environment in OoCs, is illustrated in figure 1. This includes custom ECM topology, the integration of sensors and actuators for monitoring and electrical/mechanical stimuli, control of microfluidic channel dimensions, and temporal and spatial flow profiles for pulsatile flow and chemical stimuli. Moreover, the precise microfluidic flow control enables an optimal growing environment (influx of nutrients and efflux of cell-waste) as well as the circulation of drugs, signaling molecules, or immune cells.

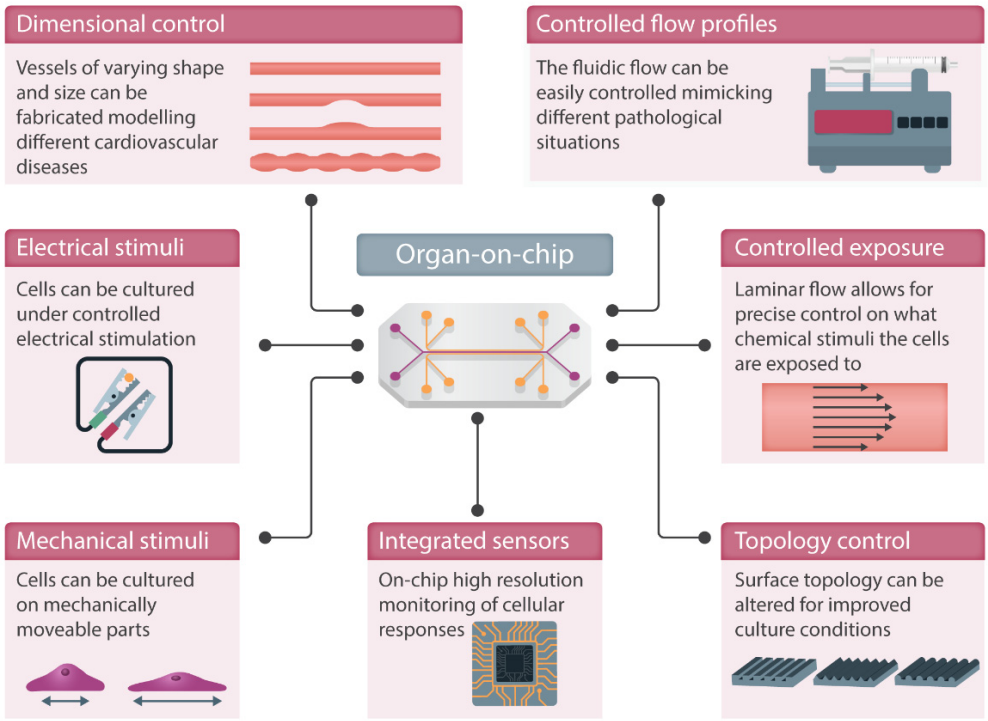

Figure 2-1: Fabricating vessel-on-chip models using micromachining allows for integration of several advanced features.

2.1.2 Organs-on-chips in Drug Development

Apart from the "standard" OoC systems, which are generated to mimic healthy organs or parts of organs, disease models on chips are also being developed. These disease models range from breast cancer models and polycystic kidney disease to Parkinson's disease[15,23–25]. These OoC disease models can provide insights into disease mechanisms and responses of the diseased tissue to drugs as well as the target organ tissue[15]. Recent technology development has focused on connecting multiple OoCs, making it possible to observe specific systemic interactions in drug toxicity and efficacy[12,14,26,27], and on combining OoC systems with human pluripotent stem cells, creating organs-on-chips with potential for personalized medicine[28–30].

Because of their physiological relevance, organs-on-chips are often considered as key future technology in several phases in drug development (figure 2A). The basic research phase, which consists of target identification and high throughput screening, could possibly be improved by a relatively simple OoC system. Whereas more complicated systems could be suitable to improve the preclinical development

phase, where pharmacokinetics, pharmacodynamics and in vitro- and in vivo toxicities are determined[31–33]. Potential advantages mentioned in the literature include: suitability for human toxicity screening[9,34–44], identification of biomarkers and diagnostics[12,45], possible (partial) replacement of animal experiments[9,16,34,37,38,41,42,44–51], as well as a higher sensitivity to external stimuli compared to the conventional 2D systems[26,38,39,51,52].

There is a clear need for more physiologically relevant model systems in drug development. Current assays in early phase and preclinical development are often 2D *in vitro* cell culture systems or living animals. 2D cell culture models are limited in their ability to mimic key physiological parameters like tissue geometry, flow, pressure and complex cell-cell and cell-niche interactions. Animal models do capture these features but are sensitive to possible species differences in disease characteristics or drug responses, which can lead to miscalculation of drug efficacy in patients or their risks. Drugs may be non-toxic or efficacious in animals but not in humans[39]. Furthermore, animal studies are expensive, time-consuming and there are ethical questions on the use of animals in drug development[46].

The lack of predictive models for preclinical drug screening is a major problem that contributes to the rising costs of developing new drugs. Given their unique features, OoCs have the potential to have a real impact on lowering cost and time-to-market of drugs.

2.1.3 Maximizing Impact of Organs-on-Chips in Drug Development

OoC technology is still in an early phase of development, but the first proof-of-concept systems already demonstrate how OoCs could be effectively implemented in the drug development process and compliment current high-throughput screening methods for identifying drug candidates and targets[14,47,53]. Alternatively, at the preclinical stage of drug development, OoCs could provide additional information on human relevance, which may eventually leading to partial replacement of animal testing[54].

There are challenges in OoC development particularly in the design choices. These design choices could be: what are the costs, which materials should be used, is there a preferred cell source, what on-chip sensors and analytical measures are available and should be used? A combination of these choices could also be preferred, however not all design choices can be implemented, therefore trade-offs must be made. Which choices have a higher weight according to stakeholders? There are

many ways of using OoC systems in drug development and therefore the dialogue between developers (or researchers) and other stakeholders at an early stage is important to decide the exact steps that should be taken in the development. On one hand, the developers are important stakeholders with respect to their knowledge of the possibilities and limitations of the technology. For example there are still several challenges to overcome before multiple organs can be connected[47,55]. On the other hand, future end-users should also be included to give their view on how OoC technology could have an impact on drug development. The exact purpose of the model is an important factor that can be defined by asking questions like: "Do the users need a model for general toxicity screening or for a specific target organ?" and "What are the most valuable read-outs for toxicity?".

Furthermore, the specific pharmacological information that the model should yield is an important factor. Examples of questions related to this factor are: "Do the users need a system to model the effects of different drug dosages or the properties of the drug at certain dosages?", "How long does the model need to be viable?", "How can a drug best be delivered?". Another factor that can be surveyed is how different end-users think about concrete design choices, for example by asking questions like: "Does this model need to be organ or tissue specific?" "Would end-users prefer a more specific disease model?", "How many target cell types should be included?", "Is it easier to use than the current golden standard models?" and "Is it important to include multiple connected organs on one chip?".

Finally, an essential consideration is how to factor in the cost and economic impact of OoCs in drug development, for example by asking: "What would be the acceptable cost per data point?". Different users can have different opinions. The users could be academic researchers in a university (biomedical research) or pharmaceutical companies. These two groups can differ significantly in opinions due to the different purposes of the systems. One difference in purpose can be where in the drug development process the system will be used. Pharmaceutical companies can be inclined to want a simple model which works faster than the now used well-plate, whereas stakeholders from a university could be more interested in understanding the mechanism behind an organ system and being able to publish.

Another important stakeholder group is the regulators. Even if a decision can be made on how the technology development should proceed, regulators have to approve the use of data from OoC systems as a substitute for current drug safety

screening methods. Thorough validation in comparison to existing regulatory requirements is essential.

It is complex to consider all aspects of stakeholder preferences and possible applications of technology development in a comprehensive manner and therefore it is imperative to have a formal method of deciding what should be prioritized in the development and what will be the possible benefits of this prioritization.

2.1.4 Early Health Technology Assessment

Early health technology assessment (HTA), including early Health Economic Modeling, is increasingly promoted as an approach to determine added value of potential new technologies early in the development pipeline. Such assessments would be useful to (1) decide about further development of the technology, (2) to define minimum performance thresholds for the new technology compared to currently available technologies and (3) to support pricing and reimbursement in early stages of development[56–58].

Early HTA can help developers in their decisions about the design of a device while it is still under development. This is possible even at the stage where there is still no proof-of-concept prototype to convince regulatory decision makers or end-users[59]. A systematic assessment can still be made in a phase in which the developers can still make meaningful changes to the design. Therefore, by applying early HTA, developers can improve the chances of developing a successful product that will find acceptance by end-users and regulatory agencies[60].

There are various methods that can be used in early HTA: these include assessment of potential impact by conducting surveys, analysis of costs and benefits by economic modelling, and scenario-driven computer simulations of clinical trials. Which method is most suitable for early HTA depends on the stage of technology development and the intended party for decision making[59]. For the translational stage of development of current OoC technology – a stage that revolves around making crucial decisions in terms of design – the most dominant perspective is to identify the most promising OoC application area, and to assess its societal impact. This would help to justify allocating resources to its development and hopefully increase the likelihood of delivering societal impact.

In such analysis, multi-criteria decision analysis (MCDA) may be particularly useful as an aid for decision making about the design of technological innovations by comparing several organs-on-chips alternatives on a set of relevant development

criteria. The criteria can be conflicting and may require a trade-off with regards to their importance. The importance of criteria, i.e., their weights can be elicited from various stakeholders, such as R&D or academic representatives. An MCDA study usually comprises 5 sections (supplementary figure 1). The first step is structuring the decision problem. The decision problem and goal are structured, and the decision criteria and alternatives identified. The next step is capturing performance for the alternatives, for instance how would the organ-on-a-chip perform in toxicity testing. This performance evidence can either be obtained by a systematic literature review or by interacting with stakeholders and is usually converted into a partial value-function to allow comparison across criteria. The next step is the elicitation of criteria weights for the organs-on-chips alternatives, such as that for cost of development and for toxicity testing in phase I trials. The final step is the aggregate value by multiplying criteria weights and performance values for the alternatives[61,62]. We will not go further into the details of how to carry out an MCDA in this chapter, the reader is recommended to read the following contributions for framework and set-up of the MCDA process[59,61–63].

When performing early HTA, it is also important to include all relevant stakeholder groups so they can provide input on key aspects of the MCDA like identification of the criteria and the alternatives to prioritize. If not all stakeholders are included or if there is a failure to communicate between all stakeholders, then this could lead to errors in the description of the problem or the deliberation[64]. Including all stakeholders can therefore help in understanding the needs and position of developers as well as users and can prevent conflicts later on in the development process[65].

When including all stakeholders early in the HTA process, differences between groups can become clear and therefore the technology developers can anticipate on the needs of the end-users.

2.1.5 Stakeholders and Organ-on-Chip Technology Development

As an illustration of the importance of involving stakeholders in early health technology assessment HTA of OoCs, we have carried out a pilot study in which mostly university employees (involved in the development of OoC systems or drug development) and pharmaceutical company employees were included. This study was not a full MCDA process, but merely shows the expectations of the two stakeholder groups. This survey can therefore not be used to elicit weight and to prioritize alternatives but is an important part at the beginning of an MCDA process

to capture evidence to structure the problem by defining key issues and criteria. These key issues and criteria can be used for a full MCDA study.

The stakeholders were asked to give their opinion on various aspects of OoC technology in the context of drug development. The survey was designed to observe whether there were significant differences of opinions between different stakeholder groups, proving the importance of including all stakeholders in the development process. For details of the survey (including results) and study plan, see online data supplement[66].

The survey was sent out to approximately 150 people using an e-mail invitation. It was filled out by 50 stakeholders. Of these 50 stakeholders 18 people (36%) were working in a pharmaceutical company and 22 (44%) were working for a university. Other respondents indicated to be working for a commercial company (n= 5 or 10%), non-profit organization (n=4 or 8%) or other (n=1 or 2%). The two main groups were the pharmaceutical stakeholders (participant's work ranging from general scientists to scientific directors) and the university stakeholders (participants ranging from general researchers to professors in the field of either drug development and/or OoC development). No distinction was made with regards to the individual's job description due to the lack of statistical certainty for such small groups.

One of the main questions in the survey was where OoCs could be beneficial in drug development. Figure 2A shows an overview of opinions of all stakeholders. There were no significant differences between the opinions of the stakeholders, therefore all stakeholder groups were combined in one sample. The three main phases of drug development are basic research, preclinical research, and clinical trials. The stakeholders were asked which phase of drug development could be improved by implementation of OoC systems. 90% of the stakeholders see improvement possibilities in the basic research phase, 88% thinks the preclinical development phase can be improved and 22% is of opinion that the clinical trial phase can be improved. In the squares (which contain subcategories of the main development phases) it can be observed that 70% of all stakeholders see possibilities for improvement in (drug and disease) target identification in basic research. More possibilities were predicted in the preclinical development stage: 78% of all stakeholders see OoCs as a means of reducing animal use in drug development and 74% expect an improvement in toxicity screening. The opinions of different stakeholder groups were similar in this example.

A

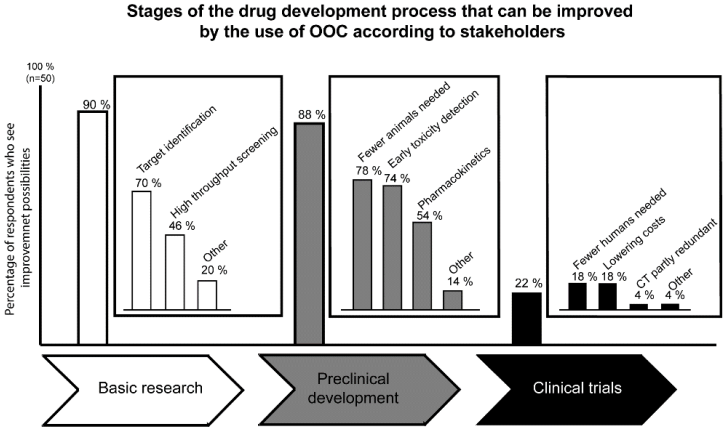
Stages of the drug development process that can be improved by the use of OOC according to stakeholders
100 % (n=50)
Percentage of respondents who see improvemnet possibilities
90 %
Target identification
70 %
High throughput screening
46 %
Other
20 %
88 %
Fewer animals needed
78 %
Early toxicity detection
74 %
Pharmacokinetics
54 %
Other
14 %
22 %
Fewer humans needed
18 %
Lowering costs
18 %
CT partly redundant
4 %
Other
4 %
Basic research
Preclinical development
Clinical trials

B

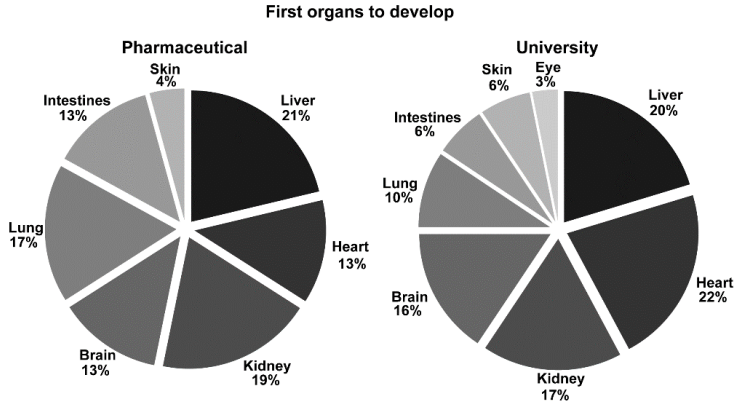
First organs to develop
Pharmaceutical
Skin 4%
Intestines 13%
Liver 21%
Lung 17%
Heart 13%
Brain 13%
Kidney 19%
University
Skin 6%
Eye 3%
Intestines 6%
Liver 20%
Lung 10%
Heart 22%
Brain 16%
Kidney 17%

C

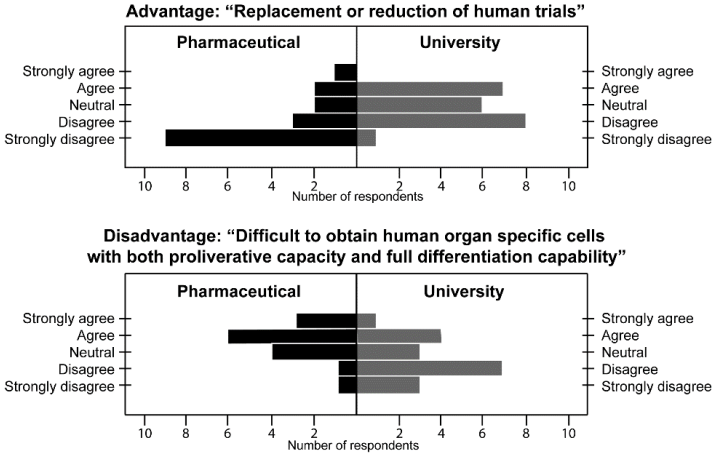
Advantage: "Replacement or reduction of human trials"
Pharmaceutical
University
Strongly agree
Agree
Neutral
Disagree
Strongly disagree
10 8 6 4 2 2 4 6 8 10
Number of respondents
Disadvantage: "Difficult to obtain human organ specific cells with both proliverative capacity and full differentiation capability"
Pharmaceutical
University
Strongly agree
Agree
Neutral
Disagree
Strongly disagree
10 8 6 4 2 2 4 6 8 10
Number of respondents

Figure 2-2: The importance of involving stakeholders in the early HTA process. A) No differences between stakeholder groups were observed when asked about the possibilities of improving the drug development process. The basic research and preclinical phase and subsections (squares) were mostly selected by both stakeholder groups. B) Also, when asked which organs an organ-on-chip model should be developed first, both stakeholder groups showed broad agreement. C) The responses of the two stakeholder groups showed significant differences when asked to score the importance of the advantage "replacement or reduction of human trials" and the disadvantage "Difficult to obtain human organ specific cells with both proliferative capacity and full differentiation capability" of organ-on-chip technology. The differences were evaluated with a Mann-Whitney U test; p = 0.015 for the top graph, p = 0.025 for the bottom graph.

Stakeholders were also asked which organ model should be developed with the highest priority as an OoC. The three highest scoring organs were the liver, heart, and kidney. However, stakeholders with a pharmaceutical background rated the development of the lung as more important than the development of the heart, whereas university stakeholders scored the heart as most important to develop first (figure 2B). There was no significant difference between the groups.

When the stakeholders were asked for their opinion on specific advantages and disadvantages of using OoCs in drug development, a significant difference was observed between stakeholders. They were asked to rank the advantage from 1 (none) to 5 (very important). The first statistically significant difference was the overall average score between university stakeholders and stakeholders working in a pharmaceutical company, where the average score of advantages and average inverse score of the disadvantages were used. The opinion of university stakeholders was more positive (3.5063) compared to the more neutral (3.1462) ranking of pharmaceutical stakeholders (T-test, p = 0.000129).

Further statistical analysis showed a significant difference between those working in pharmaceutical companies versus those working in universities on the advantage for "replacement/reducing human trials". Figure 2C shows the distribution of ranking of both groups. The university stakeholders see a higher potential for the replacement or reduction of human trials.

Other advantages with significant differences in ranking between pharmaceutical company stakeholders and university stakeholders were "shorten the length of the drug development" and "personalized medicine can be developed easier". Both were ranked higher by university stakeholders.

The first two advantages are based on conjecture and can most likely be proven when OoCs are accepted into the drug development process and fully developed. University stakeholders ranked the advantage "personalized medicine" significantly

higher than stakeholders working at a pharmaceutical company. A reason could be that pharmaceutical companies do not see enough profits from personalized medicines and therefore the pharmaceutical company stakeholders are not as familiar with the concept and underlying human stem cell technology as university stakeholders are.

There were also disadvantages of OoC technology that were rated significantly different by university versus pharmaceutical stakeholders. Stakeholders from pharmaceutical companies considered the disadvantages as "difficult to obtain human organ specific cells with both proliferative capacity and full differentiation capability" and "more expensive than well-plates" greater than university stakeholders.

These examples clearly demonstrate the need to include all stakeholders in the decision-making process. The stakeholder groups differed significantly when asked to attribute importance to various aspects of the OoC technology. This information should be taken into account in further development of OoCs and form part of the dialogue between academics and industry.

Figure 2B shows the consensus from both stakeholder groups to develop a heart model as one of the first OoC systems in drug development. Part of the heart and the circulatory system are the blood vessels. The vascular system was not included explicitly as a discussion point in the stakeholder analysis but is particularly important in drug development as most drugs enter the body via the blood stream and are then transferred to the organ that needs treatment, e.g., the heart. Next to that, vascular diseases are often a precursor for other life-threatening events such as stroke and heart attack. The following sections will therefore focus on the current state of the development of vessel-on-chips (VoCs) and its current limitations as well as prospects.

2.2 Fabrication of blood vessels-on-chips

To fabricate VoC models, it is imperative to consider the geometry as this affects the flow profile, wall shear stress, culture area, and the total number of cells used in the specific model. The material most commonly used for proof-of-concept models is poly(dimethylsiloxane) (PDMS), a polymer developed in the late 1990s[67] to fabricate microfluidic channels. PDMS has several advantages for miniaturized cell cultures, such as simple fabrication, gas permeability, and optical transparency. Using PDMS, supportive microfluidic channels can be moulded off a master that has the reverse

topographical features. By removing the PDMS from the mould and bonding the structure onto a glass slide, a sealed channel structure can be created (figure 3). Inlet and outlet holes for connecting tubing for perfusion can easily be punched into the PDMS.

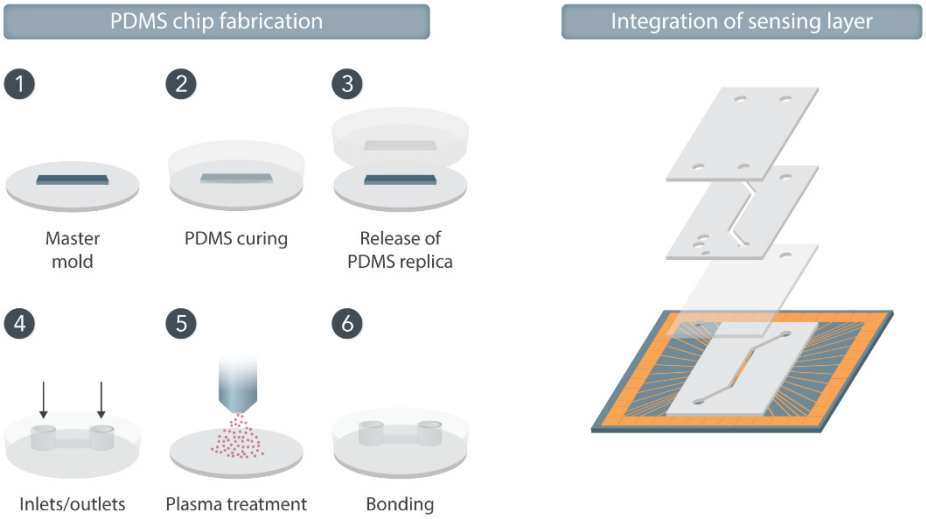

Figure 2-3: Schematic drawing showing the six basic steps of PDMS moulding to form a microfluidic channel that can be used in organs-on-chip. 1) A master is prepared having the inverse topography of the final channel structures, 2) PDMS pre-polymer is poured onto the master and polymerized upon heat treatment, 3) The moulded channels are released from the master, 4) Holes for connecting tubing for media perfusion are prepared in the PDMS by punching, 5) The PDMS surface is activated for bonding via plasma treatment, 6) The microfluidic channels are sealed by bonding the PMDS slab onto a glass microscope slide which may include patterned electrodes.

In order to mimic vessels, the microfluidic channels can then be coated with human ECs, forming artificial intima layers of vessels in which blood, plasma, or other cells of interest (e.g. monocytes and platelets) can be perfused (figure 4A, figure 5)[68]. Specific culture media with different added stimuli or drugs can be added to the system, and real-time observation of the system under a microscope can be used to evaluate the effect of certain stimuli. At the same time, variations in flow and shear stress can provide more information than static cultivation in well plates. To study disease onset, systems with higher complexity, including 3D lumen-chips that incorporate the media layer populated by SMCs, are required (figure 4B, 4D). A recent example of a perfusable artery-on-chip was published by Cho and Park[69], where SMCs and human umbilical vein ECs (HUVECs) were co-cultured in a PDMS channel. To induce the proper morphology and orientation of SMCs, wrinkles

were formed on the circular PDMS channel surface during the moulding as contact guidance, and the HUVECs were aligned by medial perfusion. Another method to study vascular networks, such is present in the blood-brain-barrier, is by self-assembly of blood vessels (figure 4C)[70–72].

One major disadvantage of using PDMS is that the material is porous, thus absorbing especially hydrophobic compounds, which can lead to false-negative read-outs from drug-screening studies[73]. Also, the polymer is not inert, which can lead to silicon leaching from the structure into the cell culture environment[74]. Developments of more inert yet biocompatible materials are therefore currently a major focus within the field[75].

In an effort to make the vascular structure more biomimetic, a system can be designed to include multiple microfluidic compartments where some can be filled with a biomimetic cell-culture scaffold to recreate the physiological environment of the vasculature (figure 4A)[70,76–78]. Alternatively, a device can be moulded using only a biological material such as collagen[79,80]. Cells can further be introduced into the biomimetic scaffolds. This set-up allows investigation of the tissue-blood interface in a controlled environment that cannot be monitored in animals or patients. It can also be utilized to study the interaction with adjacent cells on disease sub-phenotypes, such as endothelial permeability, communication with blood cells, or platelet aggregation. Another approach to fabricate VoC models in a biomimetic material is to utilize the method of viscous finger patterning (VFP) or bioprinting (figure 4B, 4D)[10,81–83], thus forming centered channels instead of adjacent ones. The VFP approach also has the advantage of generating circular vessel structures, which cannot be obtained *using* conventional PDMS moulding. The method has been used to study cell–cell interactions in 600 µm wide[84] and 250 µm[82] diameter VoC models. Although very interesting from a biological perspective, there are several technical challenges with integrating biomimetic scaffolds into OoC systems[85,86].

One option to exploit the angiogenic potential of the cells themselves is to increase the biological relevance of the vasculature models even further. In such systems, vascular cells are seeded in the biomimetic scaffold and exposed to mechanical stimuli *via* slow perfusion[87] or a chemical gradient of growth factors[76]. This results in a vascular bed formation after 2–3 weeks, including both larger macro-vessels and dense capillary microvascular networks.

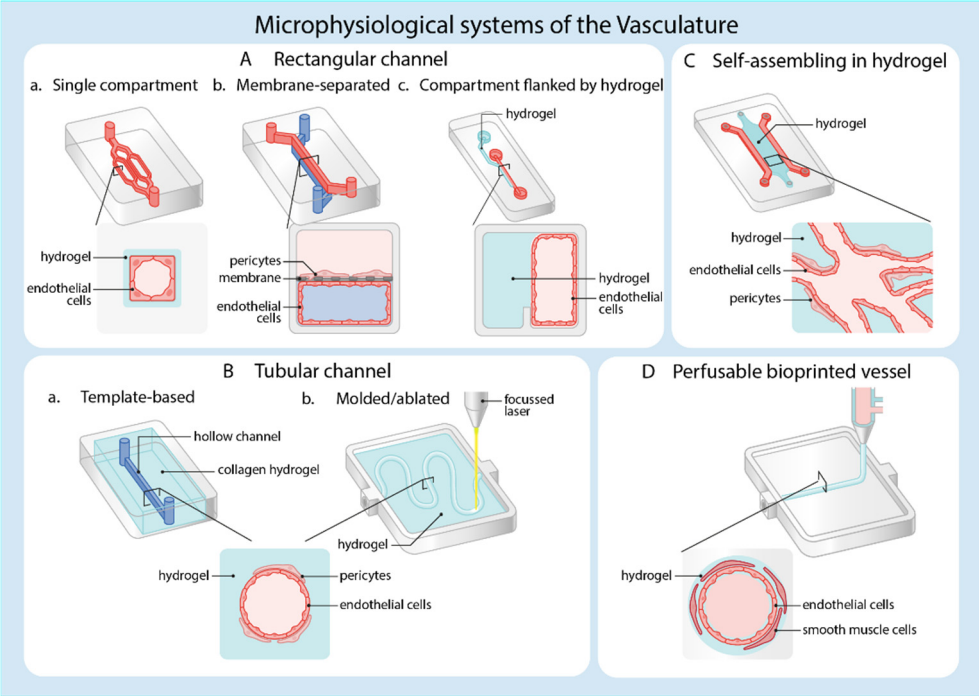

Figure 2-4: Design principles of different microphysiological systems of the human vasculature: Microphysiological systems of the vasculature: Aa) Single patterned channel, usually in PDMS although agarose gelatin hydrogel is also used. Widely used for monocultures of endothelial cells. Ab) Two aligned channels (upper and lower), separated by porous membrane. Unidirectional pressure-driven fluid flow can be introduced in both channels. The device is generated from PDMS, coated with a thin hydrogel layer. Cells can be cultured in both channels. The upper channel is usually seeded with tissue-specific cell types like astrocytes, neurons, lung- or intestinal epithelium and the lower channel with endothelial cells. Ac) Devices designed for use with gravitational bidirectional flow. Used in 2- and 3-channel formats. The side channel is used to seed endothelial cells and is flanked by a hydrogel-filled channel separated using a phase-guide. Tissue-specific cells can be seeded in the hydrogel channel. Ba) Tubular channels using templating are based on removing or replacing a structure within hydrogel. Examples include needle removal or using differences in viscosity of fluids as in viscous finger patterning. A tubular structure remains which can be seeded with cells. Bb) Molding or laser ablation can create tubular structures within hydrogels in self-designed patterns. C) Self-assembly based systems make use of the vasculogenic capacity of endothelial cells: the ability to self-organize into vascular networks. Endothelial cells are usually mixed with mural cells, seeding in a hydrogel channel to enable development of a 3D vascular network. The hydrogel channel is usually flanked by media channels to enable network perfusion. D) Several tissue engineering approaches to bio-print vessel structures are available. One is printing cell-laden hydrogel within a predetermined structure. Advanced 3D-printed structures are designed to connect to microfluidic set-ups after seeding. Aa) based on REF.[68] Ab) based on design by Emulate Inc, Boston, MA, USA and REF.[89] Ac) based on design by Mimetas, Oegstgeest, NL and REF.[90] Ba) based on REFs.[82,91] Bb) based on REF.[92,93] C) based on REF.[70–72] D) based on REF.[10,94]

Taking a completely different approach to investigating small and large artery diseases, one can utilize the advantages of microfluidics by developing advanced *ex vivo* culture platforms. They can be used if a higher complexity is needed to investigate, for example, cell–cell interactions and their relevance for the onset of a certain disease. An initial attempt to investigate structural changes occurring within the vessel wall was presented by Günther *et al.*[88]. They used a microfluidic platform for immobilizing small arteries obtained *ex vivo* from mice and long-term culturing under physiological conditions (37 °C, 45 mmHg transmural pressure). Live imaging allowed them to determine the arteries' inner and outer diameter in real time while assessing the effects of heterogeneous environmental changes on the microvascular structure and function. The different design options for VoC models are further discussed in figure 4.

2.3 Blood vessels-on-chips for vascular disease modelling

2.3.1 Studying atherosclerosis using chip-based systems

Modelling the different stages of the advancement of atherosclerosis is considered crucial in the development of vascular OoCs (summarized in table 1 and figure 5). Qiu *et al.*[68] developed a 3D microvasculature-on-chip that is able to display physiological endothelial barrier function for several weeks, therefore allowing to study how chronic endothelial dysfunction develops. To model atherosclerosis progression, several devices have been created with occlusion or stenosis of the lumen, which recreates the higher shear region commonly found in developing atherosclerotic plaques[82].

Westein *et al.*[95], Tovar-Lopez *et al.*[96], and Costa *et al.*[97] have provided excellent examples of how to investigate atherosclerosis using chip-based systems. These three models differ regarding their biological and technical complexity. The chips developed by Westein *et al.* and Tovar-Lopez *et al.* consist of a square channel in which an artificial atherosclerotic plaque is already embedded (figure 5). In order to study 3D vessel geometry in a more physiologic way, Costa *et al.*[97] created different 3D vascular structures by using 3D-printed anatomical models based on observations generated by computed tomography angiography. They were, therefore, able to closely mimic architectures found in both healthy and stenotic blood vessels.

A disadvantage of these models is the lack of the ECM, as PDMS is used to create the lumen that directly surrounds the cells. If the occlusion mechanism and pathophysiology of the development of atherosclerosis are to be studied, a more flexible model in which monocytes and macrophages can be included would be preferred.

Thrombosis is a complex process influenced by genetic and environmental factors, involving three main components: abnormalities in the vessel wall (endothelium), abnormalities in components of the blood (coagulation proteins and platelets), or abnormalities in fluid dynamics (turbulence flow and shear stress)[98,99]. Unlike static *in vitro* cell-culture models, VoCs can mimic the effect of flow and its interaction with the vessel wall while overcoming inter-species differences of animal models. Microfluidic technology has therefore been used extensively to create new *in vitro* models to study thrombotic diseases[100–104].

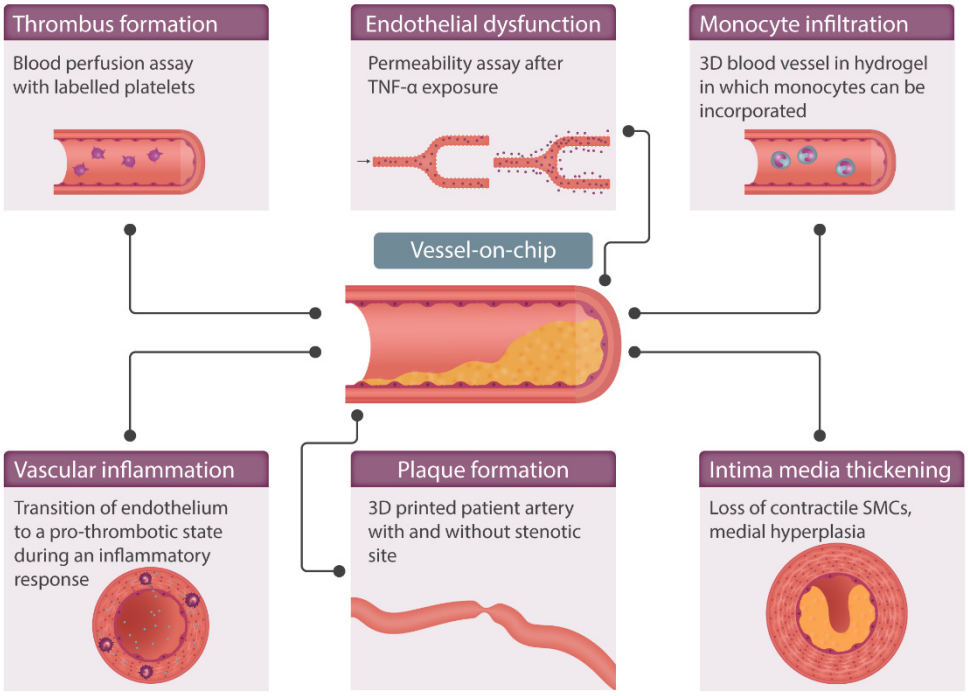

Figure 2-5: Vessel-on-chip devices are useful tools to study pathological mechanisms occurring within the vessel wall in early and later stages of atherosclerosis. Preliminary research can be performed in easier fabricated straight PDMS channels, whereas for more extensive and complicated research questions, a more elaborate model can be used by producing a 3D lumen in a hydrogel.

2.3.2 Mimicking thrombosis on-a-chip

Although previous work has been published studying thrombosis on microfluidic devices without the presence of ECs (reviewed in Westein *et al.*[101] and Zhu *et al*.[102]), we here review OoC models of thrombosis typically consisting of a tubular or rectangular mould that is covered by components of the ECM (typically fibrin or collagen). ECs form a monolayer, therefore recreating endothelial geometry and function. In healthy conditions, the endothelium has anticoagulant and anti-inflammatory properties, therefore allowing blood flow through the lumen and preventing platelet activation and fibrin clot formation[105]. Upon endothelial damage or activation, coagulation and platelet aggregation are triggered to promote the formation of a thrombus[106]. Besides endothelial damage, several stimuli and the effect of blood flow are known to activate the endothelium[105,107].

Table 1 | Aspects of human vascular physiology and disease in organs-on-chips

Vascular physiology	Perfusable 3D blood vessels with defined geometries	82,84,97,103,108–110
	Perfusable microvasculature with self-organized geometries	70,111
	Angiogenesis	70,79
	Endothelial-mural interactions	70,79,84,109
	Blood perfusion	79,95,97,104,112,113
Vascular disease modelling	Thrombosis	79,95,97,103,104,108,112,113
	Inflammation (e.g., permeability and adhesion molecules)	70,79,84,95,103,104,108,109,112
	Immune cell recruitment	70,79

Several examples of OoCs have been published that study the different triggers of clot formation through direct monitoring of platelet aggregation under a microscope. In this direction, Zheng *et al.*[79] engineered microvascular networks by seeding HUVECs intro microfluidic circuits coated with collagen and demonstrated that upon perfusion with human blood, rolling and adhesion of platelets occurred only at sites of damage—or in stimulated endothelium where long fibers of von Willebrand factor (VWF) covered the surface of the activated endothelium. These structures had not been reported in previous planar cultures or mouse models of thrombosis. Similarly, a recent study by Brouns *et al.*[104] explored the anticoagulant effect of intact endothelium (created by a microfluidic model coated with HUVECs) through natural anticoagulants while comparing with artificially damaged endothelium covering a highly thrombogenic surface created with collagen and tissue factor.

One of the key advantages of OoCs is their great capacity to tightly control vessel geometry and flow, which has contributed significantly to the understanding of flow-based changes on platelet activation and the risk of thrombosis. To better understand the contribution of atherosclerosis and vessel stenosis to thrombosis, stenotic vessels perfused with whole human blood have been developed. The results indicate that platelets aggregate at the outlet zone of constriction, therefore concluding that the shear rate is crucial for platelet adhesion and aggregation[95,97,100,108].

Although these examples clearly contribute to advancing research and understanding of the coagulation process, most of these models are not practical to enhance clinical diagnosis. Several commercial devices are emerging to provide simple tools that can be used for clinical testing. Towards this aim, Mannino *et al.*[108] proposed a commercial simple endothelial-coated cylindrical microchannel to test the effect of local vascular geometries on blood cell-endothelium interactions. Similarly, Jain *et al.*[112] demonstrated that a microfluidic device coated with ECs could be fixed and still retain their ability to modulate hemostasis under flow. The device was able to detect differences in patients taking antiplatelet medication and therefore providing a new tool for clinical laboratories for coagulation testing in more robust and practical diagnostic assays.

Mathur *et al.*[113] created a model for thrombo-inflammation where they first isolated blood outgrowth endothelial cells (BOEC) from healthy subjects and then introduced these cells to microfluidic channels. These cells were then stimulated with TNF-α and

exposed to re-calcified human whole blood to compare the inflammatory response of these cells to models using HUVECs. Due to the easy isolation method of these BOECs, and a different response of healthy and unhealthy patients, this model can be used as a tool in personalized medicine approaches for certain pathologies, in which thrombo-inflammation is an essential contributor to disease exacerbation.

Sepsis is a disease often coinciding with thrombus formation in smaller vessels and arteries, which can lead to ischemic events of the heart and subsequent heart failure (HF)[114]. Many of the models described above can be used to model thrombotic sepsis in a microfluidic chip. In sepsis, high levels of inflammation in blood vessels are observed and accompanied by an elevation of tissue necrosis factor-α (TNF-α), interleukin-1 (IL-1), and interferons. These factors activate the endothelium to a prothrombotic state and strongly induce thrombus formation[115,116]. After incubation with these factors, or other known contributors to sepsis, a blood perfusion assay can be performed to better understand more mechanisms involved in sepsis-associated thrombosis.

Finally, clinical applicability has also been demonstrated by using VoCs to predict thrombotic side effects in drug candidates prior to human clinical trials. For example, Tsai et. al. used a VoC device to perfuse blood samples from patients with sickle cell disease and test the effect of certain drugs in microvascular occlusion and thrombosis[103]. Another study by Barrile *et al.*[117] used a vascular channel coated with ECs and perfused whole human blood to study the potential for different drugs to promote blood clots. These studies serve as interesting examples for the potential of VoCs to evaluate thrombotic side effects that would otherwise be missed in prior animal or static cell culture studies. They are further proof of how OoCs can enhance drug safety during the process of developing novel treatment strategies.

2.4 Quantification of current and emerging MPS

A systematic review was performed of several key factors regarding blood vessel design. Important physiological *in vivo* features, such as fluid flow and oxygen concentrations that have already been developed extensively are shown, as well as emerging techniques such as inflammatory response and barrier integrity measurements (table 2). We describe the methods used for quantification of these features *in vivo* as well as *in vitro*, while also showing where the technique, or even *in vivo* quantification lacks. As evident, quantitative control of physiological features in MPS is still limited. This is in part due to lack of awareness on how important it is

to report quantitative data and refer them to *in vivo* physiology. In addition, however, many quantitative culture parameters are impossible to engineer or measure in the current generation of MPS. However, the table also shows the added advantage of OoC devices over the ability to measure *in vivo* when we are interested in investigating vascular biology.

Table 2 | Quantification of designed and emergent physiological features in microphysiological systems and human *in vivo*

	Category	Feature	MPS		*In vivo* (human)	Ref MPS	Ref *In Vivo*
			Method	Quantification	Quantification		
Designed	Organ architecture	Tube diameter	Laser ablation	10-500 µm	Arteries: 0.03-2.5 cm, arterioles: 10-300 µm, capillaries: 5-10 µm, venules: 8-100 µm, veins: 0.01-2 cm	92	118
			3D bioprinting	700-1000 µm		10,94	
	Fluid flow	Wall shear stress	Various pump systems	Arteries: 1.2-1.5 Pa, arterioles: 0.42 Pa, capillaries/venules; 0.03-0.72 Pa, veins: 1 Pa	Arteries: 2.23 Pa, arterioles: 6-14 Pa, capillaries: 1.2 Pa, venules: 0.3-1 Pa, veins: 0.1-0.6 Pa.	70,119–122	123,124
		Circumferential strain	Syringe pump	4-10%	5-10%	125	126,127
	Tissue elasticity	ECM elasticity	Tunable synthetic hydrogel	1-6 kPa	Arteries: 50-150 kPa, venous: 3-50 kPa (mouse)	128	129
	Oxygen concentration	Oxygen concentration	Oxygen scavenging channel	1-5%	1-13%	130	131

Emergent	Cell type diversity	Cell type diversity	scRNA-seq	NA	ECs, SMCs, Pericytes, perivascular fibroblast, Mϕ (heterogeneous between tissues and along arteriovenous axis)	-	[132]
	Cell type localization and interaction	Astrocyte coverage of endothelial layer	IF co-localization	9%	100% (rat)	[133]	[134]
		Pericyte coverage of endothelial layer	IF co-localization	16%	10-70% average all tissues, 30% BBB (rat)	[133]	[134,135]
	Inflammatory response	Cytokine secretion	Luminex. IL-6	0.3 ng/ml	0.1 - 305 ng/ml	[84]	[136]
	Barrier integrity	Permeability of the endothelial layer	Leakage assay 20 kDa	$3x10^{-6}$ cm/s	$2.4x10^{-7}$ cm/s (rat)	[90]	[137]
			Leakage assay 70 kDa	$4x10^{-7}$ cm/s	$1.5x10^{-7}$ cm/s (rat)	[68]	[137]
	Renewal	Angiogenesis	Imaging	16 µm/h	NA	[138]	-

Data was included based on the criteria as stated in Supplemental Information Note 1. Abbreviations: MPS=microphysiological system, NA=not available, ref=reference, , ECM=extracellular matrix, EC=endothelial cell, SMC=smooth muscle cell, Mϕ=macrophage, BBB=blood-brain barrier, IF=immunofluorescence, scRNA-seq=single-cell RNA-sequencing, IL=interleukin, m=meter, Pa=Pascal, h=hour, min=minute, s=second.

2.5 Future importance of organs-on-a-chip in personalized cardiovascular medicine

Animal and genetic studies have implicated specific genes conferring increased susceptibility to many human diseases. Together with other emerging techniques (e.g., genome editing), OoCs have the potential to significantly enhance our understanding of how certain genes and epigenetic regulators are capable of influencing our personal CVD risk.

The novel genome editing CRISPR/Cas9 technology enables the introduction of targeted mutations or specific gene knock-outs into human cells[139]. This methodology has allowed the generation of stable cell lines carrying the desired genetic mutation/knock-out while eliminating the effect of inter-individual variations due to the genetic background.

Although primary cells from specific individuals can be difficult to obtain and cannot be cultured indefinitely, stable organ specific cells with the desired genomic background can be generated from human induced pluripotent stem cells (hiPSCs). hiPSCs are obtained from a somatic cell and can be differentiated into all cell types[140–143]. They can therefore be derived from accessible adult tissues of any patient, such as the blood or the skin. There are current protocols available for the generation of ECs as well as pericytes and vascular SMCs[72,144,145].

Another interesting approach is the integration of clinical data with the fabrication of OoC devices was used by Costa *et al.*[97], as described in detail in the atherosclerosis section above. Here, CTA data of a coronary artery formed the basis to construct personalized chips with the measured grade of stenosis. This method allowed the researchers to reproduce *in vitro* the unique (personalized) flow profile of individual patients and to observe the formation of thrombi dynamically. Similarly, BVoCs can be perfused with human blood from individuals treated with different anticoagulant therapies to assess drug response of specific patients in a personalized manner[146].

The opportunity to build OoCs with disease-relevant cells can minimize the current challenges of most genomic studies. For example, VoC designs could be used to test whether genetic associations emerging from recent coronary artery disease, VTE, HF, or ischemic heart disease will increase the disease risk through an effect in the vascular system. At the same time, blood from individuals with a known genetic

background can be perfused into different microchannels to study interactions between blood cells and the endothelium. Overall, the advanced possibilities of OoCs using novel available technologies offer great potential to finally elucidate the effect of genetic factors on CVD phenotypes, therefore enabling us to move towards the era of personalized medicine and pharmacogenomics more rapidly and efficiently. OoCs have already demonstrated their potential to support clinical trials of certain drug candidates[14]. The opportunity to create patient specific OoCs could therefore pave the way for the development of precise and individualized therapies.

References

1. Allison, M. Feature: Reinventing clinical trials. *Nat. Biotechnol.* **30**, 41–9 (2012).
2. The Independent Institute. Drug development and approval process. http://www.fdareview.org/approval_process.shtml.
3. Schuster, D., Laggner, C. & Langer, T. Why Drugs Fail - A Study on Side Effects in New Chemical Entities. in *Antitargets: Prediction and Prevention of Drug Side Effects* (eds. Vaz, R. J. & Klabunde, T.) 1–18 (Wiley-VCH Verlag GmbH & Co. KGaA, 2008). doi:10.1002/9783527621460.ch1.
4. World Health Organization. Leading causes of death worldwide in 2016 (in millions). Statista. https://www.statista.com/statistics/288839/leading-causes-of-death-worldwide/ (2019).
5. Townsend, N. *et al.* Cardiovascular disease in Europe: Epidemiological update 2016. *Eur. Heart J.* **37**, 3232–3245 (2016).
6. Libby, P. *et al.* Atherosclerosis. *Nat. Rev. Dis. Prim.* **5**, 1–18 (2019).
7. Basatemur, G. L., Jørgensen, H. F., Clarke, M. C. H., Bennett, M. R. & Mallat, Z. Vascular smooth muscle cells in atherosclerosis. *Nat. Rev. Cardiol.* **16**, 727–744 (2019).
8. Phillippe, H. M. Overview of venous thromboembolism. *Am. J. Manag. Care* **23**, S376–S382 (2017).
9. Huh, D. *et al.* Microfabrication of human organs-on-chips. *Nat. Protoc.* **8**, 2135–57 (2013).
10. Gao, W. *et al.* One-Step Formation of Protein-Based Tubular Structures for Functional Devices and Tissues. *Adv. Healthc. Mater.* **10**, (2021).
11. Moyer, M. W. Organs-on-a-Chip for Faster Drug Development. http://www.scientificamerican.com/article/organs-on-a-chip/.
12. Bhatia, S. N. & Ingber, D. E. Microfluidic organs-on-chips. *Nat. Biotechnol.* **32**, 760–772 (2014).
13. Polini, A. *et al.* Organs-on-a-chip: a new tool for drug discovery. *Expert Opin. Drug Discov.* **9**, 335–52 (2014).
14. Ingber, D. E. Human organs-on-chips for disease modelling, drug development and personalized medicine. *Nat. Rev. Genet.* **23**, 467–491 (2022).
15. Benam, K. H. *et al.* Engineered In Vitro Disease Models. *Annu. Rev. Pathol. Mech. Dis.* **10**, 195–262 (2015).
16. Bhise, N. S., Ribas, J., Manoharan, V., Shrike, Y. & Polini, A. Organ-on-a-chip platforms for studying drug delivery systems. *J. Control. Release* **190**, 82–93 (2014).
17. Middelkamp, H. H. T. *et al.* Cell type-specific changes in transcriptomic profiles of endothelial cells, iPSC-derived neurons and astrocytes cultured on microfluidic chips. *Sci. Rep.* **11**, 1–12 (2021).
18. van Dijk, C. G. M. *et al.* A new microfluidic model that allows monitoring of complex vascular structures and cell interactions in a 3D biological matrix. *Lab Chip* **20**, 1827–1844 (2020).
19. Maoz, B. M. *et al.* A linked organ-on-chip model of the human neurovascular unit reveals the metabolic coupling of endothelial and neuronal cells. *Nat. Biotechnol.* (2018) doi:10.1038/nbt.4226.
20. van der Meer, A. D., Poot, A. A., Duits, M. H. G., Feijen, J. & Vermes, I. Microfluidic technology in vascular research. *J. Biomed. Biotechnol.* **2009**, (2009).
21. van der Helm, M. W., van der Meer, A. D., Eijkel, J. C. T., van den Berg, A. & Segerink, L. I. Microfluidic organ-on-chip technology for blood-brain barrier research. *Tissue barriers* **4**, e1142493 (2016).
22. Quirós-Solano, W. F. *et al.* Microfabricated tuneable and transferable porous PDMS membranes for Organs-on-Chips. *Sci. Rep.* **8**, 1–11 (2018).
23. Pediaditakis, I. *et al.* Modeling alpha-synuclein pathology in a human brain-chip to assess blood-brain barrier disruption. *Nat. Commun.* **12**, 1–17 (2021).
24. Moccia, C. & Haase, K. Engineering Breast Cancer On-chip—Moving Toward Subtype Specific Models. *Front. Bioeng. Biotechnol.* **9**, 1–20 (2021).

25. G. Valverde, M. *et al.* Organs-on-chip technology: a tool to tackle genetic kidney diseases. *Pediatr. Nephrol.* **37**, 2985–2996 (2022).
26. Wagner, I. *et al.* A dynamic multi-organ-chip for long-term cultivation and substance testing proven by 3D human liver and skin tissue co-culture. *Lab Chip* **13**, 3538–47 (2013).
27. Low, L. A., Mummery, C., Berridge, B. R., Austin, C. P. & Tagle, D. A. Organs-on-chips: into the next decade. *Nat. Rev. Drug Discov.* **20**, 345–361 (2021).
28. Hartogh, S. C. Den & Passier, R. Fluorescent Reporters in Human Pluripotent StemCells: Contributions to Cardiac Differentiation andTheir Applications in Cardiac Disease and Toxicity. *Stem Cells* [Epub ahead of print] (2015) doi:http://dx.doi.org10.1002/stem.2196.
29. Sung, J. H., Kam, C. & Shuler, M. L. A microfluidic device for a pharmacokinetic-pharmacodynamic (PK-PD) model on a chip. *Lab Chip* **10**, 446–455 (2010).
30. Sung, J. H. *et al.* Microfabricated mammalian organ systems and their integration into models of whole animals and humans. *Lab Chip* **13**, 1201–12 (2013).
31. Sung, J. H., Kam, C. & Shuler, M. L. A microfluidic device for a pharmacokinetic-pharmacodynamic (PK-PD) model on a chip. *Lab Chip* **10**, 446–455 (2010).
32. Lee, H. *et al.* A pumpless multi-organ-on-a-chip (MOC) combined with a pharmacokinetic–pharmacodynamic (PK–PD) model. *Biotechnol. Bioeng.* **114**, 432–443 (2017).
33. Komen, J., van Neerven, S. M., van den Berg, A., Vermeulen, L. & van der Meer, A. D. Mimicking and surpassing the xenograft model with cancer-on-chip technology. *EBioMedicine* **66**, 103303 (2021).
34. Sutherland, M. L., Fabre, K. M. & Tagle, D. a. The National Institutes of Health Microphysiological Systems Program focuses on a critical challenge in the drug discovery pipeline. *Stem Cell Res. Ther.* **4 Suppl 1**, I1 (2013).
35. Valencia, P. M., Farokhzad, O. C., Karnik, R. & Langer, R. Microfluidic technologies for accelerating the clinical translation of nanoparticles. *Nat. Nanotechnol.* **7**, 623–629 (2012).
36. Wen, Y., Zhang, X. & Yang, S.-T. MEDIUM TO HIGH THROUGHPUT SCREENING: Microfabrication and Chip-Based Technology. in *New technologies for toxicity testing* (eds. Balls, M., Combes, R. D. & Bhogal, N.) 181–206 (Springer science+business Media, LLC Landes bioscience, 2012).
37. Huh, D. *et al.* Reconstituting Organ-Level Lung Functions on a Chip. *Science (80-.).* **328**, 1662–1668 (2010).
38. Stolpe, A. Van De & Toonder, J. M. J. Den. Workshop meeting report Organs-on-Chips: human disease models. *Lab Chip* **13**, 3449–3470 (2013).
39. Marx, U. Trends in cell culture technology. in *New technologies for toxicity testing* (eds. Balls, M., Combes, R. D. & Bhogal, N.) 26–46 (Springer science+business Media, LLC Landes bioscience, 2012).
40. Meer, A. D. van der & Berg, A. van den. Organs-on-chips: breaking the in vitro impasse. *Integr. Biol.* **4**, 461–470 (2012).
41. Huh, D., Torisawa, Y., Hamilton, G. a., Kim, H. J. & Ingber, D. E. Microengineered physiological biomimicry: Organs-on-Chips. *Lab Chip* **12**, 2156 (2012).
42. Huh, D., Hamilton, G. a. & Ingber, D. E. From 3D cell culture to organs-on-chips. *Trends Cell Biol.* **21**, 745–754 (2011).
43. Fabre, K. M., Livingston, C. & Tagle, D. A. Organs-on-chips (microphysiological systems): tools to expedite efficacy and toxicity testing in human tissue. *Exp. Biol. Med.* **239**, 1073–1077 (2014).
44. van Midwoud, P. M., Verpoorte, E. & Groothuis, G. M. M. Microfluidic devices for in vitro studies on liver drug metabolism and toxicity. *Integr. Biol. (Camb).* **3**, 509–521 (2011).
45. Sackmann, E. K., Fulton, A. L. & Beebe, D. J. The present and future role of microfluidics in biomedical research. *Nature* **507**, 181–9 (2014).
46. Viravaidya, K., Sin, A. & Shuler, M. L. Development of a Microscale Cell Culture Analog to Probe Naphthalene Toxicity. *Biotechnol. Prog.* **20**, 316–323 (2004).

47. Luni, C., Serena, E. & Elvassore, N. Human-on-chip for therapy development and fundamental science. *Curr. Opin. Biotechnol.* **25**, 45–50 (2014).
48. Organs-on-chips. http://wyss.harvard.edu/viewpage/461/ (2015).
49. Balls, M., Combes, R. D. & Bhogal, N. The use of integrated and intelligent testing strategies in the prediction of toxic hazard and in risk assessment. in *New technologies for toxicity testing* (eds. Balls, M., Combes, R. D. & Bhogal, N.) 221–253 (Springer science+business Media, LLC Landes bioscience, 2012).
50. Marx, U. *et al.* 'Human-on-a-chip' developments: A translational cuttingedge alternative to systemic safety assessment and efficiency evaluation of substances in laboratory animals and man? *ATLA Altern. to Lab. Anim.* **40**, 235–257 (2012).
51. Zhang, C., Zhao, Z., Abdul Rahim, N. A., van Noort, D. & Yu, H. Towards a human-on-chip: culturing multiple cell types on a chip with compartmentalized microenvironments. *Lab Chip* **9**, 3185–3192 (2009).
52. Wolbers, F. *et al.* Breast cancer research on chip. 87–90 (2011).
53. Gold, K., Gaharwar, A. K. & Jain, A. Emerging trends in multiscale modeling of vascular pathophysiology: Organ-on-a-chip and 3D printing. *Biomaterials* **196**, 2–17 (2019).
54. Abaci, H. E. & Shuler, M. L. Human-on-a-chip design strategies and principles for physiologically based pharmacokinetics/pharmacodynamics modeling. *Integr. Biol.* **7**, 383–391 (2015).
55. Wikswo, J. P. *et al.* Engineering challenges for instrumenting and controlling integrated organ-on-chip systems. *IEEE Trans. Biomed. Eng.* **60**, 682–690 (2013).
56. Guitouni, A. & Martel, J.-M. Tentative guidelines to help choosing an appropriate MCDA method. *Eur. J. Oper. Res.* **109**, 501–521 (1998).
57. Markiewicz, K., van Til, J. a & IJzerman, M. J. Medical devices early assessment methods: systematic literature review. *Int. J. Technol. Assess. Health Care* **30**, 137–46 (2014).
58. Hummel, J. M., Rossum, W. van, Verkerke, G. & Rakhorst, G. Assessing Medical Technologies in Development; A New Paradigm of Medical Technology Assessment. *Int. J. Technol. Assess. Health Care* **16**, 1214–9 (2000).
59. Ijzerman, M. J. & Steuten, L. M. G. Early Assessment of Medical Technologies to Inform Product Development and Market Access. *Appl. Health Econ. Health Policy* **9**, 331–47 (2011).
60. Pietzsch, J. B. & Paté-Cornell, M. E. Early technology assessment of new medical devices. *Int. J. Technol. Assess. Health Care* **24**, 36–44 (2008).
61. Thokala, P. & Duenas, A. Multiple Criteria Decision Analysis for Health Technology Assessment. *Value Heal.* **15**, 1172–1181 (2012).
62. Hummel, J. M., Bridges, J. F. P. & IJzerman, M. J. Group decision making with the analytic hierarchy process in benefit-risk assessment: A tutorial. *Patient* **7**, 129–140 (2014).
63. Belton, V. & Stewart, T. *Multiple Criteria Decision Analysis: An Integrated Approach*. (Kluwer Academic Publishers, 2002).
64. Chilcott, J. B. *et al.* Avoiding and identifying errors in health technology assessment models. *Heal. Technol. Assess. Database* **14**, 1 (2010).
65. Guston, D. H. & Sarewitz, D. Real-time technology assessment. **24**, 93–109 (2002).
66. Middelkamp, H. H. T. Additional materials: Organs-on-chips in Drug Development: The Importance of Involving Stakeholders in Early Health Technology Assessment. *figshare* http://dx.doi.org/10.6084/m9.figshare.1613536 (2015) doi:http://dx.doi.org/10.6084/m9.figshare.1613536.
67. Duffy, D. C., McDonald, J. C., Schueller, O. J. A. & Whitesides, G. M. Rapid prototyping of microfluidic systems in poly(dimethylsiloxane). *Anal. Chem.* **70**, 4974–4984 (1998).
68. Qiu, Y. *et al.* Microvasculature-on-a-chip for the long-term study of endothelial barrier dysfunction and microvascular obstruction in disease. *Nat. Biomed. Eng.* **2**, 453–463 (2018).
69. Cho, M. & Park, J.-K. Fabrication of a Perfusable 3D In Vitro Artery- Mimicking Multichannel System for Artery Disease Models. *ACS Biomater. Sci. Eng.* (2020)

doi:10.1021/acsbiomaterials.0c00748.
70. Kim, S., Lee, H., Chung, M. & Jeon, N. L. Engineering of functional, perfusable 3D microvascular networks on a chip. *Lab Chip* **13**, 1489–1500 (2013).
71. Campisi, M. *et al.* 3D self-organized microvascular model of the human blood-brain barrier with endothelial cells, pericytes and astrocytes. *Biomaterials* **180**, 117–129 (2018).
72. Vila Cuenca, M. *et al.* Engineered 3D vessel-on-chip using hiPSC-derived endothelial- and vascular smooth muscle cells. *Stem Cell Reports* **16**, (2021).
73. van Meer, B. J. *et al.* Small molecule absorption by PDMS in the context of drug response bioassays. *Biochem. Biophys. Res. Commun.* **482**, 323–328 (2017).
74. Carter, S.-S. D. *et al.* PDMS leaching and its implications for on-chip studies focusing on bone regeneration applications. *Organs-on-a-Chip* **2**, 100004 (2020).
75. Campbell, S. B. *et al.* Beyond Polydimethylsiloxane: Alternative Materials for Fabrication of Organ-on-a-Chip Devices and Microphysiological Systems. *ACS Biomater. Sci. Eng.* **7**, 2880–2899 (2021).
76. Shin, Y. *et al.* Microfluidic assay for simultaneous culture of multiple cell types on surfaces or within hydrogels. *Nat. Protoc.* **7**, 1247–1259 (2012).
77. Lee, D. H., Bae, C. Y., Kwon, S. & Park, J. K. User-friendly 3D bioassays with cell-containing hydrogel modules: Narrowing the gap between microfluidic bioassays and clinical end-users' needs. *Lab Chip* **15**, 2379–2387 (2015).
78. Trietsch, S. J. *et al.* Membrane-free culture and real-time barrier integrity assessment of perfused intestinal epithelium tubes. *Nat. Commun.* **8**, 1–7 (2017).
79. Zheng, Y. *et al.* In vitro microvessels for the study of angiogenesis and thrombosis. *Proc. Natl. Acad. Sci. U. S. A.* **109**, 9342–7 (2012).
80. Wang, X. Y. *et al.* Engineering interconnected 3D vascular networks in hydrogels using molded sodium alginate lattice as the sacrificial template. *Lab Chip* **14**, 2709–2716 (2014).
81. Bischel, Lauren L; Lee, Sang-Hoon; Beebe, D. J. A Practical Method for Patterning Lumens through ECM Hydrogels via Viscous Finger Patterning. *J. Lab Autom.* **17**, 96–103 (2012).
82. de Graaf, M. N. S. *et al.* Scalable microphysiological system to model three-dimensional blood vessels. *APL Bioeng.* **3**, 026105 (2019).
83. Delannoy, E. *et al.* Multi-Layered Human Blood Vessels-on-Chip Design Using Double Viscous Finger Patterning. *Biomedicines* **10**, (2022).
84. Herland, A. *et al.* Distinct contributions of astrocytes and pericytes to neuroinflammation identified in a 3D human blood-brain barrier on a chip. *PLoS One* **11**, 1–21 (2016).
85. Tenje, M. *et al.* A practical guide to microfabrication and patterning of hydrogels for biomimetic cell culture scaffolds. *Organs-on-a-Chip* **2**, 100003 (2020).
86. Paloschi, V. *et al.* Organ-on-a-chip technology : a novel approach to investigate cardiovascular diseases . *Cardiovasc. Res.* 1–13 (2021) doi:10.1093/cvr/cvab088.
87. Hsu, Y. H., Moya, M. L., Hughes, C. C. W., George, S. C. & Lee, A. P. A microfluidic platform for generating large-scale nearly identical human microphysiological vascularized tissue arrays. *Lab Chip* **13**, 2990–2998 (2013).
88. Günther, A. *et al.* A microfluidic platform for probing small artery structure and function. *Lab Chip* **10**, 2341–2349 (2010).
89. Park, T.-E. *et al.* Hypoxia-enhanced Blood-Brain Barrier Chip recapitulates human barrier function, drug penetration, and antibody shuttling properties. *Nat. Commun.* 482463 (2019) doi:10.1101/482463.
90. Van Duinen, V. *et al.* 96 Perfusable Blood Vessels To Study Vascular Permeability in Vitro. *Sci. Rep.* **7**, 1–11 (2017).
91. Linville, R. M. *et al.* Human iPSC-derived blood-brain barrier microvessels: validation of barrier function and endothelial cell behavior. *Biomaterials* **190–191**, 24–37 (2019).
92. Brandenberg, N. & Lutolf, M. P. In Situ Patterning of Microfluidic Networks in 3D Cell-Laden Hydrogels. *Adv. Mater.* **28**, 7450–7456 (2016).

93. Enrico, A. *et al.* Three Dimensional Microvascularized Tissue Models by Laser-Based Cavitation Molding of Collagen. *Adv. Mater.* **34**, (2022).
94. Wu, Z. *et al.* Microfluidic Printing of Tunable Hollow Microfibers for Vascular Tissue Engineering. *Adv. Mater. Technol.* **6**, (2021).
95. Westein, E. *et al.* Atherosclerotic geometries exacerbate pathological thrombus formation poststenosis in a von Willebrand factor-dependent manner. *Proc. Natl. Acad. Sci.* **110**, 1357–1362 (2013).
96. Tovar-Lopez, F. J. *et al.* A microfluidics device to monitor platelet aggregation dynamics in response to strain rate micro-gradients in flowing blood. *Lab Chip* **10**, 291–302 (2010).
97. Costa, P. F. *et al.* Mimicking arterial thrombosis in a 3D-printed microfluidic: In vitro vascular model based on computed tomography angiography data. *Lab Chip* (2017) doi:10.1039/c7lc00202e.
98. Lowe, G. D. O. Virchow ' s Triad Revisited : Abnormal Flow. 455–457 (2004).
99. Rajeeva Pandian, N. K., Walther, B. K., Suresh, R., Cooke, J. P. & Jain, A. Microengineered Human Vein-Chip Recreates Venous Valve Architecture and Its Contribution to Thrombosis. *Small* **16**, 1–13 (2020).
100. Nesbitt, W. S. *et al.* A shear gradient – dependent platelet aggregation mechanism drives thrombus formation. **15**, (2009).
101. Westein, E. *et al.* Monitoring in vitro thrombus formation with novel microfluidic devices. **7104**, (2012).
102. Zhu, S., Herbig, B. A., Li, R., Colace, T. V & Muthard, R. W. In microfluidico : Recreating in vivo hemodynamics using miniaturized devices. **52**, 303–318 (2015).
103. Tsai, M. *et al.* In vitro modeling of the microvascular occlusion and thrombosis that occur in hematologic diseases using microfluidic technology. *J. Clin. Invest.* **122**, 408–418 (2012).
104. Brouns, S. L. N., Provenzale, I., van Geffen, J. P., van der Meijden, P. E. J. & Heemskerk, J. W. M. Localized endothelial-based control of platelet aggregation and coagulation under flow: A proof-of-principle vessel-on-a-chip study. *J. Thromb. Haemost.* **18**, 931–941 (2020).
105. Hinsbergh, V. W. M. Van. Endothelium — role in regulation of coagulation and inflammation. 93–106 (2012) doi:10.1007/s00281-011-0285-5.
106. Versteeg, H. H., Heemskerk, J. W. M., Levi, M. & Reitsma, P. H. New fundamentals in hemostasis. *Physiol Rev* **93**, 327–358 (2013).
107. Chen, Z. *et al.* Real-time observation of leukocyte-endothelium interactions in tissue-engineered blood vessel. *Lab Chip* **18**, 2047–2054 (2018).
108. Mannino, R. G. *et al.* Do-it-yourself in vitro vasculature that recapitulates in vivo geometries for investigating endothelial-blood cell interactions. *Sci. Rep.* **5**, 1–12 (2015).
109. Hasan, A., Paul, A., Memic, A. & Khademhosseini, A. A multilayered microfluidic blood vessel-like structure. *Biomed. Microdevices* **17**, 1–13 (2015).
110. Jia, L. *et al.* Microfluidic Fabrication of Biomimetic Helical Hydrogel Microfibers for Blood-Vessel-on-a-Chip Applications. **1900435**, 1–10 (2019).
111. Loessberg-zahl, J., Meer, A. D. Van Der, Berg, A. Van Den & Eijkel, J. C. T. Flow focusing through gels as a tool to generate 3D concentration profiles in hydrogel-filled microfluidic chips. *Lab Chip* 206–213 (2019) doi:10.1039/c8lc01140k.
112. Jain, A. *et al.* Assessment of whole blood thrombosis in a microfluidic device lined by fixed human endothelium. *Biomed. Microdevices* **18**, 1–7 (2016).
113. Mathur, T. *et al.* Organ-on-chips made of blood: endothelial progenitor cells from blood reconstitute vascular thromboinflammation in vessel-chips. *Lab Chip* **19**, 2500–2511 (2019).
114. Gami, A. S., Hayman, S. R., Grande, J. P. & Garovic, V. D. Incidence and prognosis of acute heart failure in the thrombotic microangiopathies. *Am. J. Med.* **118**, 544–547 (2005).
115. Albers, H. J., Passier, R., van den Berg, A. & van der Meer, A. D. Automated analysis of platelet aggregation on cultured endothelium in a microfluidic chip perfused with human whole blood. *Micromachines* **10**, (2019).

116. Belair, D. G. *et al.* Human Vascular Tissue Models Formed from Human Induced Pluripotent Stem Cell Derived Endothelial Cells. *Stem Cell Rev. Reports* 1–15 (2014) doi:10.1007/s12015-014-9549-5.
117. Barrile, R. *et al.* Organ-on-Chip Recapitulates Thrombosis Induced by an anti-CD154 Monoclonal Antibody: Translational Potential of Advanced Microengineered Systems. *Clin. Pharmacol. Ther.* **104**, 1240–1248 (2018).
118. Pollet, A. M. A. O. & den Toonder, J. M. J. Recapitulating the vasculature using Organ-on-Chip technology. *Bioengineering* **7**, 1–18 (2020).
119. Song, J. W. *et al.* Computer-controlled microcirculatory support system for endothelial cell culture and shearing. *Anal. Chem.* **77**, 3993–3999 (2005).
120. Arora, S., Lam, A. J. Y., Cheung, C., Yim, E. K. F. & Toh, Y. C. Determination of critical shear stress for maturation of human pluripotent stem cell-derived endothelial cells towards an arterial subtype. *Biotechnol. Bioeng.* **116**, 1164–1175 (2019).
121. Chen, H. *et al.* Cardiac-like flow generator for long-term imaging of endothelial cell responses to circulatory pulsatile flow at microscale. *Lab Chip* **13**, 2999–3007 (2013).
122. Satoh, T. *et al.* A pneumatic pressure-driven multi-throughput microfluidic circulation culture system. *Lab Chip* **16**, 2339–2348 (2016).
123. Popel, A. S. & Johnson, P. C. Microcirculation and hemorheology. *Annual Review of Fluid Mechanics* vol. 37 43–69 (2005).
124. Callaghan, F. M. & Grieve, S. M. Normal patterns of thoracic aortic wall shear stress measured using four-dimensional flow MRI in a large population. *Am. J. Physiol. - Hear. Circ. Physiol.* **315**, H1174–H1181 (2018).
125. Dessalles, C. A., Ramón-Lozano, C., Babataheri, A. & Barakat, A. I. Luminal flow actuation generates coupled shear and strain in a microvessel-on-chip. *Biofabrication* **14**, (2021).
126. Dobrin, P. B. Mechanical properties of arteries. *Physiol. Rev.* **58**, (1978).
127. Morrison, T. M., Choi, G., Zarins, C. K. & Taylor, C. A. Circumferential and longitudinal cyclic strain of the human thoracic aorta: Age-related changes. *J. Vasc. Surg.* **49**, 1029–1036 (2009).
128. Trappmann, B. *et al.* Matrix degradability controls multicellularity of 3D cell migration. *Nat. Commun.* **8**, (2017).
129. Gordon, E., Schimmel, L. & Frye, M. The Importance of Mechanical Forces for in vitro Endothelial Cell Biology. *Front. Physiol.* **11**, (2020).
130. Lam, S. F., Shirure, V. S., Chu, Y. E., Soetikno, A. G. & George, S. C. Microfluidic device to attain high spatial and temporal control of oxygen. *PLoS One* **13**, 1–16 (2018).
131. Carreau, A., Hafny-Rahbi, B. El, Matejuk, A., Grillon, C. & Kieda, C. Why is the partial oxygen pressure of human tissues a crucial parameter? Small molecules and hypoxia. *J. Cell. Mol. Med.* **15**, 1239–1253 (2011).
132. Winkler, E. A. *et al.* A single-cell atlas of the normal and malformed human brain vasculature. *Science (80-.).* **7377**, 1–23 (2022).
133. Winkelman, M. A. *et al.* Interstitial flow enhances the formation, connectivity, and function of 3D brain microvascular networks generated within a microfluidic device. *Lab Chip* **22**, 170–192 (2022).
134. Mathiisen, T. M., Lehre, K. P., Danbolt, N. C. & Ottersen, O. P. The perivascular astroglial sheath provides a complete covering of the brain microvessels: An electron microscopic 3D reconstruction. *Glia* **58**, 1094–1103 (2010).
135. Armulik, A., Genové, G. & Betsholtz, C. Pericytes: Developmental, Physiological, and Pathological Perspectives, Problems, and Promises. *Dev. Cell* **21**, 193–215 (2011).
136. Calandra, T., Gerain, J., Heumann, D., Baumgartner, J. D. & Glauser, M. P. High circulating levels of interleukin-6 in patients with septic shock: Evolution during sepsis, prognostic value, and interplay with other cytokines. *Am. J. Med.* **91**, 23–29 (1991).
137. Yuan, W., Lv, Y., Zeng, M. & Fu, B. M. Non-invasive measurement of solute permeability in cerebral microvessels of the rat. *Microvasc. Res.* **77**, 166–173 (2009).

138. Kim, S., Chung, M. & Jeon, N. L. Three-dimensional biomimetic model to reconstitute sprouting lymphangiogenesis in vitro. *Biomaterials* **78**, 115–128 (2016).
139. Hsu, P. D., Lander, E. S. & Zhang, F. Development and applications of CRISPR-Cas9 for genome engineering. *Cell* **157**, 1262–1278 (2014).
140. Lin, Y., Gil, C. H. & Yoder, M. C. Differentiation, evaluation, and application of human induced pluripotent stem cell?derived endothelial cells. *Arterioscler. Thromb. Vasc. Biol.* **37**, 2014–2025 (2017).
141. Orlova, V. V *et al.* Generation, expansion and functional analysis of endothelial cells and pericytes derived from human pluripotent stem cells. *Nat. Protoc.* **9**, 1514–31 (2014).
142. Takahashi, K. & Yamanaka, S. Induction of Pluripotent Stem Cells from Mouse Embryonic and Adult Fibroblast Cultures by Defined Factors. *Cell* **126**, 663–676 (2006).
143. Inoue, H. & Yamanaka, S. The use of induced pluripotent stem cells in drug development. *Clin. Pharmacol. Ther.* **89**, 655–661 (2011).
144. Shen, M., Quertermous, T., Fischbein, M. P. & Wu, J. C. Generation of Vascular Smooth Muscle Cells from Induced Pluripotent Stem Cells: Methods, Applications, and Considerations. *Circ. Res.* 670–686 (2021) doi:10.1161/CIRCRESAHA.120.318049.
145. Faal, T. *et al.* Induction of Mesoderm and Neural Crest-Derived Pericytes from Human Pluripotent Stem Cells to Study Blood-Brain Barrier Interactions. *Stem Cell Reports* **12**, 451–460 (2019).
146. Jain, A. *et al.* A shear gradient-activated microfluidic device for automated monitoring of whole blood haemostasis and platelet function. *Nat. Commun.* **7**, 1–10 (2016).

Supplementary information

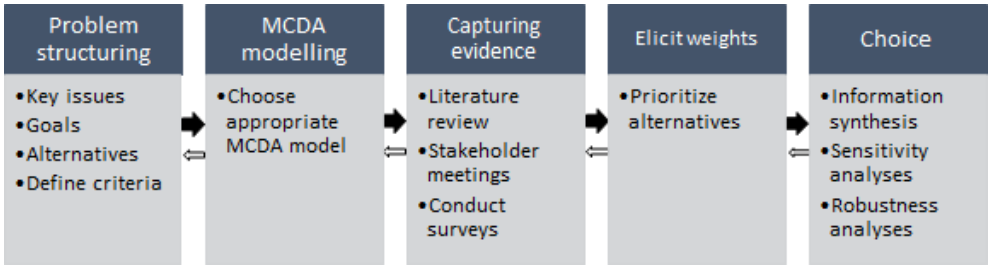

Supplementary figure 1: Schematic overview of the MCDA process. MCDA starts with defining the problem, after which an appropriate MCDA model can be chosen.39 The evidence is collected, which can be used to understand the criteria and alternatives better and to capture hard evidence for the next step where a quantitative measurement of the values is performed. A choice can be made after considering the results of the analysis. It is worth noting that it is always possible to take a step back in the process and repeat a step with evidence gathered in later in the process. Adapted from "Thokala and Duenas[61]" and "Hummel, Bridges and IJzerman[62]".

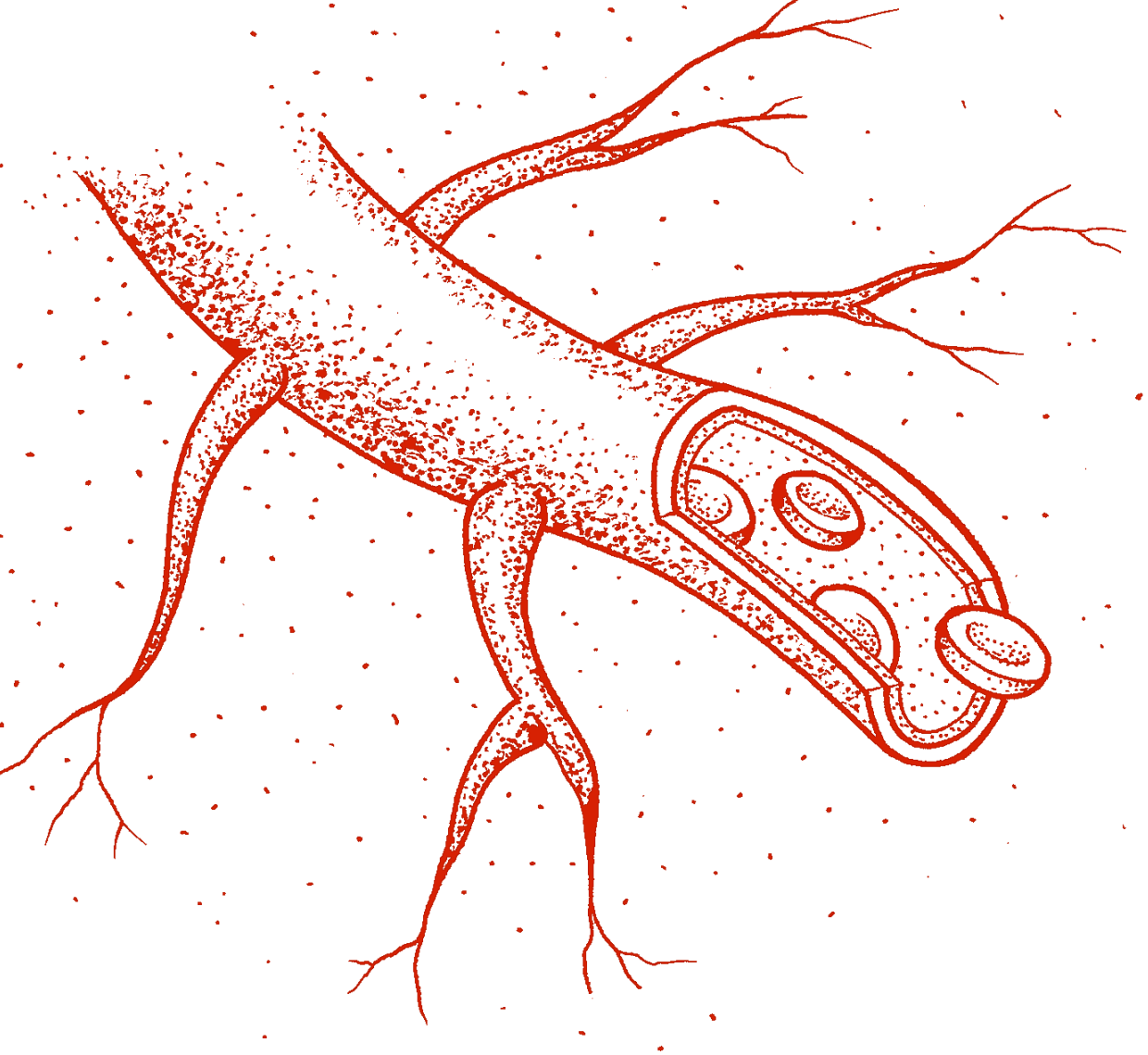

3

Trained immunity of endothelial cells in blood vessels-on-chip

H.H.T. Middelkamp*
K. Le*
N. Keurs
L. Do
M. Netea
I. Jonkers
V. Orlova
A. van den Berg
S. Withoff
V. Kumar
A.D van der Meer

Presented as poster at:
EUROoCS21; EUROoCS22; µTAS22
Manuscript in preparation
*Equal author contribution

Abstract

Immune memory is not restricted to adaptive immune cells. Recent studies show that endothelial cells as well as innate immune cells exhibit a memory after pathogen and cytokine exposure, showing a stronger immune response when exposed a second time, which is called *trained immunity*. Although endothelial cells do exhibit trained immunity on the level of gene expression, it is currently not known if this also leads to functional changes, such as immune cell recruitment. Using enzyme-linked immunosorbent assay for the cytokine interleukin-6 and flow cytometry for the endothelial adhesion molecules *intercellular adhesion molecule-1* (ICAM-1) and *vascular cell adhesion molecule-1* (VCAM-1), responses were measured in human umbilical vein endothelial cells when stimulated once or twice (with resting days in between) with the inflammatory cytokine tumor necrosis factor-α in a well-plate. For some donors, we observed a higher expression level of surface markers and secretion of cytokines on endothelial cells that were exposed twice to stimuli compared to cells that were stimulated only once.

We have developed a monocyte adhesion assay in 3D blood vessels-on-chip in which we can observe functional changes in endothelial cells after different stimulation conditions. Cells were stimulated with tissue necrosis factor-α, after which fluorescently labelled monocytes were flowed through the channel. Live images of the cells in the channels were made using a fluorescence microscope and the number of monocytes attached to the endothelial layer was determined. For two high-responding donors an increase was observed in the number of monocytes attached to the endothelial layer after 2 hits of TNF-α compared to cells that were exposed once. Furthermore, the low responding donor did not show an increase in monocytes adhered when stimulated twice.

We have successfully set up a functional assay for monocyte adhesion in a blood-vessel-on-chip model and have observed preliminary evidence of trained immunity in endothelial cells on a functional level. Next steps include performing RNA-seq and ATAC-seq to observe a possible training effect on respectively transcriptomic or chromatin levels. This model may shine light on personalized immune responses in e.g., sepsis and chronic inflammation, and can help in personalized drug development for these diseases.

3.1 Introduction

Immune memory is not restricted to adaptive immune cells. Recent studies show that endothelial cells as well as innate immune cells exhibit a memory after pathogen and cytokine exposure, showing a stronger immune response when exposed a second time, which is called *trained immunity*[1–3]. Trained immunity is hallmarked by the ability of cells to exhibit a memory effect after exposure to a pathogen. After the inflammatory response upon a first exposure to a pathogen the cell reverts to a baseline state, but its inflammatory response is exacerbated upon a second exposure to the same pathogen later in time (figure 1a). This process differs from other similar responses in the context of immunity, such as *priming* and *tolerance*. In priming, the basic functional state of the cells is changed, and their immune response does not return to baseline before a second exposure to a pathogen. In tolerance, the cells do return to a baseline reaction but exhibit a lower response at second encounter with the same pathogen[4,5]. By exhibiting a 'training effect', innate immune cells such as monocytes and macrophages can drive an enhanced response against a broad spectrum of infectious pathogens.

Other innate immune cell types such as natural killer (NK-)cells acquire a species-specific memory and are present in smaller amounts than monocytes and take longer to respond as monocytes activate the NK-cells[6,7]. In fact, after the first response to pathogens, the innate immune cells undergo metabolic and epigenetic changes that facilitate a higher expression of cytokines interleukin-1, tissue necrosis factor-α, and interferon-γ (IL-1, TNF-α and IFN-γ) in the next infection[8,9]. It is well known that immune cells are not the only cell type regulating the host responses to infection[10]. Endothelial cells are also known to modulate inflammation by cytokine release and e.g. immune cell activation[11].

Endothelial cells, lining the blood vessels, actively regulate inflammation by secreting cytokines such as interleukin-6 and interleukin-8 (IL-6, IL-8) as well as recruiting immune cells to the site of infection. Interestingly, endothelial activity is driven by key cytokines IL-1 and TNF-α secreted by the immune cells in fungal and gram-positive bacterial infection[10]. Moreover, epigenetic changes in trained monocytes indicate modifications in genes involved in vascular endothelial growth factor (VEGF) pathway, endothelin pathway and trans-endothelial migration pathway[12,13]. These are necessary pathways for the immune cells to interact with endothelial cells to regulate inflammation and coagulation, the hallmarks among blood infection symptoms. Interestingly, studies have now demonstrated that endothelial cells, at

least on the level of adhesion marker and proinflammatory cytokine release, exhibit signs of trained immunity[12,14]. Relatively little is known about the mechanism and (patho)physiological importance of this effect.

Upon infection, endothelial cell adhesion markers such as vascular cell adhesion molecule-1 (VCAM-1), intercellular adhesion molecule-1 (ICAM-1) and e-selectin are upregulated to attract the first responder white blood cells, monocytes[15–18]. To better understand the effect of trained endothelial cells in regulating inflammation, we will focus on its interaction with innate immune cells. Since endothelial cells do not recognize specific infectious pathogens, such as *Candida albicans* and *Streptococcus pneumonia* but do respond to inflammatory factors such as IL-1 and TNF- α, these factors can be used to simulate infection.

Although well plate experiments with endothelial monolayers can give an abundance of data with regards to epigenetics and cytokine expression levels, they cannot give us a representative insight in any functional changes of the cells, such as immune cell recruitment because they do not give a representative insight of the *in vivo* situation by lacking e.g., flow and *in vivo* geometries. Next to that, without the ability to actively flow immune cells over the endothelial surface, differences in immune response on the functional level of immune cell recruitment cannot be determined.

A relatively new method to investigate organ-specific diseases and to mimic specific organs are organs-on-chips (OoCs). Currently there are multiple vessel-on-chip (VoC) models to investigate the endothelial layer and its condition[19–24]. They typically consist of an actively perfused microfluidic channel or network of channels lined by endothelial cells and are widely used to investigate disease processes. Multiple models have a monocyte adhesion assay as an end point measurement[25–29]. Especially the more complex models in which 3D viscous finger patterned, endothelial cell lined lumens are used are promising models to use for a realistic functional assay. The more complex viscous finger patterned lumens have been used for endothelial cell culture for more than 2 decades and are robust in setting up and keeping in culture for longer periods of time[23,30–32]. These models also have the advantage of a more physiological environment of collagen surrounding the cells. 3D VoC with perfusable, viscous finger-patterned lumens were used in this study to identify presence or absence of trained immunity on a level of immune cell recruitment in human umbilical vein endothelial cells (HUVECs).

We hypothesize that the effect of trained immune cells in its interaction with endothelial cells, converges on endothelial responses to repeated exposure to cytokines such as TNF-α. Lately, more evidence points towards patient-specific immune reactions in for example sepsis and chronic inflammation[14,33,34], with some patients reacting more strongly when exposed to a pathogen for a second time. Therefore, there might be a donor-specific training response to repeated exposure to a pathogen[35,36].

In this research project, we strive to determine trained immunity in pooled and individual HUVECs. We will describe the responses of primary endothelial cells from different donors. From these individual donors we chose 3 different responders to test our hypothesis of trained immunity on a functional level. We have set up a monocyte adhesion assay on a VoC, to determine trained immunity in endothelial cells on a functional level.

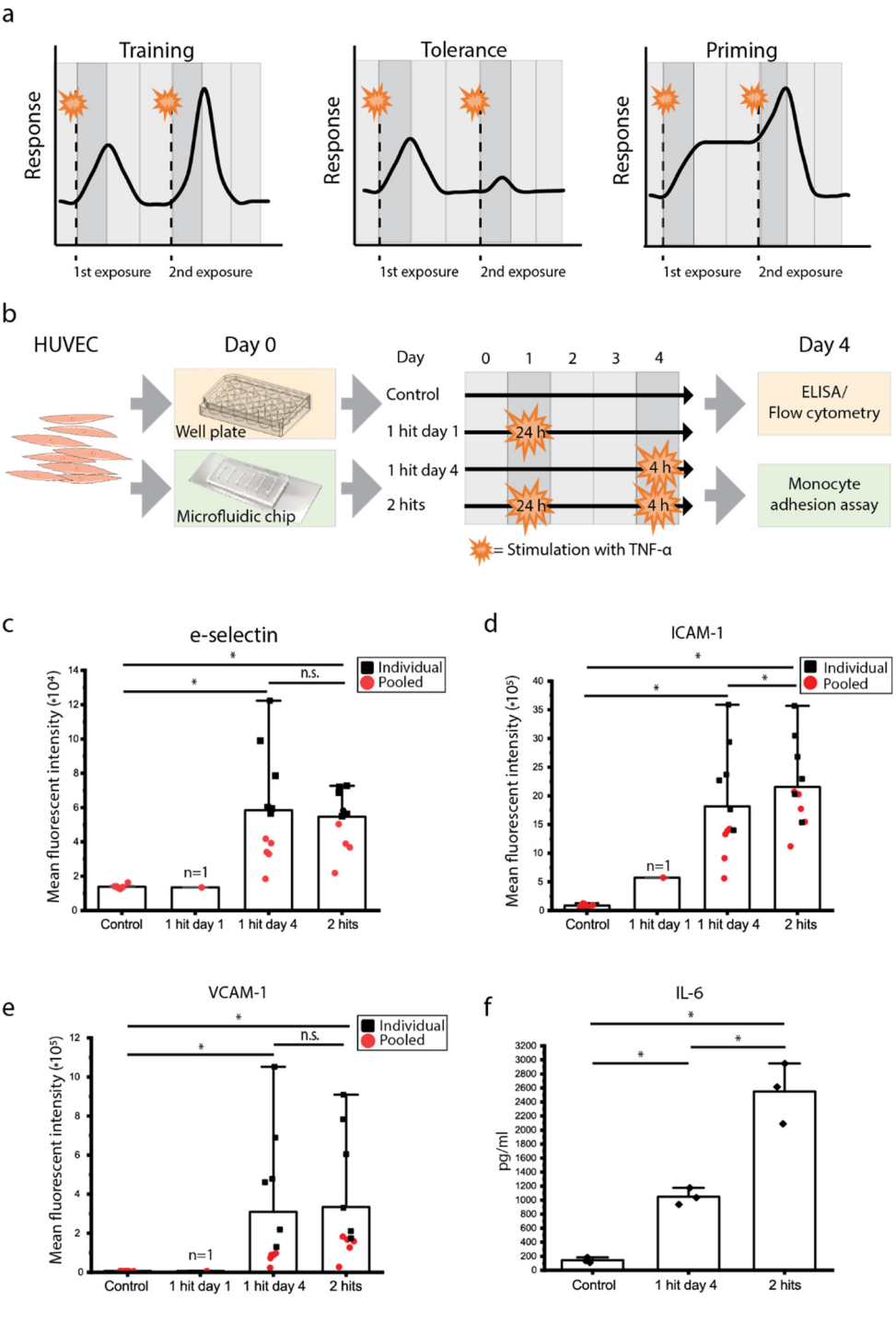
a
Training
Tolerance
Priming
Response
1st exposure
2nd exposure
b
HUVEC
Day 0
Well plate
Microfluidic chip
Day
0 1 2 3 4
Control
1 hit day 1
1 hit day 4
2 hits
24 h
4 h
Day 4
ELISA/
Flow cytometry
Monocyte
adhesion assay
= Stimulation with TNF-α
c
e-selectin
d
ICAM-1
e
VCAM-1
f
IL-6
Individual
Pooled
n.s.
n=1
Mean fluorescent intensity (*10⁴)
Mean fluorescent intensity (*10⁵)
pg/ml
Control
1 hit day 1
1 hit day 4
2 hits

Figure 3-1: Trained immunity of endothelial cells. a) Trained immunity represents itself by a higher response upon 2nd pathogen exposure. Unlike what happens in priming, immune response returns to baseline after resting phase. The reaction also differs from tolerance response, where the cells respond less to a pathogen at second exposure. B) Overview of assay presented in this chapter. (Individual donor) HUVECs were seeded on either well plate or microfluidic chip on day 0. Four separate conditions were applied to the cells after which an end-point measurement is performed (after stimulation) on day 4. c-e) HUVECs were seeded on well plates and respectively e-selectin-, ICAM-, and VCAM expression levels were measured (Flow cytometry) at different conditions. Expression levels were measured for both pooled donor (red dots) and individual donor (black squares) samples. An increase in response can be observed for all markers when stimulated on day 4 as well as a lower (ICAM) or back to baseline (e-selectin; VCAM) response when cells were stimulated on day 1. F) Excretion of IL-6 was measured (ELISA) on day 4 in a pooled donor sample. A significantly different increase in IL-6 excretion can be observed between cells stimulated for the first and second time on day 4.

3.2 Materials and Methods

3.2.1 Well plate experiments

Primary Endothelial Cell culture

To capture endothelial cell responses to repetitive stimulation, primary Human Umbilical Vein Endothelial Cells (HUVECs) from single donors were purchased (Lonza) and cultured in Endothelial cell Growth Medium (PromoCell, C-22111) supplemented with 1% Penicillin/Streptomycin (10.000U/ml) (Gibco) at 37°C, 5% CO2 and saturating humidity. Cells were stored at passage 2, thawed and seeded for well plate experiments at passage 3 and VoC experiments at passage 4.

To obtain pooled HUVECs of 7 single donors, cells at P1 were cultured to reach confluency and pooled with equal number of cells per donor. The pool was then passed for one more passage and frozen at passage 2. The pooled-donor HUVECs were thawed at P3 and seeded for experiments. Stimuli were added when cells reached 70% confluency.

Stimulation

For stimulation (figure 1b), HUVECs were treated with TNF-α (PeproTECH, 300-01A) at 10 ng/ml for 24 (day 1) or 4 (day 4) hours. At day 2 HUVECs were washed and let rest for 72 hours before the second hit of TNF-α was added for 4 hours. The responses of repetitive exposed cells (2 hits) were compared with cells that exposed only once to simulation on the day of the 2nd stimulation added (1 hit day 4). Two control conditions were also added: 1) cells that were exposed to no stimulation (Control), 2) cells that received one hit of stimulation on the day of the 1st stimulation (1 hit day 1).

Flow cytometry

To determine expression of adhesion molecules on the cell membrane, the cells were washed with PBS, detached using trypsin, washed with PBS, and fixed with Formaldehyde 4% (Thermofisher). The cell pellets were washed, resuspended in PBS, and stored at 4 °C until staining. The cells were divided equally into separate FACS tubes with ice-cold FACS buffer (PBS supplemented with 5% FCS). The cells were stained using the following antibodies: PE-conjugated anti-human e-selectin (CD62E) (Biolegend, 322606), APC-anti human VCAM-1 (CD106) (Biolegend, 305810), FITC- anti human ICAM-1 (CD54) (Biolegend, 322720) and IgG isotype controls (IgG isotype controls (Biolegend,) for 30 minutes on ice. The cells were washed once and resuspended in FACS buffer. Samples were analyzed using Agilent Quanteon system. Multi-color compensation was calibrated using positive control cell population (TNF- α activated HUVECs).

ELISA

The amount of IL-6 secreted into the medium were measured by ELISA (Human IL6 DuoSet ELISA, R&D). Supernatant was collected and stored at -20°C until measured. ELISA was performed as recommended in the manufacture kit.

3.2.2 Microfluidic chip experiments

Chip fabrication

The microfluidic chip consists of 6 channels, which are one centimeter in length and 500 x 500 µm in width and height (figure 2a-b). The chip was fabricated by conventional polydimethylsiloxane (PDMS)-based soft lithography using a poly(methyl methacrylate) (PMMA, Arkema innovative chemistry) mould. The mould was produced by micromilling (Sherline, model 5410) based on designs in SolidWorks (Dassault Systèmes, France). PDMS (10:1 base:crosslinker ratio, Sylgard 184) was added to the PMMA mould and was left to cure overnight at 65 °C after which it was removed from the mould. 1 mm inlet and outlet holes were created using biopsy punchers (Robbins Instruments). PDMS was spin coated (SPS Spin150) on a glass microscope slide and PDMS was left to cure overnight at 65 °C. The surfaces of both the microfluidic device and the microscope slide were activated by exposing them to air plasma (50 W) for 40 s (Cute, Femto Science, South Korea), after which the microfluidic chip was bonded to the microscope slide.

Microfluidic chips were further activated using a 0.22 µm filtered 2 mg/ml Dopamine Hydrochloride (Sigma Aldrich, #H8502) in 10 mM TrisHCl (pH 8.5) solution. This solution was added to the channels and incubated at room temperature for one

hour. After one hour chips were washed 3 times with sterile milliQ. Fluid was removed from the channels and microfluidic chips are ready to be used for viscous finger patterning.

Collagen solution

A 5 mg/ml rat tail collagen solution was prepared, using high concentration collagen (Corning life sciences; #354249) which was diluted using a master mix consisting of 10x PBS, 1M NaOH and dH_2O (always working on ice).

1/10 of the final volume of 10x PBS was added to the master mix. The amount of 1M NaOH added was calculated using the following formula: (volume collagen) x 0.023. The amount of dH_2O was calculated and added to the master mix: (Final volume)-(volume collagen)-(volume 10x PBS)-(volume NaOH)= volume dH_2O. The master mix was mixed thoroughly by pipetting up and down without inducing air bubbles. The collagen was added into a new ice-cold Eppendorf tube using ice-cold pipette tips. Master mix was added to the collagen and mixed gently until mixed properly. Using pH paper, the pH of the solution was checked to be between 6.5 and 7.5. Then the solution was vortexed and spun down to remove air bubbles.

Viscous finger patterning

This protocol was performed using the same method as used by de Graaf *et. al*[23]. A 200 µl pipet tip cut off to 7 mm was inserted in the outlet of the channel. 10 µl collagen solution was pipetted into the inlet of the channel until a meniscus of collagen formed on the cut pipet tip. Pipet tip was left in the inlet and a droplet of ice cold 2.2 µl PBS was added to the cut pipet tip. This droplet formed a lumen in the collagen inside the channel. After patterning, the microfluidic chip was placed inside an incubator at 37 °C and 5% CO_2 for 1 hour. After one hour pipet tips were removed from in- and outlets and replaced with new 200 µl pipet tips and filled with medium. Chips were incubated overnight at 37 °C and 5% CO_2 to have a proper level of CO_2 and heat in the chips before cell seeding.

Culturing cells in microfluidic chips

HUVEC cells (donor #SD125 (“high responder”); #SD263 (“medium responder”); #SD126 (“low responder”)) were thawed at passage 3 in a t-75 cell culture flask cultured in EGM-2 (Promocell inc.; C-22111) and passaged once to obtain enough cells for seeding in microfluidic channels. Cells were detached from t-75 flask using 3 ml of Trypsin for 3 minutes. Trypsin was neutralized using 7 ml of cell culture

medium and cell suspension was centrifuged for 5 min at 390 x*g*. Cells were counted using a LUNA cell counter and diluted to an end concentration of $5 \cdot 10^6$ cells/ml.

Cells were seeded in the channels using gel loader pipet tips, so as not to remove the present pipet tips from the collagen formed channels. After seeding cells, chips were inverted and incubated at 37 °C and 5% CO_2 for half an hour to let cells attach to the top of the microfluidic channel The bottom half of the chip was seeded using a second seeding step. After half an hour of incubation for cell adhesion, all channels were refreshed with 200 µl fresh culture medium (day 0). Chips were placed on a rocking table (10° angle, 30 sec interval; BenchBlotter™ 2D platform rocker) and after 24 hours (day 1) a monolayer was formed. Cells were kept in culture for 4 days, for the monocyte adhesion assay.

Endothelial lumens were treated in 4 different conditions: 1) 'Control' (cell medium was changed every 24 hours); 2) '1 hit day 1' (24 hour stimulation with 10 ng/ml TNF-α at day 1, with every 24 hours medium refreshment day 3-5) ; 3) '1 hit day 4' (Cell medium was changed every 24 hours from day 2-4, at day 4 cells were stimulated with 10 ng/ml TNF-α for 4 hours) ; 4) '2 hit' (24 hour stimulation with 10 ng/ml TNF-α at day 1, with every 24 hours medium refreshment day 2-3, at day 4 cells were stimulated a second time with 10 ng/ml TNF-α for 4 hours), after which the monocyte adhesion assay was performed (figure 1b).

Monocyte adhesion assay

Monocytes were stained using a cell tracker dye (Invitrogen; C2925), according to recommendations of the manufacturer using a concentration of 2.5 µM and diluted to a concentration of $2.5 \cdot 10^6$ cells/ml in RPMI 1640 + GlutaMAX medium (Gibco; 61870036). A syringe pump (Harvard Apparatus) was used to pull the monocyte solution through the channels at 2 µl/min. The pump was connected to the outlet of the channel by removing the pipet tip from the channel and adding a 14-gauge blunt needle connected to tygon tubing, which is then connected to the syringe. A brightfield microscope was used to confirm flow. After flow was confirmed, a gel loader tip, was used to remove access medium from the inlet and replaced with the monocyte solution. Monocytes were perfused through the channel for 10 minutes, after which excess monocyte solution was removed from the inlet pipet and replaced with regular EGM-2 medium (figure 2d). This was pulled through the channel for at least 2 minutes to remove all non-attached monocytes from the channel. After removing all unattached monocytes in the channel, the pump was

stopped and disconnected from the outlet of the channel. The blunt needle was replaced with a yellow pipet tip and chips are used for live imaging.

Data analysis

After the monocyte adhesion assay, live imaging of microfluidic channels was performed using and EVOS (EVOS M5000). Live images were captured at the inlet of the channel, images of the brightfield channel as well as the GFP channel (monocytes) were obtained. Confocal imaging was performed using a Zeiss LSM 880.

A pipeline was created in cell profiler[37] (CellProfiler_Version, 4.2.1). The GFP image was first converted to a grey scale image, then primary objects were identified. Thresholding strategy was Global, thresholding method Otsu. Smoothing filter was adjusted to include as many monocytes as possible. This pipeline was used to identify the number of monocytes in the GFP channel.

Graphs were made with Origin Pro 2023[38].

To determine significance in difference between different conditions a paired sample t-test was performed.

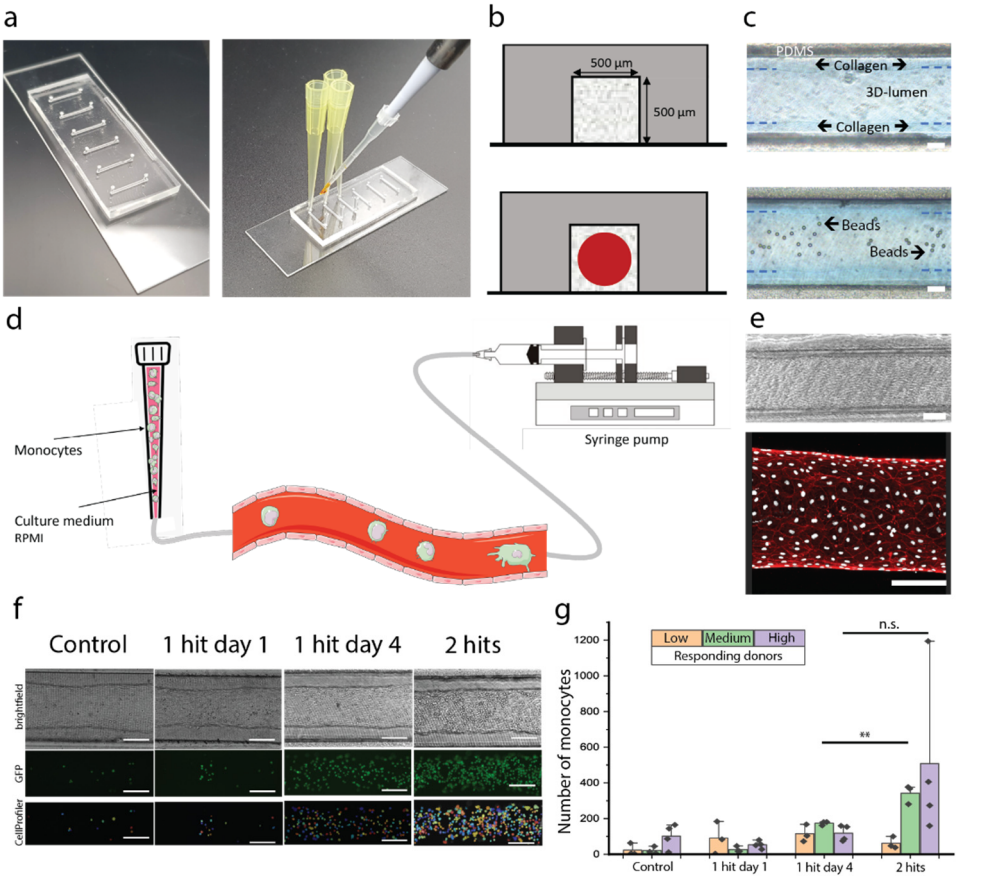

Figure 3-2: Monocyte adhesion assay. a-b) Microfluidic chip was prepared using PDMS soft-lithography and viscous finger patterning was performed to obtain a 3D lumen inside a collagen type-1 hydrogel. c) After the 3D lumen was created, beads were added to observe the ability to perfuse. d) Schematic overview of the monocyte adhesion assay. A pipette tip loaded with pre-stained monocytes was connected to the microfluidic channel. The other side of the channel is connected to a syringe pump, which pulls the monocytes through the channel. e) 3D lumen can be seeded with HUVECs, and a 3D reconstruction of the channel can be made using confocal imaging (white: nuclei; red: F-actin). f) The different functional responses of one donor to the different types of stimuli indicate a training effect of the endothelial cells. g) Three different responding donors were used in the monocyte adhesion assay. The low responding donor does not show an increase in monocytes adhered, an increase in response can be observed in both the medium and high responding donors. All scale bars represent 150 µm.

3.3 Results & Discussion

3.3.1 Re-exposure of HUVECs in well plate experiments

As previously reported, endothelial cell-monocyte interaction is mainly regulated via IL-1, TNF-α and IFNs pathways[10,39,40]. Therefore, to understand the inflammatory profile of HUVECs in the context of trained immunity, pooled HUVECs from 6 donors were stimulated with TNF-α (figure 1b). The expression of adhesion molecules ICAM-1, VCAM-1, and e-selectin, as well as secreted cytokine IL-6 were measured 4 hours after the second hit (figure 1c-f). We obtained data from both the pooled and individual donors and for ICAM-1, VCAM-1 and e-selectin combined them in the graph, with the red dots representing the pooled samples and the black squares representing individual donor measurements. For ICAM-1, VCAM-1, and e-selectin it can be observed that individual donors tend to have an overall higher response compared to the pooled data (figure 1c-e), indicating that pooling the samples may suppress the responses slightly. When plotting individual donor responses, no training effect between 1 hit day 4 and 2 hits was observed (supplementary figure 1).

We observed significant changes in ICAM-1 and IL-6 expression level between 1 hit day 4 and 2 hit stimulations. For VCAM-1 and e-selectin no significant differences were observed. The VCAM-1 and e-selectin expression of cells stimulated only on day 1 seems to return to baseline as is expected in endothelial cell training. However, these two markers are not expressed on a higher level when stimulated twice with TNF-α, indicating no training in immune response. The 1 hit day 1 condition in the e-selectin, ICAM-1, and VCAM-1 graphs represent an n=1, which was not sufficient to make statistical conclusions about the training effect. To make these observations an n=3 is recommended, therefore more repeats should be performed. The excretion of IL-6 shows a significant increase in samples which received 2 hits of stimuli compared to 1 hit on day 4, as well as a considerable increase in IL-6 excretion compared to the control sample, which received no hits with TNF-α. At individual donor level, a clear distinction could be made between different responding donors, with 3 donors chosen to continue in the follow up studies, a high-, medium-, and low responding donor (supplementary fig 1). These were selected to assess functional changes in the endothelial cell layer in a VoC. The IL-6 values were not measured for samples receiving 1 hit at day 2, therefore before starting the functional assay, it could not be assessed whether the increase in response of these donors should be interpreted as endothelial cell training or priming.

3.3.2 Re-exposure to the same stimuli alters endothelial cell's biological function in VoC.

To assess functional changes of HUVECs under different stimulation conditions and identify effects of endothelial cell training, we set up monocyte adhesion assay in a VoC model. To mimic the microphysiological environment of endothelial cells, we employed the viscous finger patterning technique to create a collagen lumen (figure 2b-c, 2e). HUVECs from 3 donors (picked from supplementary figure 1), ranging from high responder to low responder (SD125, SD263, SD126, resp.) were cultured in the 3D lumen. HUVECs were stimulated according to the stimulation scheme presented in figure 1b. On day 4, after the second exposure, cells were washed to remove excess stimuli. THP-1 cells were stained with a cell tracker dye before adding to the chip. Flow was enabled through the channel for 10 minutes at 2 µl/min, the chip was then washed, and live images were obtained for data analysis.

Figure 2f shows the results for donor SD263/medium responding in different conditions, with a brightfield image, a GFP (monocytes) image and lastly the CellProfiler monocyte count data. In the control sample, a minimal amount of monocytes adhered to the HUVEC surface. An increase could be observed in the images representing the 1 hit day 4 and 2 hits channels, with the 2 hit channel containing notably more monocytes adhered than the 1 hit day 4 channel. The channels that received a hit of TNF-α on day 1 should, in endothelial cell training, return to baseline, which can also be observed in this example. Figure 2g shows the results of the number of monocytes adhered per channel per donor. The three differently responding donors can be distinguished in orange (low responding), green (medium responding) and purple (high responding). The results of the monocyte adhesion assay seem to confirm that the excretion of IL-6 can be correlated to the immune cell recruitment capabilities of the HUVECs. The low responding donor did not show a response at all, medium and high donor did show training. Statistical significance could be established for the medium donor ($p < 0.01$), however due to broad range in response in the high responding donor, no significant difference could be established. The power calculation performed showed multiple repeats are necessary to obtain a statistically significant difference for this donor.

Figure 2 f-g confirms that endothelial cells attract more monocytes when the cells were pre-exposed to TNF-α, indicating a functional change and even training in some HUVEC donors. Interestingly, for three donors, we observe a correlation in the

magnitude of monocyte adhesion capacity and the secreted IL-6 levels. This indicates that the extent of training in endothelial cells may represent a donor-specific response. This could have clinical relevance, particularly given the fact that there is strong patient-to-patient variability in e.g., sepsis[10,41].

3.4 Conclusion & outlook

The aim of this project was to set up an assay to assess endothelial cell immune response training. We have successfully set up a 3D VoC in which we could perform a monocyte adhesion assay. Our well plate experiments indicated no different immune responses when observing adhesion markers such as VCAM-1; ICAM-1 and e-selectin. Donor specific marker expression did not indicate a training effect on a marker expression level. The excretion of IL-6 did indicate an increase in cell responses; however, no conclusions can be made whether this is a training or a priming effect. The excretion of IL-6 was our guideline for indicating 3 different donors. A low, medium, and high responding donor were used in our VoC model. These different donor channels received 4 different conditions described in fig. 1b and the monocyte adhesion assay on day 4. Preliminary results are promising. Donor-specific responses, corresponding to the IL-6 excretion profiles, to the different stimuli could be observed on a functional level. Next to that, we observed responses returning to baseline when receiving 1 hit on day 1, indicating endothelial cell training.

The next step in this project will be to observe (donor specific) differences on RNA or even chromatin levels. Using these techniques, the mechanism behind endothelial cell training can be assessed. With more knowledge on patient-specific responses, a better treatment plan or risk assessment can be made for patients with for example chronic inflammation.

References

1. Netea, M. G. *et al.* Innate Secondary Response. **352**, 1–23 (2017).
2. Netea, M. G. *et al.* Defining trained immunity and its role in health and disease. *Nat. Rev. Immunol.* **20**, 375–388 (2020).
3. Netea, M. G. *et al.* Trained immunity: A program of innate immune memory in health and disease. *Science (80-.).* **352**, 427 (2016).
4. Divangahi, M. *et al.* Trained immunity, tolerance, priming and differentiation: distinct immunological processes. *Nat. Immunol.* **22**, 2–6 (2021).
5. Byrne, K. A., Loving, C. L. & McGill, J. L. Innate Immunomodulation in Food Animals: Evidence for Trained Immunity? *Front. Immunol.* **11**, (2020).
6. Bluman, E. M., Bartynski, K. J., Avalos, B. R. & Caligiuri, M. A. Human natural killer cells produce abundant macrophage inflammatory protein-1α in response to monocyte-derived cytokines. *J. Clin. Invest.* **97**, 2722–2727 (1996).
7. Michel, T., Hentges, F. & Zimmer, J. Consequences of the crosstalk between monocytes/macrophages and natural killer cells. *Front. Immunol.* **3**, 1–6 (2012).
8. Fanucchi, S., Domínguez-Andrés, J., Joosten, L. A. B., Netea, M. G. & Mhlanga, M. M. The Intersection of Epigenetics and Metabolism in Trained Immunity. *Immunity* **54**, 32–43 (2021).
9. Crisan, T. O., Netea, M. G. & Joosten, L. A. B. Innate immune memory: Implications for host responses to damage-associated molecular patterns. *Eur. J. Immunol.* **46**, 817–828 (2016).
10. Le, K. T. T. *et al.* Leukocyte-released mediators in response to both bacterial and fungal infections trigger ifn pathways, independent of il-1 and tnf-α, in endothelial cells. *Front. Immunol.* **10**, 1–13 (2019).
11. Amersfoort, J., Eelen, G. & Carmeliet, P. Immunomodulation by endothelial cells — partnering up with the immune system? *Nat. Rev. Immunol.* **22**, 576–588 (2022).
12. Nica, V. *et al.* Expert Review of Clinical Immunology The future clinical implications of trained immunity. *Expert Rev. Clin. Immunol.* **18**, 1125–1134 (2022).
13. Arts, R. J. W. *et al.* BCG Vaccination Protects against Experimental Viral Infection in Humans through the Induction of Cytokines Associated with Trained Immunity. *Cell Host Microbe* **23**, 89-100.e5 (2018).
14. Drummer, C. *et al.* Trained Immunity and Reactivity of Macrophages and Endothelial Cells. *Arterioscler. Thromb. Vasc. Biol.* **41**, 1032–1046 (2021).
15. Kaukoranta-Tolvanen, S. S. E., Ronni, T., Leinonen, M., Saikku, P. & Laitinen, K. Expression of adhesion molecules on endothelial cell stimulated by Chlamydia pneumoniae. *Microb. Pathog.* **21**, 407–411 (1996).
16. Birnhuber, A. *et al.* Between inflammation and thrombosis: Endothelial cells in COVID-19. *Eur. Respir. J.* **58**, 1–5 (2021).
17. Kwon, S., Kurmashev, A., Lee, M. S. & Kang, J. H. An inflammatory vascular endothelium-mimicking microfluidic device to enable leukocyte rolling and adhesion for rapid infection diagnosis. *Biosens. Bioelectron.* **168**, 112558 (2020).
18. Roifman, I. *et al.* Chronic Inflammatory Diseases and Cardiovascular Risk : A Systematic Review. *CJCA* **27**, 174–182 (2011).
19. Albers, H. J., Passier, R., van den Berg, A. & van der Meer, A. D. Automated analysis of platelet aggregation on cultured endothelium in a microfluidic chip perfused with human whole blood. *Micromachines* **10**, (2019).
20. Costa, P. F. *et al.* Mimicking arterial thrombosis in a 3D-printed microfluidic: In vitro vascular model based on computed tomography angiography data. *Lab Chip* (2017) doi:10.1039/c7lc00202e.
21. Westein, E. *et al.* Atherosclerotic geometries exacerbate pathological thrombus formation poststenosis in a von Willebrand factor-dependent manner. *Proc. Natl. Acad. Sci.* **110**, 1357–1362 (2013).

22. Barrile, R. *et al.* Organ-on-Chip Recapitulates Thrombosis Induced by an anti-CD154 Monoclonal Antibody: Translational Potential of Advanced Microengineered Systems. *Clin. Pharmacol. Ther.* **104**, 1240–1248 (2018).
23. de Graaf, M. N. S. *et al.* Scalable microphysiological system to model three-dimensional blood vessels. *APL Bioeng.* **3**, 026105 (2019).
24. van Dijk, C. G. M. *et al.* A new microfluidic model that allows monitoring of complex vascular structures and cell interactions in a 3D biological matrix. *Lab Chip* **20**, 1827–1844 (2020).
25. Delannoy, E. *et al.* Multi-Layered Human Blood Vessels-on-Chip Design Using Double Viscous Finger Patterning. *Biomedicines* **10**, (2022).
26. Ohashi, K., Hayashida, A., Nozawa, A., Matsumura, K. & Ito, S. Human vasculature-on-a-chip with macrophage-mediated endothelial activation: The biological effect of aerosol from heated tobacco products on monocyte adhesion. *Toxicol. Vitr.* **89**, 105582 (2023).
27. Halaidych, O. V., van den Hil, F., Mummery, C. L. & Orlova, V. V. Microfluidic assay for the assessment of leukocyte adhesion to human induced pluripotent stem cell-derived endothelial cells (HiPSC-ECs). *J. Vis. Exp.* **2018**, 1–8 (2018).
28. Chen, Z. *et al.* Real-time observation of leukocyte-endothelium interactions in tissue-engineered blood vessel. *Lab Chip* **18**, 2047–2054 (2018).
29. Zhang, B., Peticone, C., Murthy, S. K. & Radisic, M. A standalone perfusion platform for drug testing and target validation in micro-vessel networks. *Biomicrofluidics* **7**, (2013).
30. Bischel, Lauren L; Lee, Sang-Hoon; Beebe, D. J. A Practical Method for Patterning Lumens through ECM Hydrogels via Viscous Finger Patterning. *J. Lab Autom.* **17**, 96–103 (2012).
31. Herland, A. *et al.* Distinct contributions of astrocytes and pericytes to neuroinflammation identified in a 3D human blood-brain barrier on a chip. *PLoS One* **11**, 1–21 (2016).
32. Miller, J. S. *et al.* Rapid casting of patterned vascular networks for perfusable engineered three-dimensional tissues. *Nat. Mater.* **11**, 768–774 (2012).
33. Pandolfi, F., Buisson, C. B., Guillemot, D. & Watier, L. One - year hospital readmission for recurrent sepsis : associated risk factors and impact on 1 - year mortality — a French nationwide study. *Crit. Care* 1–12 (2022) doi:10.1186/s13054-022-04212-9.
34. Wang, T. *et al.* Subsequent Infections in Survivors of Sepsis: Epidemiology and Outcomes. *J Intensive Care Med* **29**, 87–95 (2015).
35. Zhong, C., Yang, X., Feng, Y. & Yu, J. Trained Immunity: An Underlying Driver of Inflammatory Atherosclerosis. *Front. Immunol.* **11**, (2020).
36. Moorlag, S. J. C. F. M. *et al.* An integrative genomics approach identifies KDM4 as a modulator of trained immunity. *Eur. J. Immunol.* **52**, 431–446 (2022).
37. Stirling, D. R. *et al.* CellProfiler 4: improvements in speed, utility and usability. *BMC Bioinformatics* **22**, 1–11 (2021).
38. Origin(Pro), Version 2023. OriginLab Corporation, Northampton, MA, USA.
39. Kany, S., Vollrath, J. T. & Relja, B. Cytokines in Inflammatory Disease. *Int. J. Mol. Sci.* **20**, 1–31 (2019).
40. Dinarello, C. A. Overview of the IL-1 family in innate inflammation and acquired immunity. *Immunol Rev* **281**, 8–27 (2018).
41. Van Der Poll, T., Van De Veerdonk, F. L., Scicluna, B. P. & Netea, M. G. The immunopathology of sepsis and potential therapeutic targets. *Nat. Rev. Immunol.* **17**, 407–420 (2017).

Supplementary information

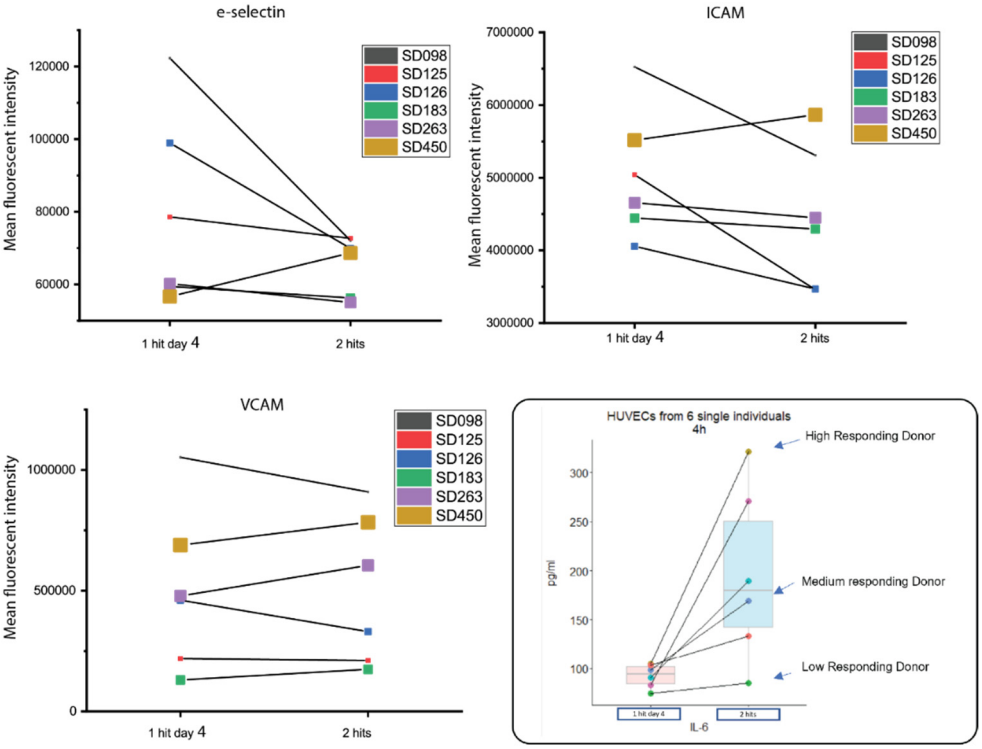

Supplementary figure 3-1: Donor specific responses to TNF-α stimulation. No specific training effect could be observed in expression levels of e-selectin, VCAM-1, and ICAM-1. IL-6 excretion does show an indication of trained immune responses. A distinguishment was made to obtain 3 differently responding donors to use for the monocyte adhesion assay.

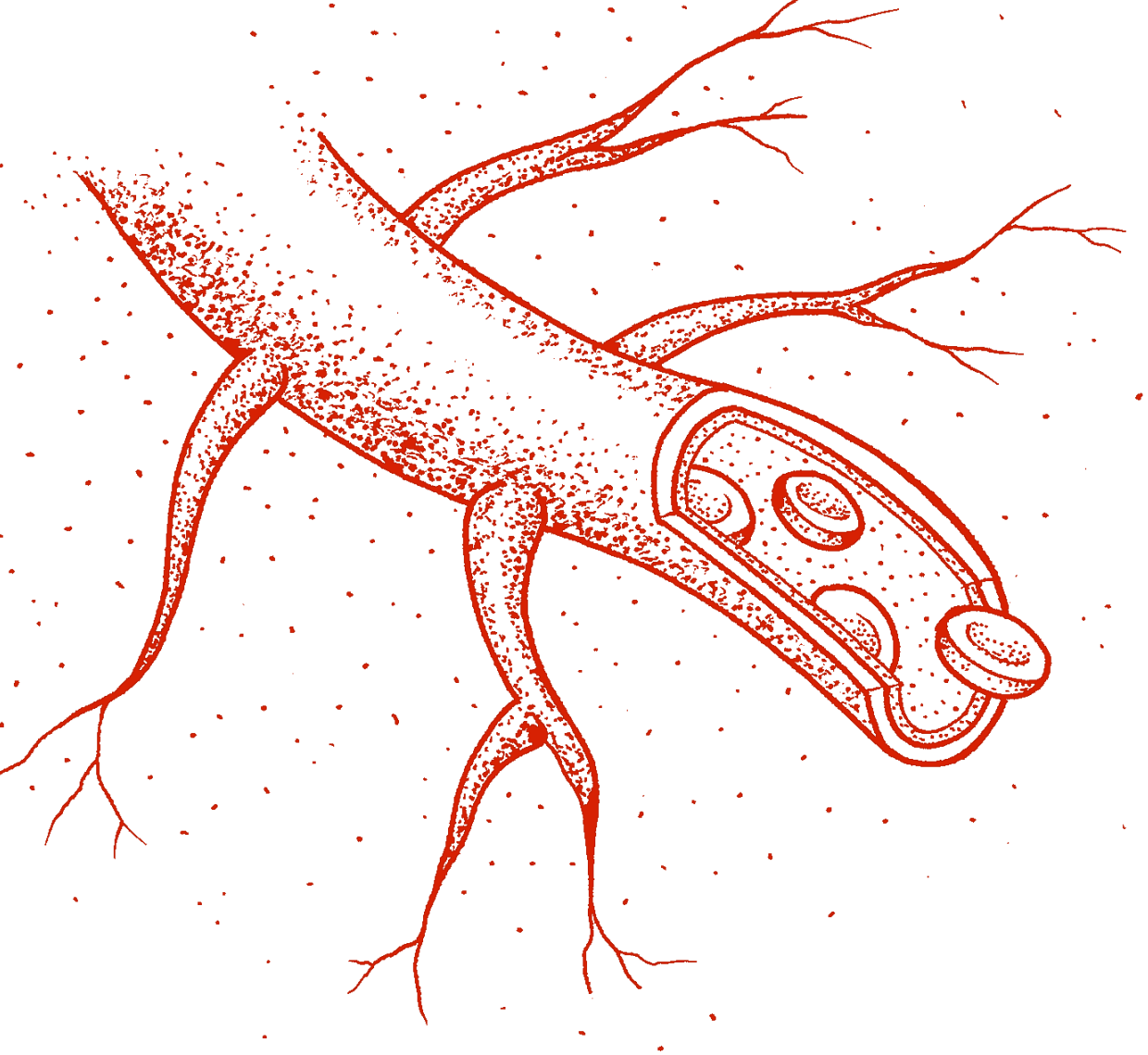

4

Embedded macrophages induce intravascular coagulation in 3D blood vessels-on-chips

H.H.T. Middelkamp
H.J. Weener
T. Gensheimer
K. Vermeul
L.E. de Heus
H.J. Albers
A. van den Berg
A.D. van der Meer

Manuscript submitted

Abstract

Macrophages are innate immune cells that prevent infections and help in wound healing and vascular inflammation. While these cells are natural helper cells, they also contribute to chronic diseases, e.g., by infiltrating the endothelial layer in early atherosclerosis and by promoting vascular inflammation. There is a crosstalk between inflammatory pathways and key players in thrombosis, such as platelets and endothelial cells – a phenomenon known as 'thromboinflammation'. The role of the embedded macrophages in thromboinflammation in the context of vascular disease is incompletely understood. Blood vessels-on-chips, which are microfluidic vascular cell culture models, have been used extensively to study aspects of vascular disease, like permeability, immune cell adhesion and thrombosis. Blood perfusion assays in blood vessel-on-chip models benefit from multiple unique aspects of the models, such as control of microvessel structure and well-defined flow patterns, as well as the ability to perform live imaging. However, due to their simplified nature, blood vessels-on-chip models have not yet been used to capture the complex cellular crosstalk that is important in thromboinflammation. Using induced pluripotent stem cell-derived endothelial cells and polarized THP-1 monocytes, we have developed and systematically set up a three-dimensional blood vessel-on-chip with embedded (lipid-laden) macrophages, which is created using sequential cell seeding in viscous finger patterned collagen hydrogels. We have set up a human whole blood perfusion assay for these three-dimensional blood vessels-on-chip. An increased deposition of fibrin in the blood vessel-on-chip models containing lipid-laden macrophages was observed. We anticipate the future use of this advanced vascular *in vitro* model in drug development for early atherosclerosis or aspects of other vascular diseases.

4.1 Introduction

Vascular diseases are the main cause of death worldwide[1]. An integral part of vascular pathophysiology is vascular inflammation. This inflammation can be induced by pathogens, vascular damage or long-term exposure of healthy blood vessels to (external) inflammatory factors such as cholesterol, toxins, and pro-inflammatory cytokines[2–5]. Vascular inflammation leads to alterations in endothelial cell functionality, including increased expression of endothelial cell markers such as cell adhesion molecules (CAMs) and junctional adhesion molecules (JAMs)[6,7]. This upregulation can in turn lead to the activation and recruitment of innate immune cells from the blood stream. Innate immune cells, such as monocytes and macrophages, have a key role in wound healing, phagocytosis and in resolving vascular inflammation. These cells can be activated by an inflamed endothelial layer and are an integral part in the pathogenesis of many arterial diseases such as atherosclerosis and aneurysms[8]. After activation, monocytes can polarize towards macrophages, promoting their ability to pass through the endothelial barrier and embed underneath the endothelial layer. Macrophages have been proven to interact with endothelial cells when embedded underneath the endothelial layer[8]. These embedded macrophages can affect the endothelial cell layer by excreting either proinflammatory cytokines such as tissue necrosis factor-α (TNF- α) and interleukin-1β (IL-1β) (‘M1’ macrophages) or anti-inflammatory cytokines such as transforming growth factor-β (TGF-β) and interleukin-10 (IL-10) (‘M2’ macrophages)[9].

Thromboinflammation is a process in which innate immune cells such as neutrophils and monocytes, interact with an inflamed or damaged endothelial layer, leading to the activation of platelets and formation of a thrombus[10]. The processes towards thrombus formation are different in arteries compared to veins, which can largely be attributed to the enormous difference in shear rates and flow[11]. In arteries, excreted von Willebrand factor plays a large role in platelet adhesion and accumulation, leading to recruitment of more platelets, neutrophils, and red blood cells, with fibrin threads being formed to stabilize the thrombus. Blood flow through veins can be a factor 100 lower than arterial flow, giving monocytes the opportunity to roll over the endothelial layer and therefore detect inflamed endothelial cells[11,12]. The cell recruitment process in veins therefore differs from arteries, with monocytes instigating platelet recruitment but also being able to polarize and transmigrate through the endothelial barrier and excrete pro- or anti-inflammatory factors. Due

to lower flow rates in veins and the accompanying lower shear rates experienced by endothelial cells, thrombi have a distinct histopathological presentation, typically with a high content of fibrin[13].

A relatively new method to investigate mechanisms of cardiovascular disease, including thrombosis, immune cell recruitment and endothelial inflammation are vessels-on-chips (VoCs). These microphysiological systems (MPS) are designed to recapitulate the microenvironment of blood vessels in terms of geometry, flow, extracellular matrix and cellular composition[14–21]. VoCs typically consist of an actively perfused microfluidic channel or network of channels lined by endothelial cells. They are widely used to investigate disease processes. Multiple VoCs have already been reported to model the endothelial layer and its role in the context of thrombosis by using blood perfusion assays as an end-point measurement[22–31]. Due to limitations in microfabrication, many of these VoC models have square and rectangular cross-sections, which do not mimic the human vessel structure. Advanced fabrication techniques provide the ability to make more physiologically relevant models, for example by using a viscous finger patterned hydrogel as a three-dimensional (3D) lumen to contain the required cell types[32–35]. Such models can also be used to incorporate multiple cell types for studies of disease. For example, incorporation of vascular smooth muscle cells and neurovascular cells such as pericytes and astrocytes has been accomplished in multiple designs[33,36].

To study vascular inflammation in VoC models, a very important factor is the realistic incorporation of immune cells such as monocytes and macrophages. The incorporation of monocytes flowing through the blood vessel has been performed when using monocyte adhesion as an end point measurement[37]. Even though monocyte activation, extravasation and polarization into macrophages is a long process which is hard to mimic in a VoC model, it can be an integral part of the vascular immune response. Vascular inflammation can be either induced or reduced by respectively embedded M1 and M2 macrophages. To have a physiologically relevant model and observe the cell-to-cell crosstalk in the context of vascular inflammation, macrophages should be incorporated directly underneath the endothelial cell layer. The complexity of a model containing human induced pluripotent derived endothelial cells (hiPSC-EC) as well as embedded (lipid-laden) macrophages, which can be kept in culture for longer periods of time and can be perfused with human whole blood has not been explored yet. Such an advanced VoC

model would be a key enabling technology to unravel mechanisms of thromboinflammation, potentially even in a patient-specific manner.

By performing systematic optimization of seeding properties, medium properties, and a human whole blood perfusion assay, we can now present the first blood-perfusable 3D VoC system with incorporated (lipid-laden) macrophages. We use this new 3D VoC to demonstrate that key aspects of thromboinflammation can be captured in MPS models.

4.2 Materials and methods

4.2.1 Microfluidic chip fabrication

The microfluidic chip consists of 6 channels which are one centimeter in length and 500 x 500 µm in width and height (figure 1a). The chip was fabricated by conventional polydimethylsiloxane (PDMS)-based soft lithography using a poly(methyl methacrylate) (PMMA, Arkema innovative chemistry) mould. The mould was produced by micromilling (Sherline, model 5410) based on designs in SolidWorks (Dassault Systèmes, France). PDMS (10:1 base:crosslinker ratio, Sylgard 184) was added to the PMMA mould and was left to cure overnight at 65 °C after which it was removed from the mould. 1 mm inlet and outlet holes were created using biopsy punchers (Robbins Instruments). PDMS was spin coated (SPS Spin150) on a glass microscope slide and PDMS was left to cure overnight at 65 °C. The surfaces of both the microfluidic device and the microscope slide were activated by exposing them to air plasma (50 W) for 40 s (Cute, Femto Science, South Korea), after which the microfluidic chip was bonded to the microscope slide. The activated chip was then used for viscous finger patterning.

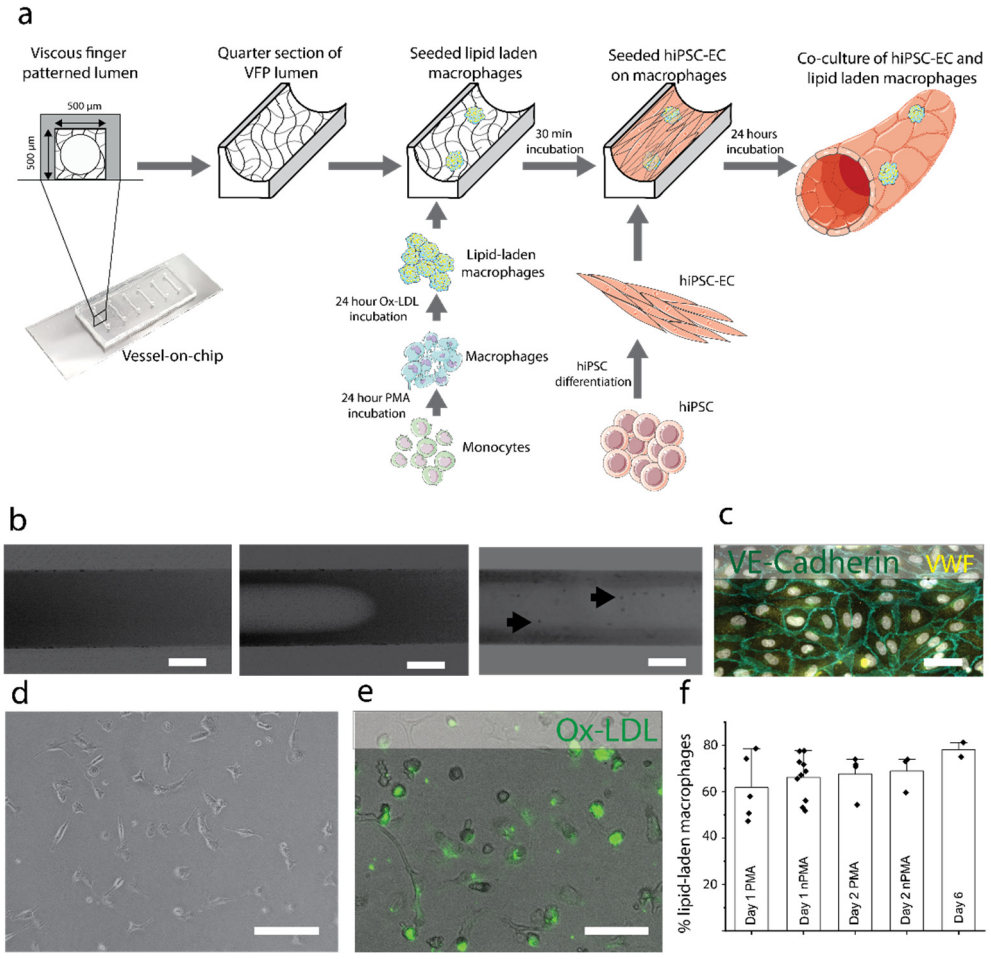

Fig 4-1: Protocol for establishing a complex 3D VoC, including characterization of its key components. a: Schematic overview of the protocol. 3D lumens are created in squared 500 x 500 µm collagen-filled channels. These channels are subsequently seeded with (lipid-laden) macrophages and hiPSC-EC; creating a 3D hiPSC-EC derived perfusable 3D blood vessel-on-chip with embedded macrophages. b: Viscous finger patterning is used to create a 3D lumen inside a channel filled with collagen type-1. Lumens can be perfused with microbeads (arrows). Scale bars represent 250 µm. c: Endothelial cell markers such as von Willebrand factor and vascular endothelial-cadherin (VE-cadherin) are present in hiPSC-derived endothelial cells. Scale bar represents 20 µm d: Polarized THP-1 macrophages. Scale bar represents 100 µm. e: Polarized THP-1 macrophages can be loaded with Ox-LDL (green). Scale bar represents 100 µm. f: Percentage of polarized, lipid-laden macrophages as analyzed by fluorescence microscopy at multiple timepoints ('Day 1', 'Day 2', 'Day 6') and in the continued presence ('PMA') or absence ('nPMA') of the polarizing phorbol myristate acetate (PMA). Day 6 represents a combination of 'PMA' and 'nPMA'.

4.2.2 Viscous finger patterning

The plasma-activated chips were coated with poly-dopamine (Merck) by adding 2 mg/ml poly-dopamine in 10 mM TrisHCl (pH 8.5) to the channels. Chips were incubated at room temperature for an hour and quickly rinsed 3 times using sterile Mili-Q water and dried. A 5 mg/ml rat tail collagen type-1 (Corning™) solution was prepared on ice, by diluting the collagen with 1/10th of the final volume of 10× PBS, supplemented with dH_2O and NaOH to obtain a pH of 6.5-7.5. The mixture was vortexed and spun down and used within 15 minutes after mixing. 3D lumens were created in the microfluidic channels using viscous finger patterning[32,33,38]. A 7 mm high pipette tip was added to the outlet of the channels. 10 µl of collagen solution was pipetted in the inlet, until a meniscus formed on the outlet tip. A droplet of 2.2 µl of ice-cold PBS solution was then pipetted onto the collagen meniscus, forming a finger-like structure inside the hydrogel (figure 1b). Chips were incubated at 37 °C and 5% CO_2 for one hour, after which pipette tips were removed and new pipette tips were added to the inlet and outlet. Further steps were performed using gel loader tips inside the pipette tips to not disturb the collagen lumens. 100 µl Endothelial Cell Growth medium 2 (EGM-2, PromoCell Inc.) was added to the channels and chips were incubated for 24 hours at 37 °C and 5% CO_2 to equilibrate, before cell seeding.

4.2.3 Cell culturing of hiPSC-derived endothelial cells and THP-1 monocytes

hiPSC-EC

Human induced pluripotent stem cell-derived endothelial cells were derived from hiPSC an adapted previously described protocol[39], by first performing a differentiation of the monolayer of hiPSC by inducing mesoderm using B(P)EL supplemented with CHIR (8 µM, Axon Medchem), followed by vascular specification using B(P)EL supplemented with VEGF (50 µg/ml, Miltenyi) and SB431542 (10 µM, R&D systems). Endothelial cells were isolated using CD31+ Dynabeads (Thermofisher). hiPSC-EC were then cultured in pre-coated collagen culture flasks (Greiner bio one) at 37 °C and 5% CO_2 using Endothelial cell serum free medium (EC-SFM (Gibco)), supplemented with 1% platelet-poor plasma-derived serum (Biomedical Technologies), 30 ng/ml VEGF (R&D systems) and 20 ng/ml bFGF (Miltenyi Biotec)[39]. To confirm the successful differentiation toward endothelial cells, the cells were stained for EC markers von Willebrand factor and VE-Cadherin (figure 1c).

Monocytes

THP-1 monocytes (ECACC) were cultured in RPMI 1640 + GlutaMAX medium (Gibco) supplemented with 1% penicillin/streptomycin (Gibco) and 10% FBS (Thermofisher) at 37 °C and 5% CO_2. Cells were used up to passage 25.

Lipid-laden macrophages

To polarize monocytes towards macrophages, cells were seeded in a 6-well plate at $4 \cdot 10^5$ cells/well and cultured overnight in serum-free RPMI 1640 medium supplemented with 50 ng/ml phorbol myristate acetate (PMA, Merck). Fresh serum-free medium supplemented with 50 ng/ml PMA and 50 µg/ml Oxidized-LDL (DiI-OxLDL from human plasma, Invitrogen) was added after 24 hours and cells were incubated for 24 hours.

4.2.4 Cell seeding in microfluidic chips

After overnight incubation of chips, cells were seeded sequentially, starting with the (lipid-laden) macrophages. Macrophages were removed from the well plate using a cell scraper and centrifuged for 5 minutes at 100 ×*g*. Cells were counted using a cell counter (Luna™ automated cell counter (brightfield cell counter)) and seeded in the channel at $1 \cdot 10^5$ cells/ml. To make sure cells attached to the top of the channel, the microfluidic chips were incubated invertedly for 15 minutes at 37 °C and 5% CO_2 after cells were added to the channel, after which chips were placed upright and incubated at 37 °C and 5% CO_2 for another 15 minutes.

HiPSC-EC were seeded at passage number 3. To seed the hiPSC-EC, cells were removed from the cell culture flask, by incubating cells with 3 ml TrypLE (Gibco) for 3 minutes at 37 °C and 5% CO_2. TrypLE was inactivated by adding 7 ml of cell culture medium to the flask. Cells were centrifuged for 5 minutes at 300 ×*g* and counted. Cells were seeded at $5 \cdot 10^6$ cells/ml. To assure the cell attachment to both the top and the bottom of the channel, the microfluidic chips were first inverted after cells were added to the channel for at least half an hour, after which the procedure was repeated, and microfluidic chips were incubated upright at 37 °C and 5% CO_2 for at least 30 minutes. 150 µl EGM-2 was added to the microfluidic channels. Microfluidic chips were placed on a rocking table (10° angle, 30 sec interval; BenchBlotter™ 2D platform rocker) inside the incubator for 24 hours.

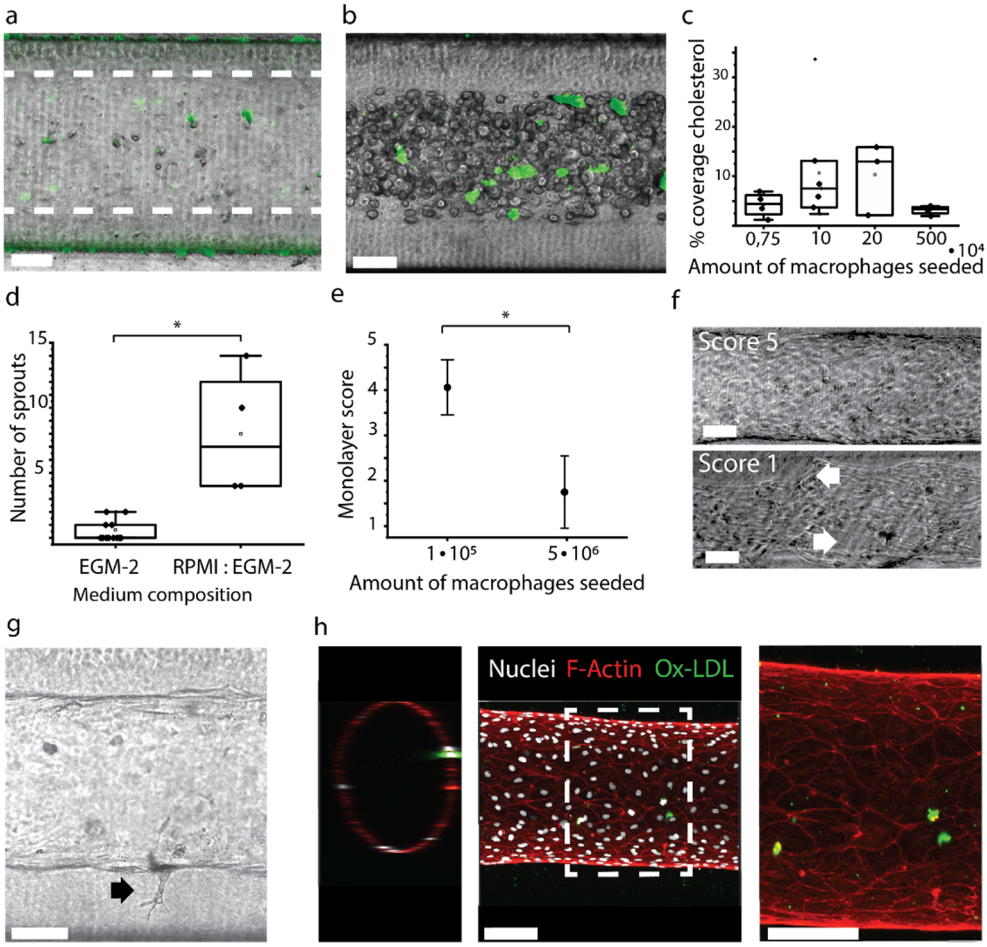

Fig 4-2: Embedded lipid-laden macrophages in 3D blood vessel-on-chip. a: Collagen lumen (dashed lines) loaded with lipid-laden macrophages (green Dil-OxLDL) seeded at $1{\cdot}10^5$ cells/ml. b: After lipid-laden macrophages were incubated for 30 minutes, hiPSC-EC were seeded to the channel at $5{\cdot}10^6$ cells/ml. Lipid laden-macrophages are visibly embedded underneath the hiPSC-EC suspension (green Dil-OxLDL). c: Percentage of the vessel area covered with green, fluorescent signal when seeding macrophages at multiple concentrations; d: Number of sprouts observed in three representative figures of a vessel lumen, in conditions with only endothelial medium ('EGM-2') or a mixture of endothelial and macrophage medium ('RPMI:EGM-2'). e: Effect of seeding densities of macrophages on monolayer quality ('Monolayer score') of hiPSC-EC after 24 hours of incubation, with a bad monolayer scored as a 1 and a very good monolayer as 5. f: Representative example of a high-quality ('Score 5') and low-quality ('Score 1') monolayer channel. The blood vessel scoring 5 has a quiescent monolayer with no wholes, whereas the blood vessel scoring 1 had multiple wholes (arrows) and therefore no monolayer. g: Example of endothelial cell sprouting. h: 3D confocal images show a monolayer of hiPSC-EC in the channel after 5 days of co-culture. Ox-LDL is still visibly embedded in the endothelial layer after 5 days of incubation (Nuclei: white; Actin: Red; Ox-LDL: Green). All scale bars represent 100 µm.

4.2.5 Medium optimization in microfluidic chips

Medium optimization was performed for the co-culture of hiPSC-EC and macrophages. Cells were incubated overnight with either EGM-2 or a combination of EGM-2 and RPMI 1640. After 24 hours 4x magnification brightfield images were obtained. Two separated operators individually counted the number of sprouts per channel.

4.2.6 Blood perfusion assay

Blood was provided by the Experimental Centre for Technical Medicine (ECTM, Techmed Centre, University of Twente) and was used within 4 hours of blood draw. This research did not fall in the scope of the Dutch Medical Research Involving Human Subjects Act. In agreement with the Declaration of Helsinki, informed consent was obtained from all volunteers. Furthermore, the blood collection procedure was approved by the local medical research ethics committee (METC Twente). Whole blood was collected in vacuvette tubes, containing 3.2 % citrate. The first tube was always discarded. Platelets and fibrin were stained with respectively CD41-FITC (40 µl/ml; Beckmann-Coulter) and conjugated fibrinogen (10 µg/ml; Fibrinogen from human plasma, Invitrogen) for 10 minutes. Immediately before perfusion, blood was recalcified using a recalcification buffer containing HEPES; 63.2 mM $CaCl_2$ and 31.6 mM $MgCl_2$.

The pipette tip at the outlet was removed and replaced by a bent 14-gauge blunt needle to which tubing (Tygon) was connected, which in turn was connected to a syringe on a syringe pump (Harvard PHD Ultra). Blood was pulled through the channel at 6 µl/min for 20 minutes. After perfusion, channels were flushed manually with EGM-2 and fixated with 4% formaldehyde for 15 minutes and subsequently washed 3 times with PBS and imaged for data analysis.

4.2.7 Staining and imaging

After fixation, cells were permeabilized with 0.1% Triton X-100 solution for 10 min at room temperature. Cells were incubated with Nucblue (nuclei, Thermofisher) and actinRed (Thermofisher) or actinGreen (Thermofisher).

Immunocytochemistry imaging data was collected using a Zeiss LSM 510 confocal microscope at 10× magnification. Images for data analysis after blood perfusion were obtained using an EVOS M5000 imaging system (Thermo Fisher) at 4× magnification.

4.2.8 Data analysis

To calculate the fibrin and Ox-LDL area coverage percentage, the thresholding function in FIJI image analysis software[40] was used. To avoid human error, two operators individually performed a blind assessment of the coverages and values were then compared and averaged. A paired sample t-test was performed for both the area coverage and clot size calculations.

The scoring of endothelial cell layer was performed by two operators, who individually observed endothelial cell layers and scored them from 1 (very bad) to 5 (very good). While scoring the endothelial layer, operators assessed cells morphology, monolayer formation, and holes.

4.2.9 Generation of figures

3D images were generated using Imaris software (Oxford Instruments). Parts of the figure were drawn by using pictures from Servier Medical Art. Servier Medical Art by Servier is licensed under a Creative Commons Attribution 3.0 Unported License (https://creativecommons.org/licenses/by/3.0/).

4.3 Results and discussion

4.3.1 3D blood vessels-on-chip

To achieve a VoC model with embedded macrophages, we followed the scheme in figure 1a. 3D lumens were created in a collagen I hydrogel in a PDMS chip. These chips were acclimated in an incubator overnight before cell seeding. (Lipid-laden) macrophages were seeded, followed by hiPSC-EC. After 24 hours of incubation on a rocking table, a functional 3D VoC with embedded macrophages was achieved. To attain this model, multiple optimization steps were performed.

Firstly, circular lumen-shaped channels in a square PDMS chip by using viscous finger patterning in a collagen 1 hydrogel had to be created (figure 1b). Viscous finger patterning of lumens in collagen is a difficult process due to manual handling, but by standardizing the protocol, high success rates can be achieved[32]. The most important parameters to optimize were the PBS droplet size and NaOH concentration to effectively drive flow upon viscous finger patterning and to promote proper gelation after patterning, respectively.

We systematically incorporated different cell types in our 3D blood vessel-on-chip. THP-1 monocytes were polarized, and loaded with Ox-LDL (figure 1d,e). The lipid-laden macrophages remained stable for up to 6 days (figure 1f). No difference in the

number of lipid-laden macrophages was observed in well-plate experiment, when loading the cells with or without the presence of PMA. After seeding the cells at $1{\cdot}10^5$ cells/ml we observed dispersed cells throughout the channel (figure 2a,b). Macrophages polarized from THP-1 monocytes using PMA are widely used in research, but due to differences in protocols it can be challenging to arrive at a single definitive protocol. For example, PMA incubation times can vary between 3-72 hours, giving the cells a completely different stimulation time[41]. We have stimulated the THP-1 cells for 24 hours and, without a resting period afterwards, loaded them immediately by incubating with Ox-LDL and PMA for 24 hours, before seeding them in the lumen.

Medium optimization for the co-culture of hiPSC-EC and macrophages was performed by combining different ratios of EGM-2 and RPMI 1640. Figure 2d shows the difference in endothelial layers when cultured in different types of medium. It was observed that when culturing cells in anything other than EGM-2, the endothelial cells were more actively migrating and started sprouting into the hydrogel (figure 2d,g). A significantly higher amount of sprouts was observed for cells cultured in 1:1 (RPMI 1640 : EGM-2) compared to merely EGM-2 ($p < 0.05$, figure 2d). Therefore, it was determined that for long-term culture of the combination of macrophages and hiPSC-EC in our VoCs, individual EGM-2 was most effective. EGM-2 is a widely used endothelial cell growth medium, optimized for primary endothelial cells and has been widely used in other projects as it contains antibiotics recommended for MPS culture[42–45].

Different macrophage seeding concentrations were tested, ranging from $7.4{\cdot}10^3$ to $5{\cdot}10^6$ cells/ml. Interestingly, we observed no difference between these conditions in terms of LDL coverage inside the VoC after 24 hours of co-culture with hiPSC-EC (figure 2c). However, VoCs seeded with high concentrations of macrophages were not able to survive for more than 24 hours. This suggests a negative effect of an abundance of macrophages on the endothelial layer. Scoring the endothelial layers of VoCs containing $1{\cdot}10^5$ macrophages/ml versus $5{\cdot}10^6$ macrophages/ml showed a significantly better endothelial cell layer at lower macrophage seeding densities after 24 hours ($p < 0.05$, figure 2f). Seeding the macrophages at a lower density ($7.4{\cdot}10^3$-$2{\cdot}10^5$) and subsequent seeding of hiPSC-EC at $5{\cdot}10^6$ cells/ml resulted in a full monolayer, covering the whole microfluidic channel (figure 2h) and enabled the VoCs to be cultured for at least 5 days. Actin staining of the channels show a quiescent monolayer of cells. We show that after 5 days, channels previously seeded

with lipid-laden macrophages still contain these lipid-laden macrophages in the channel (figure 2h).

The VoC was kept on a rocking table set to a 10° angle with a 3 second interval, giving it continuous bidirectional flow, which was calculated to yield a maximum shear rate of 140 s^{-1}. This bidirectional flow enabled the cells to experience some shear stress, and we achieved culture times of up to 5 days. However, bidirectional flow is not physiologically accurate in blood vessels and preferably cells experience unidirectional flow at relevant shear stresses[46]. Recent developments show the possibility of maintaining unidirectional flow in similar blood vessel-on-chip models at relevant shear stress, which is recommended for future research[46–48].

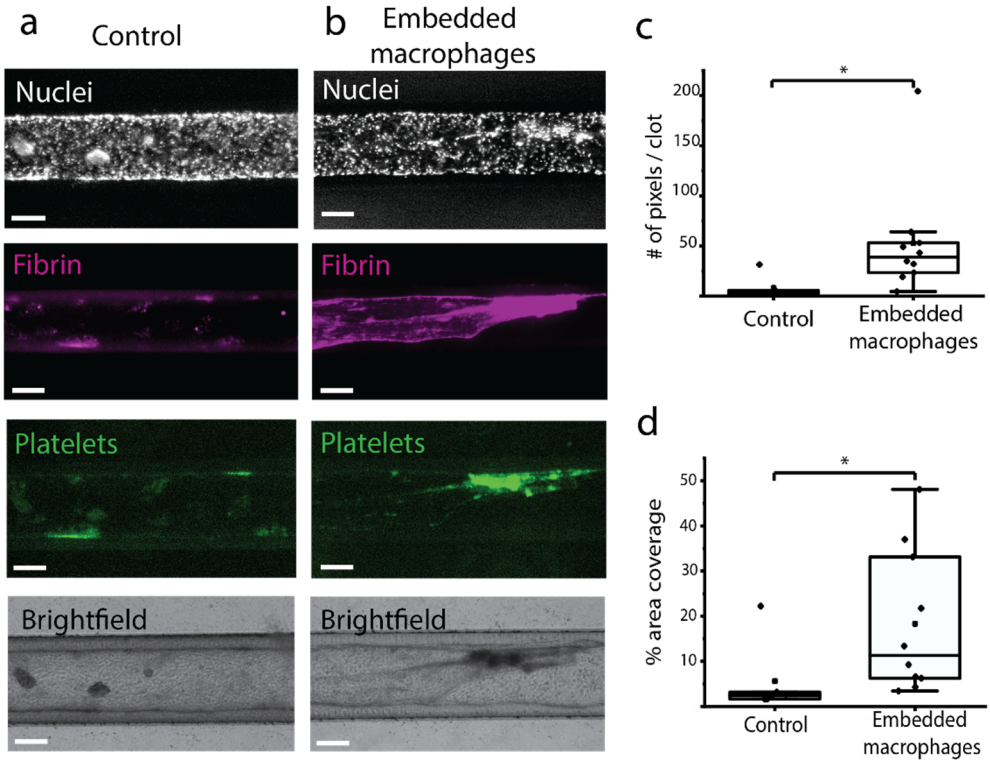

Fig 4-3: Blood perfusion assay results in a higher deposition of fibrin in the channels containing embedded macrophages; a: Blood vessel channel with a monoculture of hiPSC-EC ('Control'). b: Blood vessel channel with co-cultured macrophages with a high % area coverage of fibrin; c-d: fibrin clot size and % area of fibrin coverage in monoculture ('Control') conditions and co-culture ('Embedded macrophages) conditions. All scale bars represent 150 µm.

4.3.2 Blood perfusion assay

We successfully have set up a blood perfusion assay for the 3D blood vessels-on-chip. Blood was perfused at 6 µl/min, representing a shear rate of approximately 35 s^{-1}, which is 3 times higher than the lowest shear rate in the human veins[12]. We observed a different deposition of fibrin in the blood vessels containing embedded macrophages, compared to the control samples without embedded macrophages (figure 3a,b). Analysis of the area covered by deposited fibrin showed a significant difference between the two groups ($p < 0.05$, figure 3d). Moreover, average analysis of clot size showed a significantly bigger fibrin clot size in the blood vessels containing embedded macrophages ($p < 0.05$, figure 3c), indicating the formation of bigger fibrin networks in this vascular inflammation model. The fibrin content in the clots is higher than what is typically seen in blood perfusion assays in vessels-on-chips with activated endothelial monocultures at high shear rates (750-1000 s^{-1})[49]. This difference may reflect a more vein-like response in our model, which is expected with the flow rates used[13].

Interestingly, these results suggest the immediate negative effect of embedded macrophages on the endothelial cell layer, even without any additional external stimulation. THP-1 polarization with PMA leads to M0 macrophages, leaving them free to differentiate into either M1 or M2. The phenotype of the embedded macrophages was not determined in the current study, but future monitoring and control over this aspect could provide further insight in the model and its predictive value in disease modeling. Embedding of M1 or M2 macrophages or lipid-laden macrophages can possibly lead to a different endothelial response[50,51]. Future studies could then focus on investigating the different effects of different types of (lipid-laden) macrophages on the endothelial layer and thromboinflammatory processes.

During the blood perfusion assay, platelet aggregation was observed. However, after the chips were fixated, washed, and prepared for analysis by fluorescence microscopy, no significant difference in platelet aggregation was observed between control conditions and conditions of co-culture. Supplementary figure 1 shows the difference of a channel before and after preparing it for microscopic analysis. The pressure of washing clearly reduces the big platelet aggregates. To study the effect of platelet aggregation, live imaging during the blood perfusion assay would be recommended.

To obtain arterial responses and shear rates, the flow rate should be increased to approximately 160 µl/min. Instantaneous high flow rate on the channels resulted in loss of cells and therefore monolayer. Optimization of the system is required if arterial rates are desired. Using unidirectional continuous flow during cell culture overnight with increasing flow rates, might assist the cells to get adjusted to the constant shear.

4.4 Conclusion

The aim of this project was to set up a 3D vascular model containing embedded macrophages in an hiPSC-EC layer. For the first time, we have systematically set up and presented the protocol for a hiPSC-EC-loaded blood vessel-on-chip model with embedded macrophages arranged underneath the hiPSC-EC layer to study the effect of macrophages on the endothelial layer. We have successfully set up a blood perfusion assay for this vessel-on-chip model, which contains embedded (lipid-laden) macrophages and have studied the effect of these macrophages on the endothelial cell layer. Our results demonstrate a significantly higher area coverage of fibrin in the channels containing embedded macrophages, suggesting a proinflammatory effect of these macrophages and therefore endothelial response. In future studies, this blood vessel-on-chip will be used as a model to study mechanisms of vascular disease, thereby contributing to (personalized) drug development.

Acknowledgements

This work was supported by the Netherlands Organ-on-Chip Initiative, an NWO Gravitation project (024.003.001) funded by the Ministry of Education, Culture and Science of the government of the Netherlands. This project has received funding from the European Union's Horizon 2020 research and innovation program under the Marie Skłodowska-Curie grant agreement No 812954. This work was supported by the Impulse grant 2018 awarded to the PHAEDRA-IMPACT consortium (Grant number: CVON-2018-29 PHAEDRA-IMPACT), which includes collective funding by the Dutch Heart Foundation, Dutch Federation of University Medical Centers, The Netherlands Organization for Health Research and Development, and the Royal Netherlands Academy of Sciences. Mees de Graaf is kindly acknowledged for his help in establishing protocols for viscous finger patterning.

References

1. World Health Organization. Leading causes of death worldwide in 2016 (in millions). Statista. https://www.statista.com/statistics/288839/leading-causes-of-death-worldwide/ (2019).
2. Jia, G., Aroor, A. R., Jia, C. & Sowers, J. R. Endothelial cell senescence in aging-related vascular dysfunction. *Biochim. Biophys. Acta - Mol. Basis Dis.* 0–1 (2018) doi:10.1016/j.bbadis.2018.08.008.
3. Grootaert, M. O. J. *et al.* Vascular smooth muscle cell death, autophagy and senescence in atherosclerosis. *Cardiovasc. Res.* **114**, 622–634 (2018).
4. Phillipson, M. & Kubes, P. The neutrophil in vascular inflammation. *Nat. Med.* **17**, 1381–1390 (2011).
5. Teague, H. L. *et al.* Unraveling Vascular Inflammation: From Immunology to Imaging. *J. Am. Coll. Cardiol.* **70**, 1403–1412 (2017).
6. Weber, C., Fraemohs, L. & Dejana, E. The role of junctional adhesion molecules in vascular inflammation. *Nat. Rev. Immunol.* **7**, 467–477 (2007).
7. Krieglstein, C. F. & Granger, D. N. Adhesion molecules and their role in vascular disease. *Am. J. Hypertens.* **14**, 44–54 (2001).
8. Shirai, T., Hilhorst, M., Harrison, D. G. & Weyand, Cornelia, M. Macrophages in Vascular Inflammation – From Atherosclerosis to Vasculitis. *Autoimmunity* **48**, 139–151 (2015).
9. Chistiakov, D. A., Melnichenko, A. A., Myasoedova, V. A., Grechko, A. V. & Orekhov, A. N. Mechanisms of foam cell formation in atherosclerosis. *J. Mol. Med.* **95**, 1153–1165 (2017).
10. Rayes, J., Bourne, J. H., Brill, A. & Watson, S. P. The dual role of platelet-innate immune cell interactions in thrombo-inflammation. *Res. Pract. Thromb. Haemost.* **4**, 23–35 (2020).
11. Li, J., Han, X., Knauss, E. A., Woulfe, D. S. & Nieman, M. T. *GPCRs in thromboinflammation and hemostasis*. *GPCRs: Structure, Function, and Drug Discovery* (Elsevier Inc., 2019). doi:10.1016/B978-0-12-816228-6.00019-2.
12. Sakariassen, K. S., Orning, L. & Turitto, V. T. The impact of blood shear rate on arterial thrombus formation. *Futur. Sci. OA* **1**, (2015).
13. Chandrashekar, A., Singh, G., Garry, J., Sikalas, N. & Labropoulos, N. Mechanical and Biochemical Role of Fibrin Within a Venous Thrombus. *Eur. J. Vasc. Endovasc. Surg.* **55**, 417–424 (2018).
14. Paloschi, V. *et al.* Organ-on-a-chip technology : a novel approach to investigate cardiovascular diseases . *Cardiovasc. Res.* 1–13 (2021) doi:10.1093/cvr/cvab088.
15. Song, H. H. G., Rumma, R. T., Ozaki, C. K., Edelman, E. R. & Chen, C. S. Vascular Tissue Engineering: Progress, Challenges, and Clinical Promise. *Cell Stem Cell* **22**, 340–354 (2018).
16. Ko, J., Park, D., Lee, S., Gumuscu, B. & Jeon, N. L. Engineering Organ-on-a-Chip to Accelerate Translational Research. *Micromachines* **13**, (2022).
17. Cable, J. *et al.* Engineering multicellular living systems—a Keystone Symposia report. *Ann. N. Y. Acad. Sci.* **1518**, 183–195 (2022).
18. Ko, E. & Kamm, R. D. Neurovascular models for organ-on-a-chips. *Vitr. Model.* **1**, 125–127 (2022).
19. Myers, D. R. & Lam, W. A. Vascularized Microfluidics and Their Untapped Potential for Discovery in Diseases of the Microvasculature. *Annu. Rev. Biomed. Eng.* **23**, 407–432 (2021).
20. Pandian, N. K. R., Mannino, R. G., Lam, W. A. & Jain, A. Thrombosis-on-a-chip: Prospective impact of microphysiological models of vascular thrombosis. *Curr. Opin. Biomed. Eng.* **5**, 29–34 (2018).
21. Branchford, B. R., Ng, C. J., Neeves, K. B. & Di Paola, J. Microfluidic technology as an emerging clinical tool to evaluate thrombosis and hemostasis. *Thromb. Res.* **136**, 13–19 (2015).
22. Albers, H. J., Passier, R., van den Berg, A. & van der Meer, A. D. Automated analysis of platelet aggregation on cultured endothelium in a microfluidic chip perfused with human whole blood. *Micromachines* **10**, (2019).

23. Westein, E. *et al.* Atherosclerotic geometries exacerbate pathological thrombus formation poststenosis in a von Willebrand factor-dependent manner. *Proc. Natl. Acad. Sci.* **110**, 1357–1362 (2013).
24. Costa, P. F. *et al.* Mimicking arterial thrombosis in a 3D-printed microfluidic: In vitro vascular model based on computed tomography angiography data. *Lab Chip* (2017) doi:10.1039/c7lc00202e.
25. Barrile, R. *et al.* Organ-on-Chip Recapitulates Thrombosis Induced by an anti-CD154 Monoclonal Antibody: Translational Potential of Advanced Microengineered Systems. *Clin. Pharmacol. Ther.* **104**, 1240–1248 (2018).
26. van Dijk, C. G. M. *et al.* A new microfluidic model that allows monitoring of complex vascular structures and cell interactions in a 3D biological matrix. *Lab Chip* **20**, 1827–1844 (2020).
27. Tsai, M. *et al.* In vitro modeling of the microvascular occlusion and thrombosis that occur in hematologic diseases using microfluidic technology. *J. Clin. Invest.* **122**, 408–418 (2012).
28. Mannino, R. G. *et al.* Do-it-yourself in vitro vasculature that recapitulates in vivo geometries for investigating endothelial-blood cell interactions. *Sci. Rep.* **5**, 1–12 (2015).
29. Hasan, A., Paul, A., Memic, A. & Khademhosseini, A. A multilayered microfluidic blood vessel-like structure. *Biomed. Microdevices* **17**, 1–13 (2015).
30. Jia, L. *et al.* Microfluidic Fabrication of Biomimetic Helical Hydrogel Microfibers for Blood-Vessel-on-a-Chip Applications. **1900435**, 1–10 (2019).
31. Zheng, Y. *et al.* In vitro microvessels for the study of angiogenesis and thrombosis. *Proc. Natl. Acad. Sci. U. S. A.* **109**, 9342–7 (2012).
32. de Graaf, M. N. S. *et al.* Scalable microphysiological system to model three-dimensional blood vessels. *APL Bioeng.* **3**, 026105 (2019).
33. Herland, A. *et al.* Distinct contributions of astrocytes and pericytes to neuroinflammation identified in a 3D human blood-brain barrier on a chip. *PLoS One* **11**, 1–21 (2016).
34. Bischel, L. L., Lee, S. H. & Beebe, D. J. A Practical method for patterning lumens through ECM hydrogels via viscous finger patterning. *J. Lab. Autom.* **17**, 96–103 (2012).
35. Miller, J. S. *et al.* Rapid casting of patterned vascular networks for perfusable engineered three-dimensional tissues. *Nat. Mater.* **11**, 768–774 (2012).
36. Saili, K. S., Zurlinden, T. J. & Knudsen, T. B. *Modeling the Neurovascular Unit In Vitro and In Silico*. *Handbook of Developmental Neurotoxicology* (Elsevier Inc., 2018). doi:10.1016/B978-0-12-809405-1/00011-0.
37. Halaidych, O. V., van den Hil, F., Mummery, C. L. & Orlova, V. V. Microfluidic assay for the assessment of leukocyte adhesion to human induced pluripotent stem cell-derived endothelial cells (HiPSC-ECs). *J. Vis. Exp.* **2018**, 1–8 (2018).
38. Bischel, Lauren L; Lee, Sang-Hoon; Beebe, D. J. A Practical Method for Patterning Lumens through ECM Hydrogels via Viscous Finger Patterning. *J. Lab Autom.* **17**, 96–103 (2012).
39. Orlova, V. V *et al.* Generation, expansion and functional analysis of endothelial cells and pericytes derived from human pluripotent stem cells. *Nat. Protoc.* **9**, 1514–31 (2014).
40. Schindelin, J. *et al.* Fiji: An open-source platform for biological-image analysis. *Nat. Methods* **9**, 676–682 (2012).
41. Lund, M. E., To, J., O'Brien, B. A. & Donnelly, S. The choice of phorbol 12-myristate 13-acetate differentiation protocol influences the response of THP-1 macrophages to a pro-inflammatory stimulus. *J. Immunol. Methods* **430**, 64–70 (2016).
42. Gu, M. *et al.* Patient-Specific iPSC-Derived Endothelial Cells Uncover Pathways that Protect against Pulmonary Hypertension in BMPR2 Mutation Carriers. *Cell Stem Cell* **20**, 490-504.e5 (2017).
43. Olmer, R. *et al.* Differentiation of Human Pluripotent Stem Cells into Functional Endothelial Cells in Scalable Suspension Culture. *Stem Cell Reports* **10**, 1657–1672 (2018).
44. Zhou, D. *et al.* Patient-specific iPSC-derived endothelial cells reveal aberrant p38 MAPK signaling in atypical hemolytic uremic syndrome. *Stem Cell Reports* **16**, 2305–2319 (2021).

45. Bezenah, J. R., Kong, Y. P. & Putnam, A. J. Evaluating the potential of endothelial cells derived from human induced pluripotent stem cells to form microvascular networks in 3D cultures. *Sci. Rep.* **8**, 1–14 (2018).
46. Wang, Y. I. & Shuler, M. L. UniChip enables long-term recirculating unidirectional perfusion with gravity-driven flow for microphysiological systems. *Lab Chip* **18**, 2563–2574 (2018).
47. de Graaf, M. N. S., Vivas, A., van der Meer, A. D., Mummery, C. L. & Orlova, V. V. Pressure-Driven Perfusion System to Control, Multiplex and Recirculate Cell Culture Medium for Organs-on-Chips. *Micromachines* **13**, (2022).
48. de Graaf, M. N. S. *et al.* Multiplexed fluidic circuit board for controlled perfusion of 3D blood vessels-on-a-chip. *Lab Chip* **23**, 168–181 (2022).
49. Jain, A. *et al.* Assessment of whole blood thrombosis in a microfluidic device lined by fixed human endothelium. *Biomed. Microdevices* **18**, 1–7 (2016).
50. Binnemars-Postma, K. A., Ten Hoopen, H. W., Storm, G. & Prakash, J. Differential uptake of nanoparticles by human M1 and M2 polarized macrophages: Protein corona as a critical determinant. *Nanomedicine* **11**, 2889–2902 (2016).
51. Kim, K. *et al.* Transcriptome analysis reveals nonfoamy rather than foamy plaque macrophages are proinflammatory in atherosclerotic murine models. *Circ. Res.* **123**, 1127–1142 (2018).

Supplementary information:

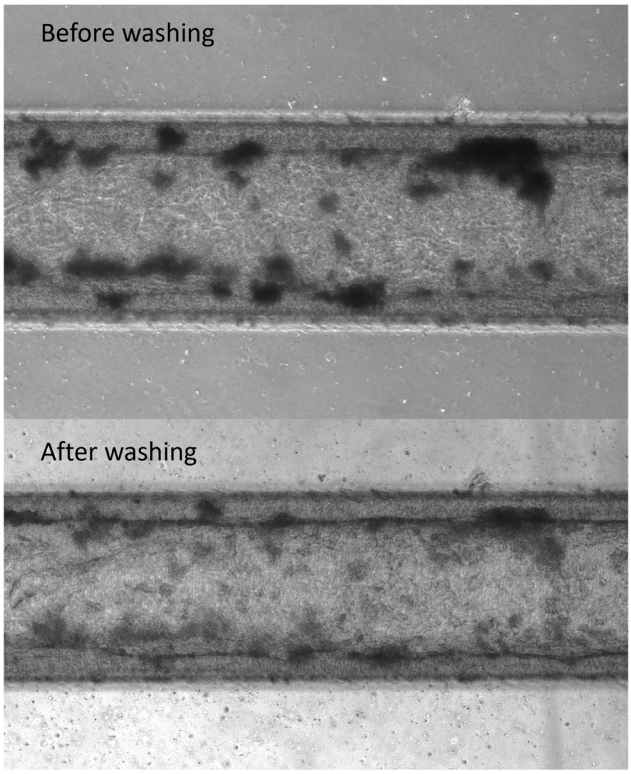

Supplementary figure 4-1: Washing the channel for fixation and staining, puts high amounts of pressure on the channels, therefore flushing big clots out of the channel.

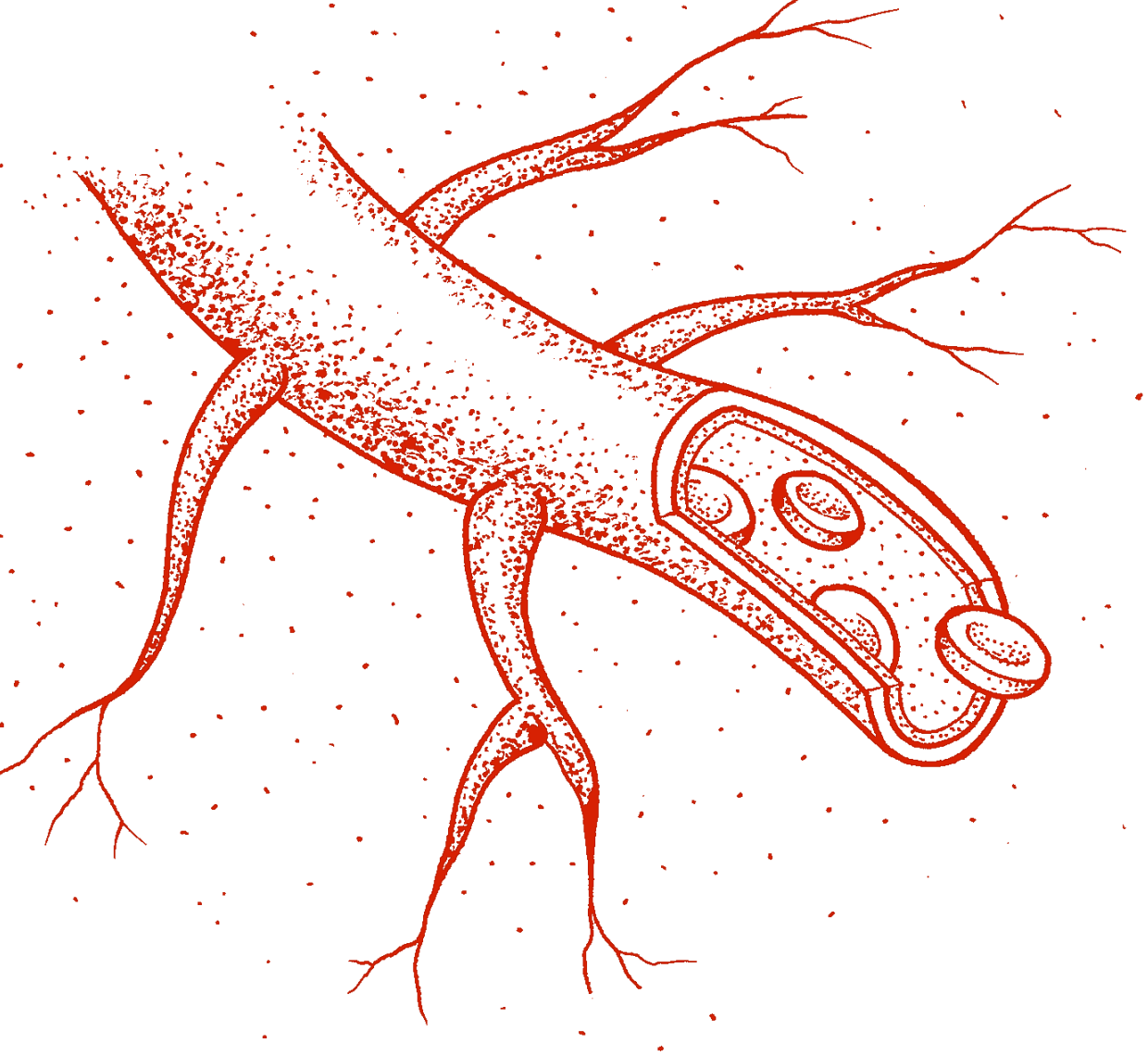

5

Cell type-specific changes in transcriptomic profiles of endothelial cells, iPSC-derived neurons and astrocytes cultured on microfluidic chips

H.H.T. Middelkamp*
A.H.A. Verboven*
A.G. De Sá Vivas
C. Schoenmaker
T. M. Klein Gunnewiek
R. Passier
C.A. Albers
P.A.C. 't Hoen
N. Nadif Kasri
A.D. van der Meer

Sci Rep 11, 2281 (2021)
*Equal author contribution

Abstract

In vitro neuronal models are essential for studying neurological physiology, disease mechanisms and potential treatments. Most *in vitro* models lack controlled vasculature, despite its necessity in brain physiology and disease. Organ-on-chip models offer microfluidic culture systems with dedicated micro-compartments for neurons and vascular cells. Such multi-cell type organs-on-chips can emulate neurovascular unit (NVU) physiology, however there is a lack of systematic data on how individual cell types are affected by culturing on microfluidic systems versus conventional culture plates. This information can provide perspective on initial findings of studies using organs-on-chip models, and further optimizes these models in terms of cellular maturity and neurovascular physiology. Here, we analysed the transcriptomic profiles of co-cultures of human induced pluripotent stem cell (hiPSC)-derived neurons and rat astrocytes, as well as one-day monocultures of human endothelial cells, cultured on microfluidic chips. For each cell type, large gene expression changes were observed when cultured on microfluidic chips compared to conventional culture plates. Endothelial cells showed decreased cell division, neurons and astrocytes exhibited increased cell adhesion, and neurons showed increased maturity when cultured on a microfluidic chip. Our results demonstrate that culturing NVU cell types on microfluidic chips changes their gene expression profiles, presumably due to distinct surface-to-volume ratios and substrate materials. These findings inform further NVU organ-on-chip model optimization and support their future application in disease studies and drug testing.

5.1 Introduction

Advanced *in vitro* cellular models are instrumental in understanding CNS function and mechanisms underlying neurological disease. Proper brain function depends on interaction between multiple cell types of the central nervous system (CNS) and its associated vasculature, known as the neurovascular unit (NVU)[1,2]. The NVU is important for cerebral homeostasis and is linked to neurodegenerative diseases[3–5]. Models consisting of multiple cell types are required to study cell type-specific contributions of the NVU to a disorder[6]. Furthermore, it is of interest to study neurological disorders in a patient-specific manner[1].

Current *in vitro* neuronal models are typically based on a two-dimensional (2D) cell layer cultured in a microwell plate, which are not designed to controllably mimic the three-dimensional (3D) geometry of nervous tissue. They lack a vascular compartment which prevents their use in studies of neurovascular disease or blood-brain barrier permeability. More complex *in vitro* neuronal models rely on co-culture of cells in transwell systems, in which cells are cultured on a porous synthetic membrane that is suspended in a well filled with culture medium. Though useful in studying cell-cell interactions, such transwell systems lack key aspects of the geometrical and physical microenvironment of brain tissue. For example, they lack blood vessels with perfusable lumens, and the cell-to-volume ratio of the cell culture medium is non-physiological[7]. Brain organoids are a more complex *in vitro* neuronal models, consisting of multicellular tissues with a complex 3D geometry than can include vascular structures[8–10]. These models are very useful when studying cell-cell interactions and the CNS microenvironment, however difficulties in controlling their formation results in high variability. They further lack the possibility to provide specific nutrients to individual cell types.

Organs-on-chips are *in vitro* cell culture models based on microfluidic devices ('chips') that integrate human cells, as well as possible sensors and actuators, to simulate the function of tissues or organ subunits[11–14]. The microsystems are designed to offer a specific geometry for the tissue of interest, while also allowing perfusion of liquids and a favourable cell-to-volume ratio. Moreover, the dynamic nature of the system allows for continuous alteration of culture conditions and infusion of solutes at various concentrations. The use of multiple culture compartments gives possibility to culture multiple cell types even when different media are required, and to adjust the fluid shear stress per cell type. Moreover, using

patient-specific human induced pluripotent stem cell (hiPSC)-derived cells, these devices can considerably aid the development of personalized medicine[12,15–19].

The first studies that use organs-on-chips to model the central nervous system and its associated vasculature were published in the past years[20,21,30–34,22–29]. Increased popularity of these 'brain-on-chip', 'blood brain-barrier-on-chip' and 'neurovascular unit (NVU)-on-chip' models requires a deeper understanding of the biological processes that are influenced by differentiating and culturing cells on microfluidic chips. The geometries and liquid volumes of microfluidic chips differ from those in conventional culture wells, which will likely affect the cells. Previous studies showed the effect of different culture systems, such as 3D culturing, on transcriptomic profiles of cells[35]. Also, co-culturing hiPSC-derived endothelial cells and hiPSC-derived neurons has an effect on their transcriptomes[25]. These studies demonstrate that *in vitro* cultured cells are sensitive to cues from their culture microenvironment, illustrated by changes in gene expression. Whether culturing on a microfluidic chip induces a gene expression profile associated with a more mature, physiological state of neurons remains to be determined. It is essential to identify culture system-dependent characteristics of various individually cultured cell types when setting up organ-on-chips to model the brain.

In this study we present an open-top microfluidic chip with two compartments that can be used to model the NVU. Cell sources such as iPSC-derived as well as primary cells were used to show the effect of culturing various cell types in different culture environments. The dimensions and materials of a microfluidic chip play a large role in cell behaviour and will likely influence the gene expression profiles of cells. To systematically compare cultures on microfluidic chips and on conventional well plates, we used both these culture systems to study 1) co-cultures of hiPSC-derived neurons (iNeurons) and rat astrocytes, and 2) monocultures of human endothelial cells.

iNeurons were generated by the widely used method of *Neurogenin-2* (*Ngn2*) overexpression, resulting in a homogeneous population of cortical upper-layer II/III excitatory neurons[36,37]. We cultured iNeurons and rat astrocytes together since astrocytes are essential for proper neuronal maturation[38–45]. Human umbilical vein endothelial cells (HUVECs) are a widely used primary cell source in studies of vascular biology; a lot of reference data on gene expression and cell function is available. HUVECs have also been widely used in modelling the NVU and the blood brain

barrier *in vitro* and were therefore used as the primary vascular cell type in this project[29,46,47].

For each cell type, we determined the changes in gene expression in cells cultured on the microfluidic chip relative to a conventional well plate using RNA sequencing (RNA-seq). Even though the iNeurons and rat astrocytes were cultured together, we could separate the gene expression profiles from both cell types since the cell types originated from different species, enabling us to study each cell type individually. We demonstrate that the implemented culture system affects gene expression in a cell type-specific manner, showing decreased cell division in endothelial cells, increased cell adhesion in iNeurons and astrocytes, and increased maturity of iNeurons when cultured on a microfluidic chip.

5.2 Materials and methods

5.2.1 Microfluidic chip design

The microfluidic chip consists of a straight bottom channel (500 µm width × 500 µm height) in which endothelial cells can be seeded, separated from an open-top compartment (500 µm width × 1500 µm height) by a membrane (polyester, 5 µm pore size) (figure 1A-B). The design of this chip is similar to other organ-on-chip systems designed to model the central nervous system[20,21,31,32]. The channel dimensions in such chips are optimized to provide a significant co-culture area as well as enough internal volume to culture cells with low flow rates or intermittent medium refreshing. In this study, the open-top compartment was used for differentiation of hiPSCs into iNeurons. The microfluidic chip is designed to fit into a 6-well plate (figure 1C), which can be filled with medium while the bottom channel can be perfused separately. The microfluidic chip is designed in such a way that different types of medium can be added to different types of cells (see figure 1A-B). The open top allows the treatment of hiPSCs similar to how they would be treated during differentiation to iNeurons or any other cell type in a well plate, while also giving the possibility of adding more volume to the well, therefore decreasing the need for changing medium too often. The bottom channel can be addressed separately by using medium-filled pipet tips, which can be placed on both the inlet and outlet of the channel.

5.2.2 Microfluidic chip fabrication

The microfluidic chip was fabricated by conventional polydimethylsiloxane (PDMS)-based soft lithography using poly(methyl methacrylate) (PMMA, Arkema innovative

chemistry) moulds. Two moulds (one defining the top channels, and one defining the bottom channels) were produced by micromilling (Sherline, model 5410) based on designs in SolidWorks (Dassault Systèmes, France). Polyester porous membranes (Whatman Nuclepore; 5 µm pore size) were cut and positioned on top of the structure that defines the lower channel (supplementary figure 1). Both moulds were pressed together by clamping to prevent leakage and irregularities in the end product. The space between the clamped moulds was injected with PDMS (10:1 base:crosslinker ratio) using a 10 ml syringe. PDMS was left to cure overnight at 65 °C after which it was removed from the mould. The surfaces of both the device and a round 32 mm glass coverslip (menzel-gläser) were activated by exposing them to air plasma (50W) for 40 seconds (Cute, Femto Science, South Korea), after which the microfluidic chip was bonded to the coverslip. The activated chip was then coated according to protocol in next chapter.

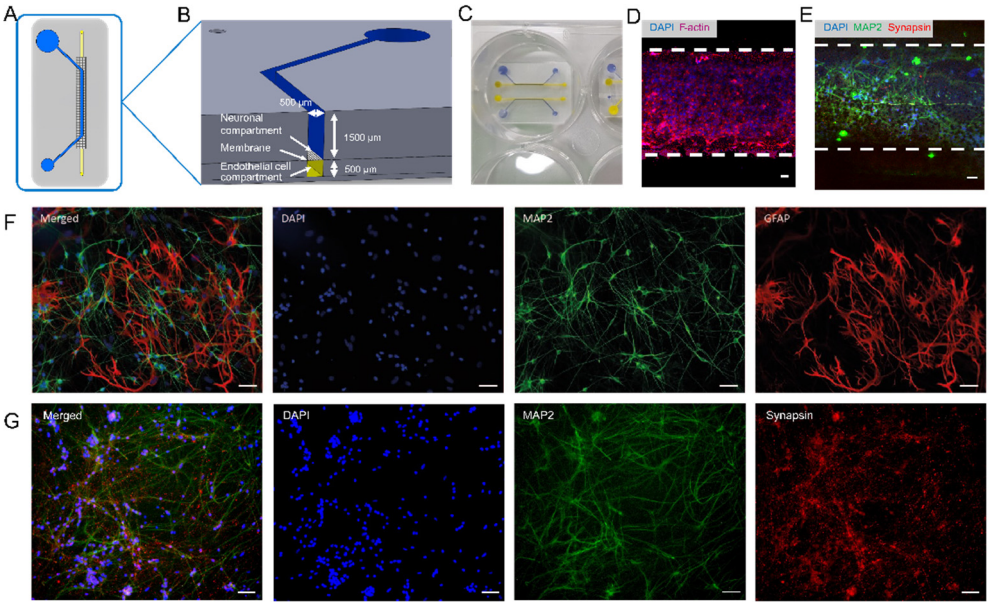

Figure 5-1: A-B: Schematic overview of the microfluidic chip. A: The open top curved channel (blue) is separated from the straight bottom channel (yellow) by a polyester membrane (5 µm pores). B: Cross-section connected channels. C,D,F: neurovascular unit (NVU)-on-a-chip microfluidic device. C: Open-top microfluidic chip in a 6-well plate, in the bottom channel (yellow) endothelial cells can be cultured, while the open top channel (blue) is used for neuronal differentiation. D: Staining performed on endothelial cell monoculture on bottom channel of the microfluidic chip on a polyester membrane. Based on the staining pattern, a monolayer was present. Blue: Nuclei; Red: F-actin. E: Staining performed on neurons differentiated in the top channel of the microfluidic chip on a polyester membrane. Blue: Nuclei; Green: Microtubule Associated Protein 2 (MAP2); Red: Synapsin-1/2 (SYN1/2). F: Staining performed on neurons co-cultured with astrocytes differentiated on a 24-well plate. Blue: Nuclei; Green: MAP2; Red: Glial fibrillary acidic protein (GFAP), a 1:1 ratio of neurons and astrocytes is visible. G: Staining of neurons differentiated on a 24-well plate. Blue: Nuclei; Green: MAP2; Red: SYN1/2. Scale bars, 50 µm.

5.2.3 Cell culturing of hiPSC-derived neurons and rat astrocyte co-cultures

hiPSC-derived neurons were co-cultured with rat astrocytes, either on a 24-well plate or on the microfluidic chip at 37 °C and 5% CO_2. For generation and culturing of iNeurons, a previously published protocol[36] was used that is based on differentiation of hiPSCs (GM25256 iPSC from Fibroblast, Coriell Institute for Medical Research) into neurons (iNeurons) by *Neurogenin 2 (Ngn2)* overexpression using a doxycycline-inducible system. hiPSCs from a commercially available cell line were used, which were transduced with two separate lentiviral vectors containing rtTA and Ngn2[48]. One day before cell plating, channels of the microfluidic chip and wells of a 24-well plate were coated overnight at 4 °C with 20 µg/ml laminin (rhLaminin-521, Gibco) diluted in cold DMEM/F12 medium (Gibco). On days *in vitro* (DIV) 1 approximately 10,000 cells were seeded per channel and 20,000 cells were seeded per well. To seed cells on the microfluidic chip, the top channels were first filled with culture medium by open-microfluidic flow[49], after which a droplet containing a high concentration of cell suspension (calculated to contain the correct number of cells) was pipetted into the channels to disperse the cells. The size of the cells prevented them from passing through the membrane to the bottom channel. Chips were incubated for two hours at 37 °C and 5% CO_2. Two hours after seeding the cells in the channels, the wells containing the microfluidic chips were filled with Essential E8 Flex Basal medium (Gibco), supplemented with 1x RevitaCell Supplement (Gibco) and 4 µg/ml doxycycline (Sigma Aldrich). For culture in wells plates, the wells were first filled with 500 µl medium, followed by seeding and dispersion of the correct number of cells. From DIV1 onwards, the steps were the same for differentiation of hiPSCs into iNeurons in a well and on the microfluidic chip. On DIV1 cell medium was changed to DMEM/F12 medium, supplemented with 0.1 mg/ml primocin (InvivoGen), 4 µg/ml doxycycline, 1x N-2 (Gibco), 1x MEM Non-Essential Amino Acids Solution (NEAA, Gibco), 10 ng/ml NT-3 Recombinant Human Protein (NT-3, Promocell) and 10 ng/ml BDNF Recombinant Human Protein (BDNF, Promocell).

On DIV2, the rat astrocytes (isolated according to earlier described protocols[36]) were added in a 1:1 ratio with the hiPSCs, similar to the hiPSC seeding. A droplet containing a highly concentrated suspension with the calculated number of cells was dispersed on top of the medium. On DIV3, medium was removed and switched to Neurobasal medium (Gibco) supplemented with 0.1 mg/ml primocin, 1x B-27 Supplement, serum free (Gibco), 1x GlutaMAX Supplement (Gibco), 4 µg/ml doxycycline, 10 ng/ml NT-3, 10 ng/ml BDNF and 2 µM Cytosine β-D-arabinofuranoside hydrochloride (Sigma Aldrich). Starting from DIV5, 50% of the

medium was refreshed every 2 days with Neurobasal medium, supplemented with 0.1 mg/ml primocin, 1X B-27, 1X GlutaMAX, 4 µg/ml doxycycline, 10 ng/ml NT-3 and 10 ng/ml BDNF. From DIV9 onwards, medium was refreshed every 2 days with this medium, which was then supplemented with 2.5% Fetal Calf Serum (Sigma Aldrich) to sustain the rat astrocytes. iNeurons were kept in culture up to DIV38.

5.2.4 Cell culturing of human umbilical vein endothelial cells (HUVECs)

Human umbilical vein endothelial cells (HUVECs, Lonza) were cultured either on a 24-well plate or on the microfluidic chip at 37 °C and 5% CO_2. Cells were seeded to the top surface of a 20 µg/ml laminin (rhLaminin-521, Gibco)-coated bottom channel of the microfluidic chip or to the bottom of a well to reach an initial number of 40,000 cells per channel and 40,000 cells per well. To make sure cells attached to the top of the channel, the microfluidic chips were inverted after cells were added to the channel for at least half an hour. After half an hour, the medium in the channel was replaced with fresh endothelial cell growth medium (ECGM-2: Basal medium (ECBM-2) with supplement mix PromoCell) and microfluidic chips were placed back to the normal upright position. Cells were cultured for 24 hours during which medium was changed twice.

5.2.5 Fixation, staining and imaging of iNeuron and rat astrocyte co-cultures, and endothelial cells

iNeuron and astrocyte co-culture: After co-culturing of iNeurons and astrocytes for 30 days on coverslips in a 24-well plate, cells were washed with ice cold phosphate buffered saline (PBS, Gibco). Subsequently, cells were fixated for 15 minutes at room temperature with 4% formaldehyde (Thermo scientific) and washed three times for 5 minutes at room temperature with PBS. Cells were permeabilized with 0.2% Triton X-100 (Sigma-Aldrich) solution for 10 minutes at room temperature. Blocking buffer (PBS (Gibco), 5% normal horse serum, 5% normal goat serum, 5% normal donkey serum, 0.1% bovine serum albumine (BSA), 0.4% triton, 0.1% lysine (all from Sigma-Aldrich)) was incubated for 1 hour at room temperature. Primary antibodies (MAP2, Mouse monoclonal, Abcam ab11267, 1:1000; GFAP, Rabbit polyclonal, Abcam ab7260, 1:1000) were diluted in blocking buffer, and were incubated overnight at 4 °C. Cells were washed three times for 5 min with PBS, followed by incubation with secondary antibodies (Goat anti-Mouse IgG Alexa Fluor 488, Thermofisher A-11029, 1:1000; Goat anti-Rabbit IgG Alexa Fluor 647, Thermofisher A-21245, 1:500) diluted in blocking buffer for 1 hour at room temperature. Subsequently, cells were washed 3 times for 5 minutes with PBS, followed by incubation with Hoechst (Thermofisher

#H3570) diluted 1:10000 in PBS for 10 minutes at room temperature. Lastly, cells were washed one time with PBS for 5 minutes at room temperature, followed by imbedding of coverslips in fluorescent mounting medium (DAKO #S3023). Cells were imaged using a Zeiss Axio Imager Z1 at a 2752 x 2208 resolution at 20X magnification (scale 1 pixel = 0.23 µm).

iNeuron synapsin: After co-culturing of iNeurons and astrocytes for 38 days on chips and well plate, cells were washed with ice cold phosphate buffered saline (PBS, Gibco), fixated for 15 minutes at room temperature with 4% formaldehyde (Thermo scientific) and subsequently washed 3 times with PBS. Cells were permeabilized with 0.2% Triton X-100 (Sigma-Aldrich) solution for 10 minutes at room temperature. 5% goat serum (Sigma Aldrich) in PBS was used as a blocking agent for 1 hour at room temperature. Primary antibodies (MAP2, Rabbit polyclonal, Abcam ab32454, 1:1000; Synapsin-1/2, Guinea Pig, Synaptic systems 106004, 1:500) were diluted in PBS with 1% goat serum and applied to the cells, which was then incubated overnight at 4 °C. Cells were washed 10 times for 1 minute with PBS. Secondary antibodies (Chicken anti-Rabbit IgG Alexa Fluor 488, ThermoFisher A-21441, 1:500; Goat anti-Guinea Pig IgG Alexa Fluor 647, ThermoFisher A-21450, 1:1000) and DAPI (Thermo fisher) were diluted in 1% goat serum and added to the cells. Cells were incubated for 1 hour at room temperature. Afterwards cells were washed 10 times for 1 minute with PBS. Cells were imaged using a Zeiss LSM 510 confocal microscope at 10X magnification.

Endothelial cells: After monoculturing HUVECs for 24 hours on a chip, cells were washed with PBS, fixated for 15 minutes at room temperature with 4% formaldehyde and subsequently washed 3 times with PBS. Cells were permeabilized with 0.1% Triton X-100 solution for 10 minutes at room temperature. 5% goat serum in PBS was used as a blocking agent for 1 hour at room temperature. Alexa Fluor 633 Phalloidin (ThermoFisher A22284, 1:40) and DAPI were diluted in 1% goat serum and added to the cells. Cells were incubated for 1 hour at room temperature. Afterwards cells were washed 3 times with PBS. Cells were imaged using a Zeiss LSM 510 confocal microscope at 10X magnification.

5.2.6 RNA sequencing

RNA was isolated from monocultured HUVEC samples (24 hours after seeding) and from iNeuron and rat astrocyte co-culture samples (DIV38) by adding 100 µl of RNA lysis buffer to the well plate and respectively bottom or top channel of the chip. After the lysis buffer was removed, both plates and chips were checked by using a brightfield microscope for remaining cells and previous step was repeated until no more cells were visible. Cells were cultured either on a microfluidic chip or on a 24-well plate. Two replicates per culture condition were taken (figure 2A), resulting in a total of 8 RNA samples. RNA was purified with the *Quick*-RNA Microprep kit (Zymo Research, R1051) according to manufacturer's instructions. RNA quality was checked using Agilent's Tapestation system (RNA High Sensitivity Screentape and Reagents, 5067-5579/80). RIN values ranged between 9.0 – 9.8. RNA sequencing (RNA-seq) library preparation was performed using the SMARTer Stranded Total RNA Sample Prep Kit (low input mammalian) (Takara Bio, 634861) according to manufacturer's instructions. RNA concentrations were determined using the Qubit RNA HS Assay kit (Invitrogen, Q32855). 50 ng of total RNA was depleted for rRNA using the included RiboGone kit (Takara Bio, 634847). After rRNA depletion the remaining amount of RNA was below 10 ng. Library amplification was performed with 12 amplification cycles. Fragment size distribution was determined using Agilent's Tapestation system (HS D1000 ScreenTape and Reagents, 5067-5584/5). Library concentrations were quantified using the KAPA Library Quantification Kit (KAPA Biosystems, KK4973). Libraries were sequenced on the NextSeq 500 platform (Illumina) using a V2 75 cycle kit (paired-end 2 x 42 bp).

5.2.7 Pre-processing of RNA-seq data

Base calls were converted to fastq format and demultiplexed using Illumina's bcl2fastq conversion software (v2.16.0.10) tolerating one mismatch per library barcode. The first three bases of all forward reads were removed using Trimmomatic (version 0.33)[50], as recommended by the manufacturer of the SMARTer Stranded RNA Sample Prep kit. Trimmed reads from HUVEC samples were mapped to the human reference genome (GRCh38.p12). Trimmed reads from iNeuron samples co-cultured with rat astrocytes were mapped to a combined human (GRCh38.p12) and rat (Rnor 6.0) reference genome, to separate reads belonging to the human iNeurons from reads belonging to the rat astrocytes. Mapping was performed using STAR[51] (version 2.5.1b) with default settings (--outReadsUnmapped None, --outFilterType Normal, --outFilterScoreMin 0, outFilterMultimapNmax 10, --outFilterMismatchNmax 10, --alignIntronMin 21, --alignIntroMax 0, --

alignMatesGapMax 0, --alignSJoverhangMin 5, --alignSJDBoverhangMin 3, --sjdbOverhang 100). Uniquely mapped reads (mapping quality of 255) were extracted. Reads from bam files were further processed to generate count matrices with HTSeq[52] (version 0.9.1) (parameters: --order=pos, --stranded=yes, --mode=union, --type=exon, --idattr=gene_id). Reference transcriptome GRCh38.p12 (GENCODE 29, Ensembl version 94) was used for bam files from HUVEC samples, and the human reference transcriptome combined with the rat reference transcriptome Rnor 6.0 (Ensembl version 94) was used for bam files from iNeuron samples co-cultured with rat astrocytes. The resulting count tables for the RNA-seq data were used directly for subsequent analyses.

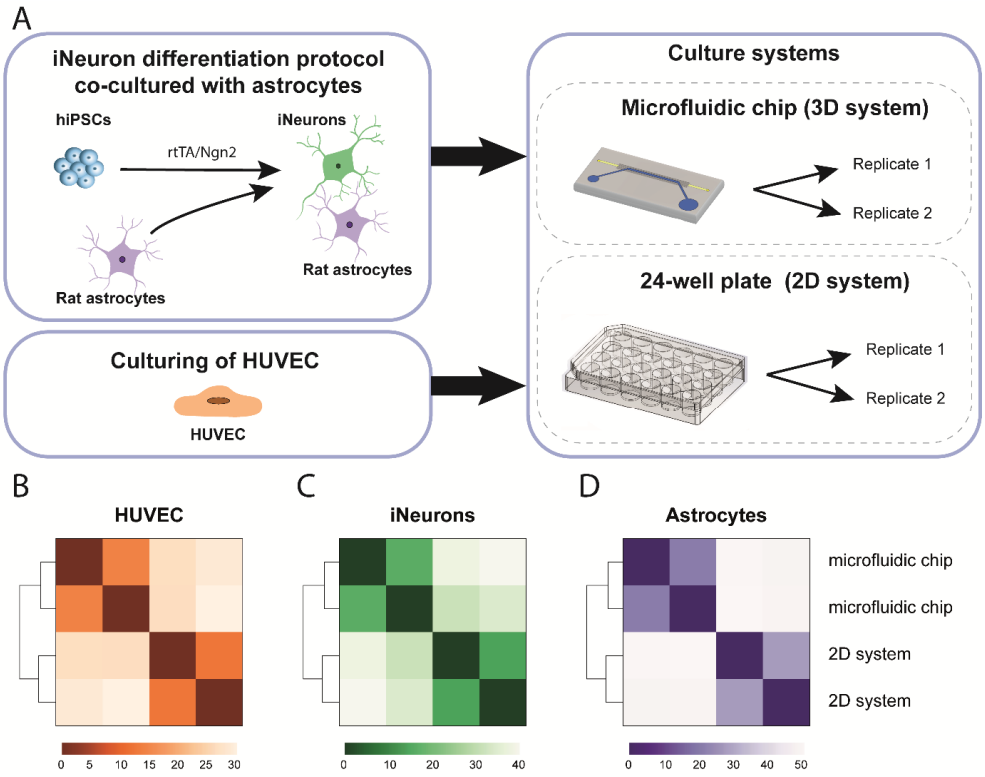

Figure 5-2: A: Set-up of RNA-seq experiment. hiPSCs transduced with two lentiviral vectors expressing rtTA and Ngn2 are treated with doxycycline to initiate differentiation into iNeurons up to DIV38. On DIV2, rat astrocytes are added to the culture to support neuron differentiation. The experiments were performed both on the microfluidic chip and on a 24-well plate. On DIV38, RNA was isolated from two replicates per culture condition. Separately, HUVECs were cultured on the microfluidic chip and on a 24-well plate as well. After 24 hours, RNA was isolated from two replicates per culture condition. B-D: Heatmaps of Euclidean distances between samples based on gene expression profiles, generated per cell type (HUVEC, iNeurons, and astrocytes). Within each cell type, samples cluster according to culture condition.

5.2.8 RNA-seq data analysis

Raw counts from count tables were transformed to counts per million (cpm) using edgeR (R package[53]). Subsequent steps were performed for each cell type individually. Transcripts with a cpm > 2 in at least two samples were included for further analysis (14,069 genes for iNeurons, 12,023 genes for astrocytes, and 12,717 genes for HUVECs). Heatmaps were generated by performing a regularized log transformation on the raw counts using the rld function from DESeq2[54]. Euclidean distances between samples were determined. Differential expression analysis was performed using DESeq2, to compare samples cultured on a microfluidic chip to samples cultured on a well plate. Raw counts were used as input. Genes with a Benjamini-Hochberg (BH)-corrected *p*-value < 0.05 were considered to be significantly differentially expressed (DE) between the two conditions.

Overrepresentation analysis (ORA) of DE genes was performed using goseq[55]. Enrichment of DE genes in Gene Ontology (GO) terms (C5 collection) and canonical pathways (C2 sub-collection CP) from the Molecular Signatures Database (MSigDB, version 7.0)[56] was determined. Gene symbols corresponding to transcripts that were not included in the DE analysis were removed from the selected gene sets. Subsequently, gene sets with remaining gene set size > 5 and < 500 were used for enrichment analysis. For DE genes identified in rat astrocyte samples, gene symbols had to be converted to its matching human homologue to match with the human gene symbols in MSigDB. Human homologues from the Ensembl homology database (version 94) were used for this conversion, by including one-to-one orthologues and one-to-many orthologues with a confidence score of 1. For 10,653 genes (out of 12,023 included in DE analysis of rat astrocyte samples) human homologues could be identified. For all cell types, human gene symbols (Ensembl version 94) from DE results were converted to gene symbols from Ensembl version 97, corresponding to the version of gene symbols used in MSigDB. DE genes were considered to be significantly overrepresented in MSigDB gene sets for which a Bonferroni-corrected *p*-value < 0.05 was obtained.

For principal component analysis (PCA) count tables from all samples of all cell types were combined. First, counts belonging to rat transcripts had to be assigned to the human homologue of each rat gene. For 16,074 rat genes a unique human homologue could be identified, using one-to-one orthologues and one-to-many orthologues with a confidence score of 1 from the Ensembl homology database (version 94). Raw counts for these 16,074 genes were selected for all samples from

HUVEC, iNeurons and rat astrocytes (gene symbols converted to human). The counts were transformed using the variance stabilizing transformation (vst) function from DEseq2. PCA was performed using the prcomp function from stats (R package).

5.3 Results

5.3.1 Microfluidic chip design and operation

We designed a microfluidic chip and studied the transcriptomic differences of different cell types when cultured on chip versus the traditional well plate method. In our system we can culture cells under similar culturing conditions as when cultured in conventional well plates. This allows us to differentiate hiPSCs into neurons on chip from 0 days *in vitro* (DIV0) using established protocols. The microfluidic chip has a design similar to other organ-on-chip microdevices that were used in modelling tissues of the central nervous system[20,21,31,32]. The chip contains two channels separated by a porous membrane (figure 1A-B). The bottom channel represents the vascular compartment and is used for endothelial cell culture, while the top channel represents the neuronal compartment in which the hiPSC-derived neurons are co-cultured with rat astrocytes. Importantly, the neuronal compartment has an open-top design, which means that it can either be selectively filled with liquids via open microfluidics, or it can be exposed to a well fully filled with medium. To seed cells in the top compartment, we used pipetting by open microfluidics (supplementary movie 1), while the long-term culturing was performed by exposing the top compartment to a well filled with medium. The endothelial compartment is a typical microchannel with a closed configuration. We seeded endothelial cells on the porous membrane that forms the top surface of the channel (figure 1D). As we directly compare cells cultured on the microfluidic chips and cells cultured in wells, we only evaluated iNeuron and astrocyte co-cultures and HUVEC monocultures in this microfluidic chip. We tested co-cultures of endothelial cells and neurons in the same device as well (see supplementary section co-culture, suppl. figure 2). However, endothelial cells do not form a full monolayer in those co-cultures, but instead seem to form 3D structures resembling pseudo capillaries. Such structures are often seen when plating endothelial cells on soft, extracellular matrix-like substrates. This may indicate long-term culture of iNeurons leads to changes in the substrate present in the channel of the microfluidic chip on which the endothelial cells are later seeded.

5.3.2 iNeuron differentiation on microfluidic chip

We generated hiPSC-derived neurons by the widely used method of *Neurogenin-2* (*Ngn2*) overexpression, resulting in a homogeneous population of cortical upper-layer II/III excitatory neurons[36,37]. hiPSCs were differentiated into neurons and co-cultured with rat astrocytes on top of the membrane in the open-top microfluidic chip as well as in a conventional 24-well plate. Because of the different surface-to-volume ratio of the channels on the microfluidic chip compared to wells in a 24-well plate, cell density was adjusted accordingly. The differentiation process was always performed without the presence of endothelial cells. On DIV2, rat astrocytes were added to support differentiation of neurons. We confirmed presence of both iNeurons and astrocytes using immunostaining (figure 1F). After 38 days *in vitro*, cells on the microfluidic chip and in the well plate were fixed and were stained for microtubule-associated protein-2 (MAP2) and synapsin-1/2 (SYN1/2). The images obtained by confocal fluorescence microscopy demonstrate that a network of iNeurons expressing MAP2 and synapsin forms in the top channel of the microfluidic chip, confirming the successful differentiation of hiPSC into neurons on the microfluidic chip (figure 1E,G). Interestingly, imaging of the microfluidic co-cultures also showed invasion of neurites from the top compartment through the membrane into the bottom compartment (suppl. figure 2).

5.3.3 Differences in gene expression patterns between cell types and culture systems

We performed RNA-seq to investigate effects of culturing cells on the microfluidic chip compared to a conventional 2D system. Raw data set have been deposited with the Gene Expression Omnibus (www.ncbi.nlm.nih.gov/geo) under accession code GSE154799[57]. RNA was isolated from HUVEC monocultures (cultured for 24 hours), and from iNeuron and rat astrocyte co-cultures (DIV38), cultured both on microfluidic chip and on a conventional well plate. We were interested in the effect of culturing cells on different culture systems for each cell type individually. Since the iNeurons and astrocytes originated from different species, we could separate reads from iNeuron and astrocyte co-culture samples by aligning them to a combined human and rat genome. Gene expression levels were quantified for iNeurons and astrocytes separately by counting reads mapping to human and rat genes, respectively. Gene expression levels for HUVEC samples were determined by aligning reads to the human genome only. As expected, the largest variation between samples on gene expression level was related to cell type differences (suppl. figure 3). Within each cell type, samples clearly cluster according to culture

condition (figure 2B-D). For further analysis, the effects of culturing cells on a microfluidic chip were studied by comparing samples cultured on the microfluidic chip versus the conventional 2D system for each cell type separately.

5.3.4 HUVECs cultured on a microfluidic chip show decreased expression of genes related to cell division

Differential expression analysis using DESeq2 was performed on HUVEC samples to identify differentially expressed (DE) genes between the two culture conditions. In HUVEC samples cultured on a microfluidic chip, 853 genes were significantly up-regulated and 1161 genes were significantly down-regulated (adj. *p*-value < 0.05) (suppl. table 1). The most significant upregulated genes include *STC1* (logFC = 2.8, adj. *p*-value = 5.64×10^{-73}), *ITGB4* (logFC = 1.7, adj. *p*-value = 2.77×10^{-41}) and *ITGA10* (logFC = 1.5, adj. *p*-value = 1.36×10^{-25}). Interestingly, both STC1 (stanniocalcin-1) and integrins are involved in regulation of tube formation, indicating a more *in vivo*-like growth pattern of the HUVECs [58–61]. The most significantly down-regulated genes included genes important for cell growth and division, including *CENPF* (logFC = -1.8, adj. *p*-value = 1.76×10^{-75}), *MKI67* (logFC = -2.1, adj. *p*-value = 1.76×10^{-75}), and *TOP2A* (logFC = -1.7, adj. *p*-value = 3.61×10^{-61}).

Overrepresentation analysis (ORA) showed enrichment of DE genes in 150 gene ontology (GO) terms (adj. *p*-value < 0.05) (suppl. table 1). Interestingly, the GO terms were mainly enriched for down-regulated genes. The top GO terms include biological processes (BP) such as regulation of cell cycle, DNA replication and repair mechanisms, and processes involved in cell division (figure 3A). The DE genes were also significantly overrepresented in many pathways orchestrating cell cycle (suppl. table 1), confirming results from GO terms analysis. Since a high percentage of DE genes in these gene sets was downregulated, this indicates HUVECs cultured on a microfluidic chip divide and proliferate less. This could be a result of depletion of growth factors in the relatively small culture volume on the microfluidic chip as well as a more *in vivo* like environment, where endothelial cells are less inclined to proliferate often, when cells are grown on the microfluidic chip.

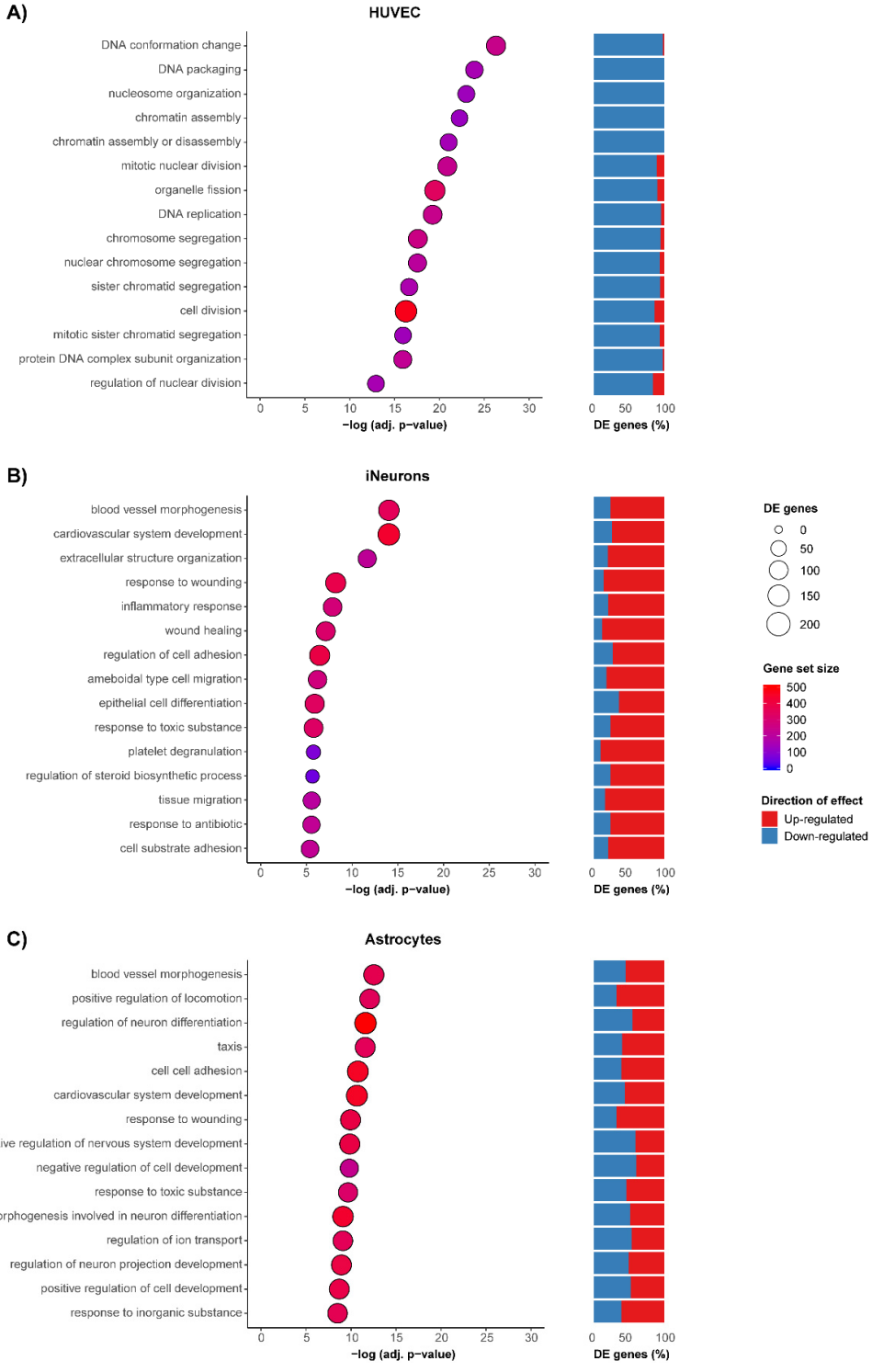
A)
HUVEC
DNA conformation change
DNA packaging
nucleosome organization
chromatin assembly
chromatin assembly or disassembly
mitotic nuclear division
organelle fission
DNA replication
chromosome segregation
nuclear chromosome segregation
sister chromatid segregation
cell division
mitotic sister chromatid segregation
protein DNA complex subunit organization
regulation of nuclear division
0 5 10 15 20 25 30
−log (adj. p−value)
0 50 100
DE genes (%)
B)
iNeurons
blood vessel morphogenesis
cardiovascular system development
extracellular structure organization
response to wounding
inflammatory response
wound healing
regulation of cell adhesion
ameboidal type cell migration
epithelial cell differentiation
response to toxic substance
platelet degranulation
regulation of steroid biosynthetic process
tissue migration
response to antibiotic
cell substrate adhesion
0 5 10 15 20 25 30
−log (adj. p−value)
0 50 100
DE genes (%)
DE genes
0
50
100
150
200
Gene set size
500
400
300
200
100
0
Direction of effect
Up-regulated
Down-regulated
C)
Astrocytes
blood vessel morphogenesis
positive regulation of locomotion
regulation of neuron differentiation
taxis
cell cell adhesion
cardiovascular system development
response to wounding
positive regulation of nervous system development
negative regulation of cell development
response to toxic substance
cell morphogenesis involved in neuron differentiation
regulation of ion transport
regulation of neuron projection development
positive regulation of cell development
response to inorganic substance
0 5 10 15 20 25 30
−log (adj. p−value)
0 50 100
DE genes (%)

Figure 5-3: Overrepresentation analysis of DE genes in GO terms was performed by comparing samples cultured on a microfluidic chip compared to a 2D system, for HUVECs (A), iNeurons (B), and astrocytes (C). Top 15 GO terms representing biological processes (BP) are shown per cell type. On the x-axis significance of the overrepresentation is represented by the -log(adj. p-value), calculated by taking the p-value corrected for multiple testing using Bonferroni correction. The gene set size represents the number of genes in each gene set for which a cpm (counts per million) value > 2 was obtained in 2 replicates per cell type, depicted by the color of the circles. The number of DE genes per GO term are depicted by circle size. For each gene set, the percentage of up-regulated (red) and down-regulated (blue) genes of all DE genes per gene set is shown.

5.3.5 iNeurons cultured on a microfluidic chip show increased expression of genes related to cell adhesion, tissue migration and activation of metabolic processes

Differential expression analysis was also performed for iNeurons co-cultured with rat astrocytes. To study gene expression changes in the iNeurons dependent on culture system, we selected reads from the co-culture samples that mapped to the human genome. In total, 1480 genes were significantly upregulated, and 1139 genes were significantly down-regulated (adj. *p*-value < 0.05) in iNeurons cultured on the microfluidic chip (suppl. table 2). Interestingly, among the top up-regulated genes were several genes involved in cell adhesion, including *FN1* (logFC = 7.5, adj. *p*-value = 1.08×10^{-118}), *THBS1* (logFC = 9.1, adj. p-value = 2.31×10^{-58}) and *MSN* (logFC = 5.4, adj. p-value = 3.47×10^{-48}). Overrepresentation analysis revealed significant overrepresentation of DE genes in 133 GO terms (adj. *p*-value < 0.05) (suppl. table 2). Indeed, these results show overrepresentation of DE genes in cell adhesion gene sets (figure 3B). Other GO terms enriched for DE genes represented processes such as extracellular matrix (ECM) organization, tissue migration, and steroid metabolic processes. The majority of these genes were upregulated, indicating increased activation of these processes in iNeurons cultured on a microfluidic chip. Pathway analysis confirmed the results from GO term analysis (suppl. table 2).

Among the top down-regulated DE genes were many transcriptional regulators important for development or involved in regulating cell growth, such as *BHLHE41* (logFC = -3.2, adj. *p*-value = 4.61×10^{-44}), *JUN* (logFC = -1.3, adj. *p*-value = 2.90×10^{-23}), *TSHZ2* (logFC = -1.9, adj. *p*-value = 6.78×10^{-23}), *KLF10* (logFC = -1.9, adj. *p*-value = 2.86×10^{-21}), and *RARB* (logFC = -3.8, adj. *p*-value = 2.98×10^{-19}). This indicated the process of neuronal differentiation might depend on culture system. Indeed, several neuronal maturation marker genes were significantly differentially expressed in the iNeurons. *SOX1* (logFC = -2.4, adj. *p*-value = 6.72×10^{-3}) and *DCX* (logFC = -0.3, adj. *p*-value = 2.45×10^{-3}), both neural progenitor (NPC) markers, and *EFNA5* (logFC = -1.3, adj. *p*-value = 5.18×10^{-12}), an immature neuronal marker, were significantly down-

regulated in iNeurons cultured on the microfluidic chip. Conversely, post-mitotic neural marker *SYP* (logFC = 0.5, adj. *p*-value = 1.89 x 10^{-4}), and synaptic markers *SLC17A6* (logFC = 0.4, adj. *p*-value = 2.45 x 10^{-3}), *SNAP25* (logFC = 1.1, adj. *p*-value = 7.78 x 10-^{16}), *SYT1* (logFC = 0.3, adj. *p*-value = 0.03), and *SYT2* (logFC = 1.6, adj. *p*-value = 7.04 x 10^{-23}) were up-regulated. These results indicate that the iNeurons cultured on a microfluidic chip are more mature compared to iNeurons cultured on the 2D well system.

5.3.6 Astrocytes cultured on a microfluidic chip exhibit differences in gene expression patterns that regulate neuronal differentiation

Finally, to compare the effect of the different culture systems on rat astrocytes, we selected reads from the iNeuron and astrocyte co-culture samples that mapped to the rat genome. DESeq2 analysis identified 768 significantly up-regulated genes and 752 significantly down-regulated genes from astrocyte samples cultured on the microfluidic chip compared to a conventional well plate (adj. *p*-value < 0.05) (suppl. table 3). Interestingly, the most significantly up-regulated gene is *Scg2* (logFC = 5.3, adj. *p*-value = 4.38 x 10^{-234}). Scg2 (secretogranin II) can be secreted by astrocytes[62,63] and is known to regulate neuronal differentiation, providing more evidence for a more mature state of the co-cultured iNeurons on a microfluidic chip. Many other genes relevant for astrocyte-neuron communication were among the most significantly DE genes as well, including *Slc7a11* (glutamate release) (logFC = 4.0, adj. *p*-value = 5.35 x 10^{-125}), *Cp* (iron metabolism) (logFC = -3.2, adj. *p*-value = 5.26 x 10^{-76}), *Hgf* (neurotrophic growth factor) (logFC = -4.0, adj. *p*-value = 1.02 x 10^{-35}), and *Atp1a2* (potassium clearance) (logFC = -2.2, adj. *p*-value = 2.94 x 10^{-34}).

We determined whether there is overrepresentation of astrocyte DE genes in GO terms and pathways (suppl. table 3). For 10,653 genes (out of 12,023 included in DE analysis) human homologues could be identified, which were used for overrepresentation analysis in gene sets. In total 1411 of these genes were significantly differentially expressed, which were overrepresented in 213 GO terms (adj. *p*-value < 0.05). We investigated whether there was overlap between GO terms identified for the different cell types and observed large overlap between GO terms identified for iNeurons and astrocytes, whereas there was hardly any overlap with GO terms identified for HUVECs (suppl. figure 4A). The overlapping GO terms between iNeurons and astrocytes include processes such as cell adhesion and tissue migration (figure 3B, figure 3C). Interestingly, the overlap in DE genes between iNeurons and astrocytes is not higher than the overlap with HUVECs and either cell

types (suppl. figure 4B). This indicates that although the same processes are changed in both iNeurons and astrocytes, these changes are caused by altered expression of different genes. GO terms that were unique for astrocytes mainly represent DE genes that have a function in regulation of cell development and neuron differentiation. Pathway analysis confirmed findings from GO term analysis, with changes observed in pathways such as ECM organization, cell adhesion, axon guidance and regulation of the neuronal system (suppl. table 3).

Overall, the results suggest the degree to which astrocytes support neuronal differentiation differs depending on the culture system used. This was shown by the highly significant differential expression of genes relevant for communication between astrocytes and neurons, as well as the significant enrichment of DE genes in GO terms that represent regulation of neuronal differentiation. The function of astrocytes and neurons are known to be closely connected. Astrocytes respond to neurotransmitters released by neurons, whereas neurons respond to factors released by astrocytes that influence synaptic activity and function of neurons[64]. In iNeurons we observed increased expression of marker genes for mature neurons, and decreased expression of marker genes for immature neurons. These findings indicate that iNeurons mature faster when cultured on a microfluidic chip compared to conventional 24-well plates. The changes in gene expression observed in the co-cultured astrocytes support these findings, as they seem to contribute to the difference in neuronal maturation. It could also be that changes in gene expression observed in astrocytes are a secondary result caused by the difference in maturity of iNeurons, rather than underlying the changes in neuronal maturation. Nevertheless, our results show that iNeurons co-cultured with astrocytes display a different, more mature state, when cultured on a microfluidic chip.

5.4 Discussion

In this study we present a new, open-top microfluidic chip for culturing multiple cell types, which we used to study transcriptomic differences of different cell types when cultured on chip versus the traditional well plate method. The chip can be used for future studies to study interaction between cell types as well. We cultured different cell types on these microfluidic chips relevant for modelling the NVU, consisting of 1) co-cultures of hiPSC-derived neurons and rat astrocytes, and 2) monocultures of HUVECs. We were interested to identify processes that are changed in each cell type when cultured on a microfluidic chip, compared to conventional culture systems. These cell type-specific changes in gene expression were investigated using RNA-

seq. HUVECs were cultured separately from hiPSC-derived neurons co-cultured with rat astrocytes, both on the microfluidic chip and on a conventional 24-well plate. We demonstrate that culturing cells on microfluidic chips has a clear, cell type-specific effect on gene expression.

Endothelial cells exhibited decreased expression of genes related to cell division and increased expression of genes related to tube formation when cultured on microfluidic chips. The medium used for culturing endothelial cells stimulates endothelial proliferation by high levels of growth factors like vascular endothelial growth factor (VEGF) and fibroblast growth factor (bFGF). The microfluidic chip has a surface-to-volume ratio that is approximately five times higher than that found in the well plate (0.01 cm^2/µl vs.0.0019 cm^2/µl respectively). Therefore, the decrease in expression of genes related to proliferation and increased expression of genes related to tube formation may be due to depletion of growth factors in the relatively small culture volume on the microfluidic chip. Under normal conditions, endothelial cells do not proliferate continuously when in contact with other endothelial cells. Thus, the decreased expression of genes related to cell division can be representative of a more *in vivo* like environment when cells are grown on the microfluidic chip. These findings stress the importance of adjusting physiological flow accordingly when setting up an organ-on-chip model. Fluid flow will continuously refresh the medium in the bottom compartment to provide endothelial cells with sufficient nutrients but can also cause shear stress; the mechanical stimulus caused by flowing liquid. Previous research has shown different gene expression patterns in HUVECs cultured in a microfluidic chip under different continuous flow profiles[65]. It is important to set the fluid flow at a level where it provides sufficient medium for cell survival, while keeping it at a minimum to prevent shear stress and maintain the cells at a less proliferative state comparable to the *in vivo* situation.

Gene expression data from co-cultured iNeurons and rat astrocytes indicated iNeurons mature more rapidly when cultured on microfluidic chips compared to conventional well plates. This was shown by increased expression of marker genes for mature neurons and decreased expression of marker genes for immature neurons. It was further supported by findings from the co-cultured astrocytes, showing expression of astrocyte genes involved in regulation of neuron differentiation was affected. The function of astrocytes and neurons are closely connected. Astrocytes respond to neurotransmitters released by neurons, and vice

versa neurons respond to factors released by astrocytes that influence synaptic activity and function of neurons[64]. This could explain the changes we find on gene expression in both neurons and astrocytes that are linked to a different neuronal maturation state of neurons.

Furthermore, both iNeurons and astrocytes exhibited increased expression of genes related to adhesion, migration, and ECM organization upon culture on the microfluidic chips. Previous studies have shown upregulation of cell motility, axon guidance and cell morphogenesis[35] in neurons when cultured in 3D *versus* 2D, in line with our findings. It is unclear which aspect of the microenvironment accounts for changes in cell adhesion and ECM organization. Both the substrate (PDMS and polyester membranes) and the geometry on the microfluidic chip are different from the flat tissue-culture treated polystyrene found in a well plate and could contribute to these factors.

We show that differentiation of hiPSCs to neurons is possible from DIV0, preventing the need to transfer neurons at a later stage during development. Using this approach, we performed, for the first time, the full differentiation process on the microfluidic chip, from hiPSC to neurons up to 38 days *in vitro.* We also show that co-culture of all three cell types together on a microfluidic chip to obtain functional iNeurons and a separate monolayer of endothelial cells is not possible if the endothelial cells are added after long-term culture of iNeurons. The incomplete endothelial monolayer formation is most likely the result of neurites extending into the endothelial compartment, thereby affecting the surface on which endothelial cells need to attach. Sances *et al*.[25] observed the same problem when co-culturing hiPSC-derived spinal cord neurons and endothelial cells and demonstrate the problem can be solved by changing the order of seeding cell types, allowing the formation of an endothelial monolayer before introducing neurons. The use of HUVECs as the primary vascular cell type in our study poses a limitation. Although HUVECs are widely used in modelling the NVU and the BBB *in vitro*[29,46,47], other cell types (e.g. primary human brain microvascular endothelial cells) may function differently when cultured with neurons in a microfluidic chip. For example, the incomplete formation of an endothelial layer that we observed upon co-culture could also be the result of not using a different brain specific cell source such as human brain microvascular endothelial cells or even induced brain microvascular endothelial cells[66]. Studies that use such cell types for co-culture with neurons in microfluidic chips have demonstrated clear monolayer formation[67]. Using iPSC-

derived cells would also enable a more patient-specific model and prevent potential issues in transcriptomic profile comparisons due to different cell sources.

Altogether, our data show clear cell type-specific responses in gene expression dependent on culture system. We show endothelial cells cultured on microfluidic chip more closely resemble *in vivo* conditions, and neurons cultured on microfluidic chip are more mature. These results show the microfluidic chip could be used as a useful tool to model the NVU. Our findings can serve as a reference point for future studies towards application of microfluidic chips in modelling the NVU to study its function and its role in pathology of neurological disorders.

5.5 Conclusion and outlook

In this paper we show a new, open-top microfluidic chip that allows for controlled integration of multiple cell types to model the neurovascular unit (NVU). We demonstrate that for different cell types (co-cultures of hiPSC-derived neurons and astrocytes, and monocultures of endothelial cells) separately cultured on the microfluidic chip, cell type-specific gene expression profiles are highly dependent on culture system. These findings can serve as a reference point for future studies to study interactions between cell types, to increase understanding on neurovascular physiology and neurovascular disease. The use of hiPSC-derived neurons from individual patients will give insight in patient variability in disease and allows identification of patient-specific responses to treatment.

Acknowledgements

Jan Eijkel is acknowledged for his help in setting up the administrative aspects of the project. We thank the department of Molecular Developmental Biology at the Radboud Institute of Molecular Life Sciences for RNA library sequencing. This study was financially supported by a pre-seed research grant from the Twente University RadBoudumc Opportunities (TURBO) program (to ADvdM, CAA and NNK), established by the University of Twente and Radboudumc. This work was supported by the Netherlands Organ-on-Chip Initiative, an NWO Gravitation project (024.003.001) funded by the Ministry of Education, Culture and Science of the government of the Netherlands (to ADvdM). This work was supported by grants from the Netherlands Organization for Health Research and Development (ZonMW grants 91217055 to N.N.K)

References

1. R.J. Jakel, B.L. Schneider, C.N. Svendsen. Using human neural stem cells to model neurological disease. *Nat. Rev. Genet.* **2004**, 5 (2), 136–144.
2. Y. Sharif, F. Jumah, L. Coplan, et al. Blood brain barrier: A review of its anatomy and physiology in health and disease. *Clin. Anat.* **2018**, 31 (6), 812–823.
3. N.J. Abbott, L. Rönnbäck, E. Hansson. Astrocyte–endothelial interactions at the blood–brain barrier. *Nat. Rev. Neurosci.* **2006**, 7, 41–53.
4. A.H. Bell, S.L. Miller, M. Castillo-Melendez, A. Malhotra. The Neurovascular Unit: Effects of Brain Insults During the Perinatal Period. *Front. Neurosci.* **2020**, 13 (January), 1–19.
5. Z. Gao, E.M. Cilento, T. StewartJ, J. Zhang. Chapter 1: Vascular Dysfunction and Neurodegenerative Disease. In *Vessel Based Imaging Techniques*; Yuan, C., Hatsukami, T. S., Mossa-Basha, M., Eds.; Springer Nature Switzerland AG, Seattle, **2020**; pp 3–16.
6. G. Potjewyd, S. Moxon, T. Wang, M. Domingos, N.M. Hooper. Tissue Engineering 3D Neurovascular Units: A Biomaterials and Bioprinting Perspective. *Trends Biotechnol.* **2018**, 36 (4), 457–472.
7. B.D. Gastfriend, S.P. Palecek, E. V. Shusta. Modeling the blood–brain barrier: Beyond the endothelial cells. *Curr. Opin. Biomed. Eng.* **2018**, 5 (i), 6–12.
8. M.T. Pham, K.M. Pollock, M.D. Rose, et al. Generation of human vascularized brain organoids. *Neuroreport* **2018**, 29 (7), 588–593.
9. O. Ham, Y.B. Jin, J. Kim, M.O. Lee. Blood vessel formation in cerebral organoids formed from human embryonic stem cells. *Biochem. Biophys. Res. Commun.* **2020**, 521 (1), 84–90.
10. B. Cakir, Y. Xiang, Y. Tanaka, et al. Engineering of human brain organoids with a functional vascular-like system. *Nat. Methods* **2019**, 16 (11), 1169–1175.
11. S.N. Bhatia, D.E. Ingber. Microfluidic organs-on-chips. *Nat. Biotechnol.* **2014**.
12. H.H.T. Middelkamp, A.D. van der Meer, J.M. Hummel, et al. Organs-on-Chips in Drug Development: The Importance of Involving Stakeholders in Early Health Technology Assessment. *Appl. Vitr. Toxicol.* **2016**, 00 (00), aivt.2015.0029.
13. P. Nikolakopoulou, R. Rauti, D. Voulgaris, et al. Recent progress in translational engineered in vitro models of the central nervous system. *Brain* **2020**.
14. D.Y. Park, J. Lee, J.J. Chung, Y. Jung, S.H. Kim. Integrating Organs-on-Chips: Multiplexing, Scaling, Vascularization, and Innervation. *Trends Biotechnol.* **2020**, 38 (1), 99–112.
15. M.W. van der Helm, A.D. van der Meer, J.C.T. Eijkel, A. van den Berg, L.I. Segerink. Microfluidic organ-on-chip technology for blood-brain barrier research. *Tissue barriers* **2016**, 4 (1), e1142493.
16. A. Van Den Berg, C.L. Mummery, R. Passier, A.D. Van der Meer. Personalised organs-on-chips: functional testing for precision medicine. *Lab Chip* **2019**, 19 (2), 198–205.
17. J. Ellis, M. Bhatia. IPSC technology: Platform for drug discovery. *Clin. Pharmacol. Ther.* **2011**, 89 (5), 639–641.
18. Y.A. Jodat, M.G. Kang, K. Kiaee, et al. Human-Derived Organ-on-a-Chip for Personalized Drug Development. *Curr. Pharm. Des.* **2019**, 24 (45), 5471–5486.
19. H. Inoue, S. Yamanaka. The use of induced pluripotent stem cells in drug development. *Clin. Pharmacol. Ther.* **2011**, 89 (5), 655–661.
20. G.D. Vatine, R. Barrile, M.J. Workman, et al. Human iPSC-Derived Blood-Brain Barrier Chips Enable Disease Modeling and Personalized Medicine Applications. *Cell Stem Cell* **2019**, 24 (6),

995-1005.e6.

21. A. Sharma, S. Sances, M.J. Workman, C.N. Svendsen. Multi-lineage Human iPSC-Derived Platforms for Disease Modeling and Drug Discovery. *Cell Stem Cell* **2020**, 26 (3), 309–329.
22. J.A. Brown, V. Pensabene, D.A. Markov, et al. Recreating blood-brain barrier physiology and structure on chip: A novel neurovascular microfluidic bioreactor. *Biomicrofluidics* **2015**, 9 (5), 1–15.
23. J.A. Brown, S.G. Codreanu, M. Shi, et al. Metabolic consequences of inflammatory disruption of the blood-brain barrier in an organ-on-chip model of the human neurovascular unit. *J. Neuroinflammation* **2016**, 13 (1), 1–17.
24. Y.I. Wang, H.E. Abaci, M.L. Shuler. Microfluidic blood–brain barrier model provides in vivo-like barrier properties for drug permeability screening. *Biotechnol. Bioeng.* **2017**, 114 (1), 184–194.
25. S. Sances, R. Ho, G. Vatine, et al. Human iPSC-Derived Endothelial Cells and Microengineered Organ-Chip Enhance Neuronal Development. *Stem Cell Reports* **2018**, 10 (4), 1222–1236.
26. T.E. Park, N. Mustafaoglu, A. Herland, et al. Hypoxia-enhanced Blood-Brain Barrier Chip recapitulates human barrier function and shuttling of drugs and antibodies. *Nat. Commun.* **2019**, 10 (1), 1–12.
27. M.R. Zanotelli, H. Ardalani, J. Zhang, et al. Stable engineered vascular networks from human induced pluripotent stem cell-derived endothelial cells cultured in synthetic hydrogels. *Acta Biomater.* **2016**, 35, 32–41.
28. M. Campisi, Y. Shin, T. Osaki, et al. 3D self-organized microvascular model of the human blood-brain barrier with endothelial cells, pericytes and astrocytes. *Biomaterials* **2018**, 180, 117–129.
29. G. Adriani, D. Ma, A. Pavesi, R.D. Kamm, E.L.K. Goh. A 3D neurovascular microfluidic model consisting of neurons, astrocytes and cerebral endothelial cells as a blood-brain barrier. *Lab Chip* **2017**, 17 (3), 448–459.
30. K.L. Sellgren, B.T. Hawkins, S. Grego. An optically transparent membrane supports shear stress studies in a three-dimensional microfluidic neurovascular unit model. *Biomicrofluidics* **2015**, 9 (6), 6–10.
31. B.M. Maoz, A. Herland, E.A. FitzGerald, et al. A linked organ-on-chip model of the human neurovascular unit reveals the metabolic coupling of endothelial and neuronal cells. *Nat. Biotechnol.* **2018**, No. July.
32. A. Herland, A.D. Van Der Meer, E.A. FitzGerald, et al. Distinct contributions of astrocytes and pericytes to neuroinflammation identified in a 3D human blood-brain barrier on a chip. *PLoS One* **2016**, 11 (3), 1–21.
33. F.R. Walter, S. Valkai, A. Kincses, et al. A versatile lab-on-a-chip tool for modeling biological barriers. *Sensors Actuators, B Chem.* **2016**, 222, 1209–1219.
34. Y. Wang, L. Wang, Y. Guo, Y. Zhu, J. Qin. Engineering stem cell-derived 3D brain organoids in a perfusable organ-on-a-chip system. *RSC Adv.* **2018**, 8 (3), 1677–1685.
35. H. Tekin, S. Simmons, B. Cummings, et al. Effects of 3D culturing conditions on the transcriptomic profile of stem-cell-derived neurons. *Nat. Biomed. Eng.* **2018**, 1–15.
36. M. Frega, S.H.C. van Gestel, K. Linda, et al. Rapid Neuronal Differentiation of Induced Pluripotent Stem Cells for Measuring Network Activity on Micro-electrode Arrays. *J. Vis. Exp.* **2017**, No. 119, 1–10.
37. S.M. Ho, B.J. Hartley, J. TCW, et al. Rapid Ngn2-induction of excitatory neurons from hiPSC-derived neural progenitor cells. *Methods* **2016**, 101, 113–124.
38. N.J. Allen, C. Eroglu. Cell biology of astrocyte-synapse interactions Nicola. *Neuron* **2017**, 96(3),

697–708.

39. Nicola J. Allen, M.L. Bennett, L.C. Foo, et al. Astrocyte glypicans 4 and 6 promote formation of excitatory synapses via GluA1 AMPA receptors. *Nature.* **2012**, 410–414.
40. M.R. Witcher, Y.D. Park, M.R. Lee, et al. Three-dimensional relationships between perisynaptic astroglia and human hippocampal synapses. *Glia* **2010**, 58 (5), 572–587.
41. A.R. Bialas, B. Stevens. TGF-β Signaling Regulates Neuronal C1q Expression and Developmental Synaptic Refinement. *Nat Neurosci.* **2013**, 16(12), 1773–1782.
42. W.-S. Chung, L.E. Clarke, G.X. Wang, et al. Astrocytes mediate synapse elimination through MEGF10 and MERTK pathways. *Nature* **2013**, 504(7480), 394–400.
43. J.T. Gonçalves, S.T. Schafer, F.H. Gage. Adult Neurogenesis in the Hippocampus: From Stem Cells to Behavior. *Cell* **2016**, 167 (4), 897–914.
44. A. Faissner, M. Pyka, M. Geissler, et al. Contributions of astrocytes to synapse formation and maturation - Potential functions of the perisynaptic extracellular matrix. *Brain Res. Rev.* **2010**, 63 (1–2), 26–38.
45. M.A. Johnson, J.P. Weick, R.A. Pearce, S.C. Zhang. Functional neural development from human embryonic stem cells: Accelerated synaptic activity via astrocyte coculture. *J. Neurosci.* **2007**, 27 (12), 3069–3077.
46. S. Bang, S.R. Lee, J. Ko, et al. A Low Permeability Microfluidic Blood-Brain Barrier Platform with Direct Contact between Perfusable Vascular Network and Astrocytes. *Sci. Rep.* **2017**, 7 (1), 1–10.
47. L.A. Rocha, E.D. Gomes, J.L. Afonso, et al. In vitro Evaluation of ASCs and HUVECs Co-cultures in 3D Biodegradable Hydrogels on Neurite Outgrowth and Vascular Organization. *Front. Cell Dev. Biol.* **2020**, 8 (June), 1–14.
48. F.R. Kreitzer, N. Salomonis, A. Sheehan, et al. A robust method to derive functional neural crest cells from human pluripotent stem cells. *Am. J. Stem Cells* **2013**, 2 (2), 119–131.
49. J. Berthier, K.A. Brakke, E. Berthier. Open Microfluidics; John Wiley & Sons, **2016**.
50. A.M. Bolger, M. Lohse, B. Usadel. Trimmomatic: A flexible trimmer for Illumina sequence data. *Bioinformatics* **2014**, 30 (15), 2114–2120.
51. A. Dobin, C.A. Davis, F. Schlesinger, et al. STAR: Ultrafast universal RNA-seq aligner. *Bioinformatics* **2013**, 29 (1), 15–21.
52. S. Anders, P.T. Pyl, W. Huber. HTSeq-A Python framework to work with high-throughput sequencing data. *Bioinformatics* **2015**, 31 (2), 166–169.
53. R Core Team. R: A Language and Environment for Statistical Computing. R Foundation for Statistical Computing, Vienna, Austria 2019.
54. M.I. Love, W. Huber, S. Anders. Moderated estimation of fold change and dispersion for RNA-seq data with DESeq2. *Genome Biol.* **2014**, 15 (12), 1–21.
55. M.D. Young, M.J. Wakefield, G.K. Smyth, A. Oshlack. Gene ontology analysis for RNA-seq: accounting for selection bias. *Genome Biol.* **2010**, 11 (2).
56. A. Subramanian, P. Tamayo, V.K. Mootha, et al. Gene set enrichment analysis: A knowledge-based approach for interpreting genome-wide expression profiles. *Proc. Natl. Acad. Sci.* **2005**, 102 (43), 15545–15550.
57. H.H.T. Middelkamp, A.H.A. Verboven, P.A.C. 't Hoen, N.N. Kasri, A.D. van der Meer. GSE154799 Metadata: Transcriptomic profiles of endothelial cells, induced pluripotent stem cell-derived neurons and astrocytes cultured on a microfluidic chip undergo changes in a cell type-specific manner https://www.ncbi.nlm.nih.gov/geo/query/acc.cgi?acc=GSE154799.

58. D.G. Stupack, D.A. Cheresh. Integrins and Angiogenesis. *Curr. Top. Dev. Biol.* **2004**, 64, 207–238.
59. S.M. Weis, D.A. Cheresh. av Integrins in Angiogenesis and Cancer. *Cold Spring Harb Perspect Med2011;1a006478* **2011**, 1–14.
60. A.Y.S. Law, C.K.C. Wong. Molecular and Cellular Endocrinology Stanniocalcin-1 and -2 promote angiogenic sprouting in HUVECs via VEGF / VEGFR2 and angiopoietin signaling pathways. *Mol. Cell. Endocrinol.* **2013**, 374 (1–2), 73–81.
61. L. He, T. Wang, Q. Gao, et al. Stanniocalcin-1 promotes tumor angiogenesis through up-regulation of VEGF in gastric cancer cells. *J. Biomed. Sci.* **2011**, 1–9.
62. X.H.J. Kim, A.M. Denli, R. Wright, et al. REST Regulates Non – Cell-Autonomous Neuronal Differentiation and Maturation of Neural Progenitor Cells via Secretogranin II. **2015**, 35 (44), 14872–14884.
63. R. Fischer-colbrie, R. Kirchmair, C. Olenik, D.K. Meyer, H. Winkler. Secretogranin II Is Synthesized and Secreted in Astrocyte Cultures. *Journul Neurochem.* **1993**, 2312–2314.
64. C.A. Durkee, A. Araque. Diversity and Specificity of Astrocyte–neuron Communication. *Neuroscience* **2019**, 396, 73–78.
65. C. Zheng, X. Zhang, C. Li, Y. Pang, Y. Huang. Microfluidic Device for Studying Controllable Hydrodynamic Flow Induced Cellular Responses. *Anal. Chem.* **2017**, 89 (6), 3710–3715.
66. R.G. Lim, C. Quan, A.M. Reyes-Ortiz, et al. Huntington's Disease iPSC-Derived Brain Microvascular Endothelial Cells Reveal WNT-Mediated Angiogenic and Blood-Brain Barrier Deficits. *Cell Rep.* **2017**, 19 (7), 1365–1377.
67. L. Delsing, P. Dönnes, J. Sánchez, et al. Barrier Properties and Transcriptome Expression in Human iPSC-Derived Models of the Blood–Brain Barrier. *Stem Cells* **2018**, 1–12.

Author contributions statement

H.H.T.M and A.H.A.V. conducted the experiments and analyzed the results. A.G.D.S.V and H.H.T.M designed the microfluidic chip. iPSC and astrocyte maintenance was performed by C.S and T.M.K.G respectively. A.D.M, N.N.K, P.A.C.H, C.A.A and R.P supervised the study. All authors wrote and revised the manuscript.

Supplementary information

Supplementary video and tables can be downloaded via:

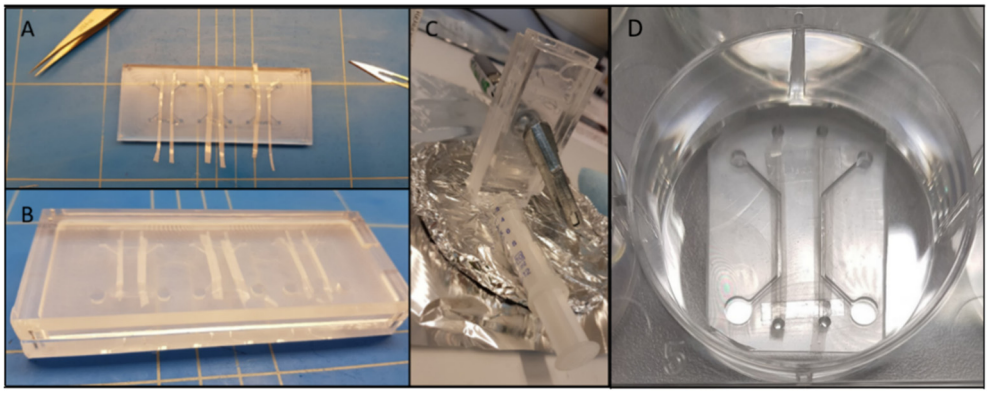

Supplementary figure 5-1: The process of incorporating the membrane of the microfluidic chip using injection moulding. A: Membranes are cut into slices slightly wider than channel. Using double sided scotch tape, the membranes are attached on top of the curved channels. B: Both sides of the mould (curved and straight channel separated by the membrane are pieced together. C: Using a 12 ml syringe needle approximately 8 ml of PDMS is pushed between the moulds and cured in an oven. D: Microfluidic chips are bonded to a round 32mm coverslip using plasma activation. Microfluidic chips fit into a 6 well plate for convenience.

Supplementary section Co-culture:

Methods:

Culturing of iNeurons and endothelial cells together on the same microfluidic chip was performed similar to culturing of the cell types separately on a microfluidic chip (See methods; section Cell culturing). The bottom channels were coated alongside the top channels with 20 µg/ml laminin on DIV 0. On DIV1 hiPSCs were plated and differentiated into iNeurons on the top channel, with addition of rat astrocytes on DIV2. On DIV37, endothelial cells were seeded onto the bottom of the membrane and co-cultured for 24 hours with the iNeurons.

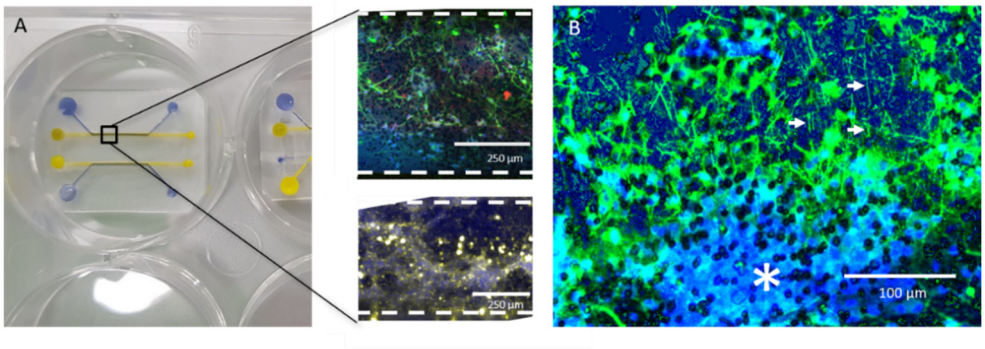

Supplementary figure 5-2: (Co-)cultures of iNeurons and endothelial cells. A: Staining performed on neurons differentiated in the top channel and endothelial cells in the bottom channel of the microfluidic chip on a polyester membrane. Endothelial cells no longer formed a monolayer but formed structures resembling typical pseudo capillaries. Blue: Nuclei; Green: Microtubule Associated Protein 2 (MAP2); Red: Synapsin-1/2 (SYN1/2); Yellow: F-actin. B: Neurite infiltration (arrows) through membrane in endothelial (asterisk) field of focus, Blue: Nuclei; Green: MAP2.

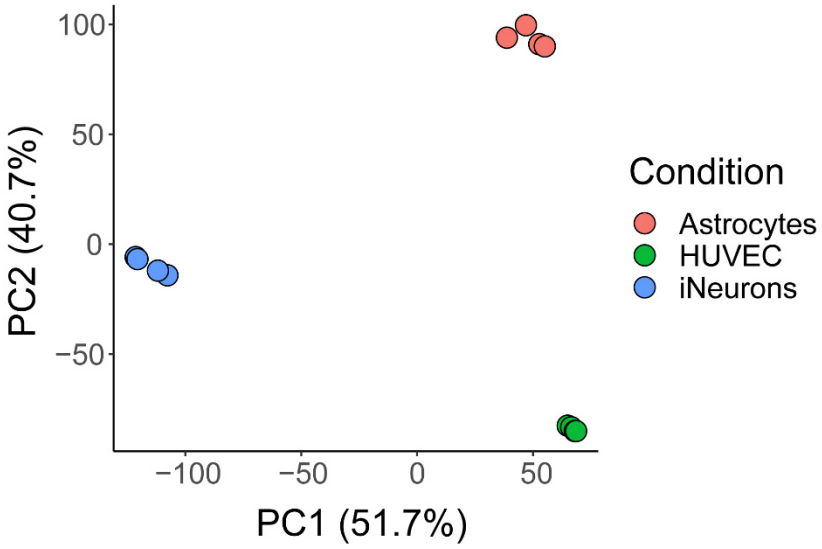

Supplementary figure 5-3: Principal component analysis (PCA) performed on HUVEC, iNeuron and astrocyte samples, including all genes for which a human homologue is available (n=16,074). PC1 and PC2 are shown. Samples are colored per cell type.

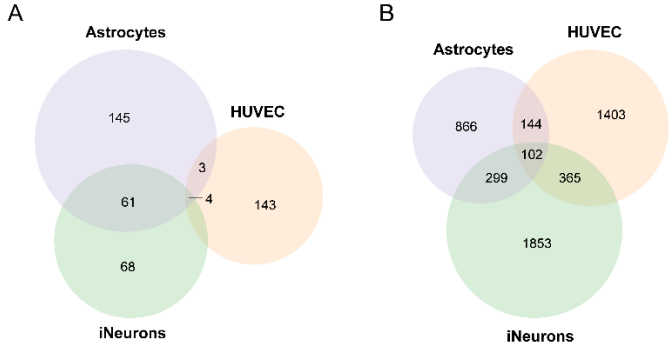

Supplementary figure 5-4. Venn diagrams showing overlap of A) GO terms and B) differentially expressed (DE) genes identified per cell type (iNeurons, astrocytes, and HUVEC) when comparing 3D to 2D culture systems (adjusted p-value < 0.05).

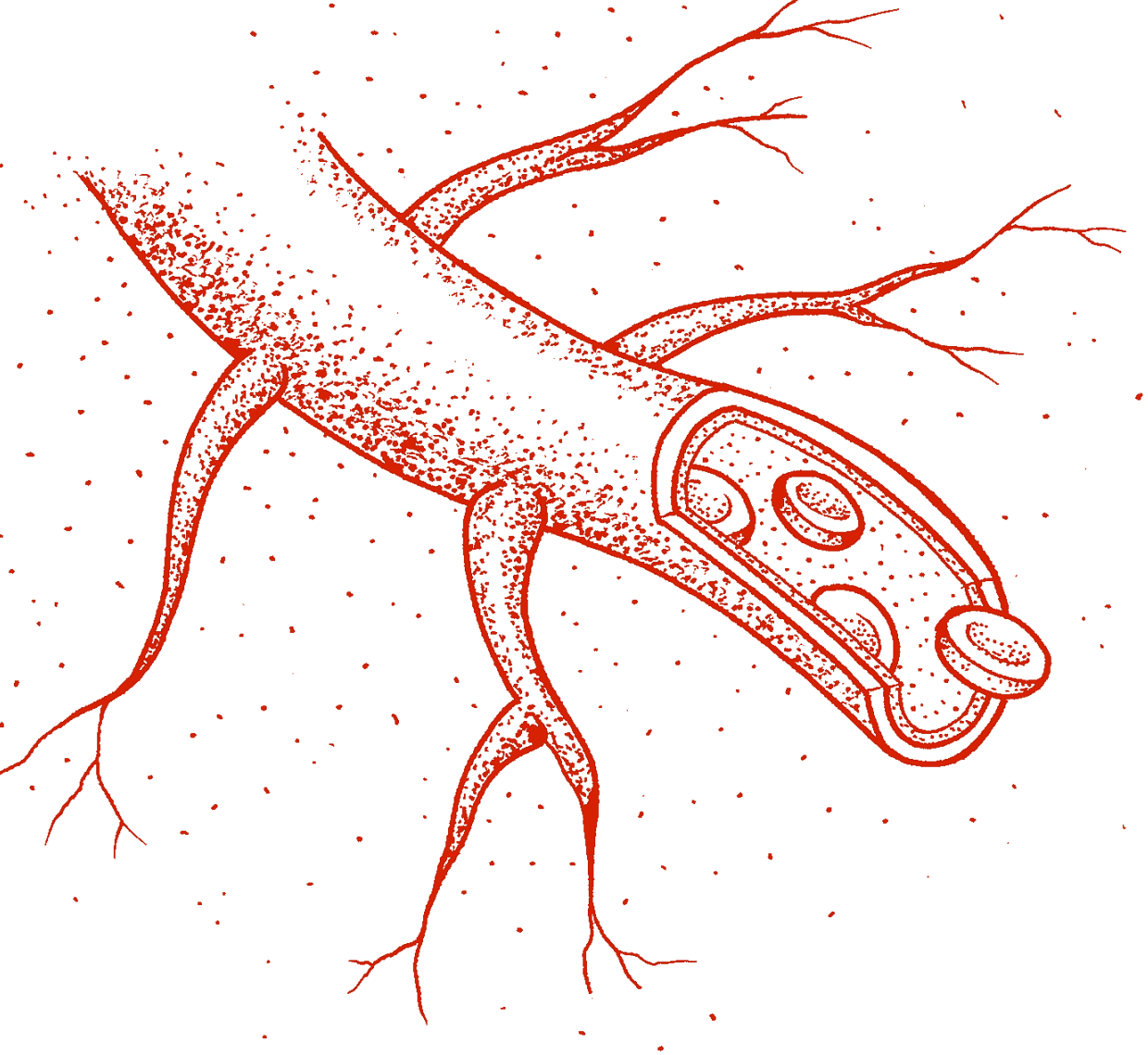

6

Blood vessel-on-chip based thrombus formation and visualization with optical coherence tomography

H.H.T. Middelkamp*
C. Cuartas-Velez*
A. van den Berg
A.D. van der Meer
N. Bosschaart

*Equal author contribution
Manuscript submitted

Abstract

Thrombus formation is a physiological response to blood vessel damage, which relies on a complex interplay of blood platelets and coagulation factors, as well as immune cells and the vessel wall. The dynamics of thrombus formation are essential for a deeper understanding of many disease processes, such as bleeding, wound healing, and thrombosis. However, monitoring thrombus formation *in vivo* is challenging due to the limited imaging options available. In this work, we use a visible-light optical coherence tomography (vis-OCT) system to monitor the dynamic process of the formation of thrombi in a microfluidic blood vessel-on-chip (VoC) device. Inside the VoC, thrombi form inside a channel that is lined with a monolayer of endothelial cells and that is perfused by human whole blood. By thresholding the decorrelation of the OCT signal during thrombus formation, we track the growth of thrombi over time. We validate our results with fluorescence microscopic imaging of fibrin and platelet markers. In conclusion, we demonstrate that the correlation of the vis-OCT signal can be used to visualize both the spatial and temporal behavior of the formation of thrombi in flowing human whole blood.

6.1 Introduction

Thrombus formation is a physiological response to prevent excessive blood loss when a blood vessel is damaged. When vascular injury occurs, platelets become activated and they interact with the extracellular matrix underneath the vascular endothelium, causing them to adhere to the injured vessel. The activated platelets form a stable plug held in place with fibrin. Under hemostatic circumstances, thrombi are dissolved during fibrinolysis and cleared by the body[1,2]. However, coagulation disorders, endothelial dysfunction and inflammation can all affect the normal formation or clearing of a thrombus, thus increasing the risk for severe health-threatening diseases such as deep vein thrombosis[3,4], pulmonary embolism[5], stroke[6,7], and heart attack[8,9]. Consequently, understanding, parameterizing, and measuring the thrombus formation is essential for developing preventive and therapeutic strategies in many cardiovascular and hematologic disorders.

Several techniques focusing on different physical properties of blood have emerged to monitor thrombus formation[10]. These techniques include electrical[11–13], and electrochemical signals[14], electro-mechanical analysis[15–17], photoacoustics[18,19], and optical detection[20–22]. Electrical signals utilize the change in the intrinsic impedance of blood during thrombus formation[12,13]. By recording the impedance over time, parameters related to thrombus formation can be precisely estimated[11]. Electrochemical methods use aptamer-based sensing to evaluate parameters related to thrombus formation, such as the clotting time[14]. Electro-mechanical signals leverage on the change of viscoelastic properties of blood during thrombus formation[15]. Using microelectromechanical (MEMS) resonators in contact with the clotting blood, the dynamics of thrombus formation and important parameters of this process (i.e., coagulation time, platelet aggregation, and tissue factor concentration) are measured[16]. Recently, Chen et al. developed a microfluidic integrated micro-clot array system to measure properties of thrombi under a simulated physiological shear flow[17]. Although these methods provide precise assessments, their main disadvantage lies in the static state or non-physiological flow of the blood. Therefore, they lack applicability to detailed studies of thrombus formation, where the shear wave velocity, tube size, and hematocrit modify the clotting process[23, 24]. Therefore, photoacoustic, and optical methods that analyze flowing blood offer an attractive alternative approach. In photoacoustics (PA), a pulsed laser beam illuminates the tissue with a given pulse rate. The tissue absorbs and reemits the energy from the pulse, producing acoustic waves measurable with

acoustic transducers[18]. Circulating thrombi are monitorable in real time since the PA signal is contactless[19]. However, its application remains restricted due to limited spatial and temporal resolution and high background noise. Other optical methods characterize thrombus formation through the interaction between blood and light[23,25]. By analyzing changes in the intensity of scattered or transmitted light, several parameters related to thrombus formation are quantifiable. Those include viscoelastic properties, shear modulus, flow velocity, and thrombus dynamics[21,22]. Moreover, optical coherence tomography (OCT) is growing in attention due to its potential application *in vivo* and capability to non-invasively characterize properties of whole blood, such as hematocrit[26], blood oxygen saturation[27], blood fibrinogen level[28], and total hemoglobin concentrations[29].

OCT uses backscattered light to create high-resolution images of tissue[30]. In the case of blood, the changes in viscoelastic properties of thrombus formation directly influence the absorption and scattering experienced by light[22,23]. Therefore, monitoring the dynamics of formation of thrombi based on the OCT signal over time has been demonstrated. By analyzing the decay of the OCT signal in thrombus formation, Xu et al. have investigated the clotting time under static and dynamic conditions for different blood flow velocities, hematocrits, tube sizes, and fibrinogen levels[23,24,28]. Furthermore, the authors developed an optical coherence elastography (OCE) method based on OCT to obtain viscoelastic properties of blood by estimating shear wave velocities and mechanical displacements[21]. However, OCE requires specialized equipment to induce mechanical waves with quantifiable movements. More recently, Tang et al. proposed a correlation-based technique to determine the coagulation time, thrombus formation duration, and thrombus strength from the OCT signal during coagulation[22]. Despite those promising results, the characterization of thrombus formation in contact with endothelial cells remains challenging due to lack of control over the process during *in vivo* experiments. Alternatively, advanced microfluidic cell culture models known as 'vessels-on-chips' (VoC) are now being used to study cellular-level interaction between thrombi and endothelial cells.

VoC devices are micro-physiological systems designed to mimic human vessels by culturing human vascular cells in a spatially controlled, dynamically perfused microenvironment[31–38]. VoC models are used for studying vascular inflammation and use blood perfusion assays to unveil the underlying mechanisms of these processes[39–47], thus thrombus formation has been previously simulated[48–50]. The dynamics of the

formation of a thrombus relies on the interplay of many parameters, such as platelet behavior[51,52]. Real-time information about the dynamic formation of a thrombus can facilitate understanding thromboembolic events that occur under different types of flow, thus easing anti-thrombotic drug development[53–55]. Using fluorescence microscopy, VoCs can reveal the aggregation of thrombus components, such as platelets and fibrin, during and after active blood perfusion. However, fluorescence microscopy is a limited read-out, as it relies on selected markers. Furthermore, these techniques only provide insight in two-dimensional end-point read-outs. Therefore, non-invasive real-time monitoring methods such as OCT present an opportunity to understand the dynamics of thrombus formation[56].

For the first time, we have combined OCT with a microfluidic VoC device to monitor thrombus formation over time. We show that decorrelation mapping OCT can follow the development of thrombi in real time. Furthermore, thrombus formation can be measured in multiple dimensions, showing not only the development of a thrombus in length and width, but also height. We use a visible-light OCT (vis-OCT) system to non-invasively monitor thrombus formation in the VoC. We argue that differences in the decorrelation signal can predict the thrombus formation and growth in flowing blood. We validate our results with microscopy images of labeled fibrin and platelets after blood perfusion assay. This OCT thrombus formation technique can be used to observe thrombus formation on other VoC devices, where multidimensional thrombus formation observations can lead to better understanding of clotting disorders and other vascular diseases.

6.2 Materials and methods

6.2.1 Microfluidic vessel-on-chip device

Microfluidic chip fabrication

The microfluidic chip consists of 4 channels which are 1 cm in length and 300 × 52 µm in width and height (as shown in figure 1a and figure 1b). The chip was fabricated by polydimethylsiloxane (PDMS, Sylgard 184, Mavom, the Netherlands)-based soft lithography using a negative wafer which was produced by SU-8-based lithography using designs made in CleWin (WieWin software, the Netherlands). PDMS was added to the wafer at a ratio of 10 : 1 (base: crosslinker), left to cure overnight at 65◦C, and removed after. Inlet and outlet holes of 1 mm were created employing biopsy punchers (RBP-10P, Robbins Instruments, USA). PDMS was spin-coated (SPS Spin150, SPS-international, The Netherlands) on a glass microscope slide (with

thickness ~ 150 µm), and it was left to cure overnight at 65◦C (figure 1a). The surfaces of the PDMS chip and the microscope slide were activated by exposing them to air plasma (50 W) for 40 s (Cute, Femto Science, South Korea), after which the microfluidic chip was bonded to the microscope slide, as displayed in figure 1a. The activated chip was then used for cell seeding (figure 1b).

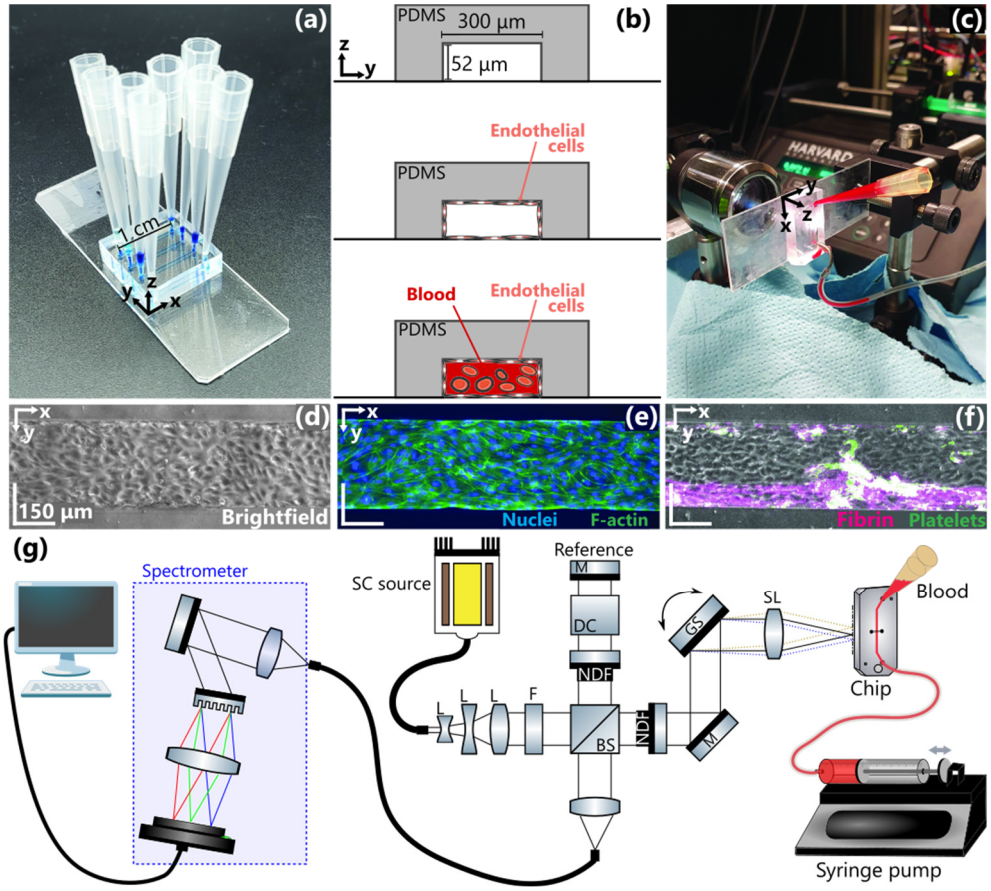

Figure 6-1: overview of blood perfusion assay using OCT imaging. (a) The microfluidic chip is made from PDMS and contains 4 straight channels which are separately assessable. (b) The microfluidic chip consists of a 1 cm long channel with 300 × 52 µm width and height. These channels are seeded with HUVECs and after 24 hours a monolayer has formed, after which blood can be perfused through the channels. (c) Overview of blood perfusion set-up when imaging using OCT. (d) Brightfield image of the quiescent cell monolayer. (e) Fluorescent microscopy image of the monolayer distinguishing nuclei in blue and F-actin in green. (f) After blood perfusion assay thrombus markers such as fibrin (in purple) and platelets (in green) are imaged using a fluorescent microscope. (g) Schematic illustration of the vis-OCT set-up used to monitor thrombus formation. L: Lens, SC: Supercontinuum, F: Filter, NDF: Neutral density filter, BS: Beam splitter, DC: Dispersion compensation element, M: Mirror, GS: Galvanometer scanner, SL: Scanning lens.

Cell culturing and seeding

Human umbilical vein endothelial cells (HUVECs LO CC-2519, Westburg, The Netherlands) were cultured in pre-coated collagen culture flasks (#690950, Greiner Bio One, The Netherlands) at 37 °C and 5% CO_2 using endothelial cell growth medium 2 (EGM-2, #C-22111, PromoCell inc., Germany). Immediately after plasma activation, chips were coated using a 0.1 mg/ml collagen solution (Collagen type-I, rat tail #A1048301, Thermofisher, The Netherlands). The coating was incubated at 37 °C and 5% CO_2 for one hour. The coated chips were flushed with EGM-2 and prepared for cell seeding. HUVECs were removed from the cell culture flask by incubation with 3 ml Trypsin-EDTA (#15400054, Thermofisher, The Netherlands) for 3 minutes at 37 °C and 5% CO_2. A cell culture medium in a 1 : 2 ratio was added to the flask to inactivate trypsin. The cells were centrifuged for 5 minutes at 390 ×*g* and counted using a brightfield cell counter (Luna™ automated cell counter, logos biosystems, France).

The cells were seeded on the top and bottom of the channel at $15 \cdot 10^6$ cells/ml for at least 30 min for HUVECs to attach (figure 1b). A total of 150 µl of EGM-2 was added to the microfluidic channels, and the chips were placed on a rocking table (BenchBlotter™ 2D platform rocker, benchmark scientific, USA) inside the incubator for 24 hours, after which a perfusable monolayer was formed (figure 1b and figure 1d). To observe the endothelial monolayer, F-actin and DNA in the cells were stained with Phalloidin-A488 and DAPI (R37110, R37605 Thermofisher, the Netherlands) as depicted in figure 1e.

Blood perfusion assay

The Experimental Centre for Technical Medicine (ECTM, Techmed Centre, University of Twente) provided human whole blood samples. This research did not fall within the scope of the Dutch Medical Research Involving Human Subjects Act. In agreement with the Declaration of Helsinki, all volunteers gave written informed consent. Furthermore, the local medical research ethics committee (METC Twente) approved the blood collection procedure. Whole blood samples were collected in vacuvette tubes containing 3.2% citrate (#455322, GreinerBio, The Netherlands). The samples were used within 4 hours of the blood draw. Due to the risk of contamination with tissue thromboplastin during the blood draw, the first tube was discarded[57]. Then, platelets and fibrin were stained with CD41-PE (1% (v/v), #MHCD4104, Thermo Fisher, The Netherlands) and fluorescein-conjugated fibrinogen (Fibrinogen from human plasma, #F13192, Invitrogen, The Netherlands) respectively for 10 minutes. A bent 14 gauge blunt needle replaced the outlet pipette tip and connected the chip

through tubing (Tygon, Fishersci, The Netherlands) to a syringe pump (Harvard PHD 2000, Harvard Apparatus, USA). Immediately before the perfusion assay, blood was recalcified using a recalcification buffer containing HEPES (15630080, Thermofisher, The Netherlands), 63.2 mM $CaCl_2$ (#21115, Merck, Germany), and 31.6 mM $MgCl_2$ (#J61014.AK, Thermofisher, The Netherlands). During blood perfusion, blood was pulled through the channel at 7.8 µl/min for ~ 15 minutes, as shown in figure 1c. After that, channels were flushed with EGM-2 and fixated with 4% formaldehyde for 15 minutes. Finally, an EVOS M5000 imaging system (Thermofisher, The Netherlands) was used to obtain microscopy validation images at 4× magnification, as shown in figure 1f.

6.2.2 Optical coherence tomography

OCT system

We use a custom-built OCT system optimized for visible light and described in detail in our previous work[29,58] and schematized in figure 1g. Briefly, light propagates from a supercontinuum broadband source (SC, SuperK EXTREME EXB-6, NKT Photonics, Denmark) through three lenses (L1: LD2746-A, L2: LD2060-A, L3: LB1471-A, Thorlabs, USA) expand and collimate the beam. A short-pass filter (FESH0700, Thorlabs, USA) filters out all wavelengths above 700 nm before the light arrives at the open-air Michelson interferometer. In the interferometer, a 10 : 90 beam splitter (BS028, Thorlabs, USA) guides 90% of the incoming light towards the reference arm and 10% towards the sample arm. In the reference arm, a variable neutral density filter (NDC-50C-2M-A, Thorlabs, USA) controls the intensity of light propagating through a dispersion compensation block composed by a microscope slide as the one where the PDMS was molded (Section 2.1.1) and a lens equivalent dispersion glass (LSM03DC-VIS, Thorlabs, USA). Then, the reference mirror (PF10-03-P01, Thorlabs, USA) reflects the beam to the beam splitter. In the sample arm, a variable neutral density filter (NDC-50C-2M-A, Thorlabs, USA) attenuates the light propagating to a galvanometer scanner (8320K, Cambridge Technology, USA) that steers the beam. After the scanner, a scanning lens (LSM03-VIS, Thorlabs, USA) with a 39 mm focal length and 12 µm e^2 diameter focuses the beam at the channel of the VoC device. Backscattered light from the VoC and light reflected at the reference arm combine at the beam splitter and is collected by a single-mode fiber (S405XP, Thorlabs, USA). The fiber guides the light into a custom-built spectrometer (HoloSpec f/1.8i, Kaiser Optical Systems, USA), where a grating disperses it on a line camera (Sprint spL4096-140km, Basler, Germany). The camera has an exposure time of 58 µs at a line rate of 16.7 kHz. The spectrometer has a spectral resolution of 0.1

nm within 480 – 660 nm. The collected spectrum has a full width at half-maximum of ~ 75 nm centered at 555 nm, leading to a theoretical axial resolution of ~ 1.8 µm in air.

Imaging protocol

At the beginning of the blood perfusion assay, VoCs were placed in the OCT setup (figure 1c) and imaged continuously for 15 minutes. During this time, OCT scans were performed in a volume of 0.9 × 2 × 0.7 mm in z, x, y with a sampling of 1024 × 156 × 512 pixels, respectively. Each B-scan (plane zx) was repeated two times to allow the calculation of the correlation between consecutive B-scans. After the assay, an additional OCT scan of the VoC flushed was performed. Each OCT volume was flattened by aligning each A-line to the top boundary of the chip's channel.

Correlation mapping

Correlation mapping is employed to distinguish between clotted regions and flowing blood. As demonstrated by Tang et al.[22], the autocorrelation of the OCT signal decreases as blood coagulates. We leverage this idea to create a spatial map of the correlation and determine the presence of a thrombus by analyzing the difference in the correlation signal. For this method, the intensity from the first B-scan It,A is correlated to the intensity of the second B-scan It,B at each spatial location (x, y, z) and time t. By evaluating the decorrelation across the entire B-scans, a correlation map Ct (z, x, y) is calculated as[22,59]:

$$C_t(z,x,y) = \frac{\sum_{i=1}^{I}\sum_{j=1}^{J}\left(\left[I_{t,A}(z_i,x_j,y)-\overline{I_{t,A}}\right]\left[I_{t,B}(z_i,x_j,y)-\overline{I_{t,B}}\right]\right)}{\sqrt{\sum_{i=1}^{I}\sum_{j=1}^{J}\left[I_{t,A}(z_i,x_j,y)-\overline{I_{t,A}}\right]^2}\sqrt{\sum_{i=1}^{I}\sum_{j=1}^{J}\left[I_{t,B}(z_i,x_j,y)-\overline{I_{t,B}}\right]^2}}$$

(1)

where $I \times J$ is a window for which the correlation is calculated around the central point (z, x, y), $\overline{I_{t,A}} = \frac{1}{IJ}\sum_{i=1}^{I}\sum_{j=1}^{J} I_{t,A}(z_i, x_j, y)$ and $\overline{I_{t,B}} = \frac{1}{IJ}\sum_{i=1}^{I}\sum_{j=1}^{J} I_{t,B}(z_i, x_j, y)$ correspond to the mean intensity within the correlation window at location (x, y, z) for the two B-scans.

The correlation window spans 5 × 5 pixels (4.4 × 19.5 µm in zx) as this offered a reasonable trade-off between resolution and noise. The resulting correlation map ranges between −1 and 1, indicating weak and strong correlations, respectively. While low correlation values indicate red blood cells undergoing rapid motion, strong correlations represent static tissue or thrombi moving at a lower velocity [22].

Commonly, high correlation values ≥ 0.6 have indicated static tissue that does not undergo any motion[59–61]. However, in the case of a thrombus, they may present slow motion and weak diffusivity. Therefore, we defined the thrombus formation when the correlation remains ≥ 0.4 in our correlation maps. The correlation maps during the blood perfusion assay were binarized by thresholding $Ct \geq 0.4$. The thresholded maps at each time interval were utilized to retrieve quantitative information from the thrombi. The thrombus size, count, and area were calculated with the function bwboundries from MATLAB (version 2022a), assuming that the total area of one xy pixel is 17.5 µm2.

6.3 Results

6.3.1 Correlation-based thrombus formation

First, we evaluated the thrombus formation by analyzing the evolution of the correlation map as a function of time. Figure 2 shows the OCT intensity and correlation map during the blood perfusion assay. En-face and cross-sectional views of the OCT intensity from the VoC at the beginning of the assay are displayed in figure 2a. From these cross-sectional views, it can be observed that flowing blood produces a homogeneous intensity distribution inside the flow channel, while the boundary of the flow channel has higher intensity due to the presence of HUVECs and medium change. En-face images were produced by averaging the intensity in the red box in the cross-sections of figure 2 within the channel boundaries. The corresponding correlation map in figure 2b presents low correlation ($Ct \leq 0.4$), which indicates homogeneous flow. Small patches with high correlation $Ct \geq 0.4$ arise at the beginning of the assay, which are attributable to early thrombus formation. As time progresses, figure 2c exhibits low-intensity regions. These can be related to developing thrombi, where the accumulation of red blood cells attenuates more light than the free-flowing erythrocytes. The correlation map in figure 2d confirms the development and expansion of thrombi as the correlation value increases over time for the regions where lower flow is expected due to thrombus formation. The two spots indicated by the red arrows show the origin of two thrombi that become visible ~ 7 minutes into the assay. In the surrounding areas, the correlation is higher as time passes and the thrombus size increases. In contrast, the blue arrow indicates an area where homogeneous flow is present, and the correlation map presents low variation compared to the areas where thrombi have formed.

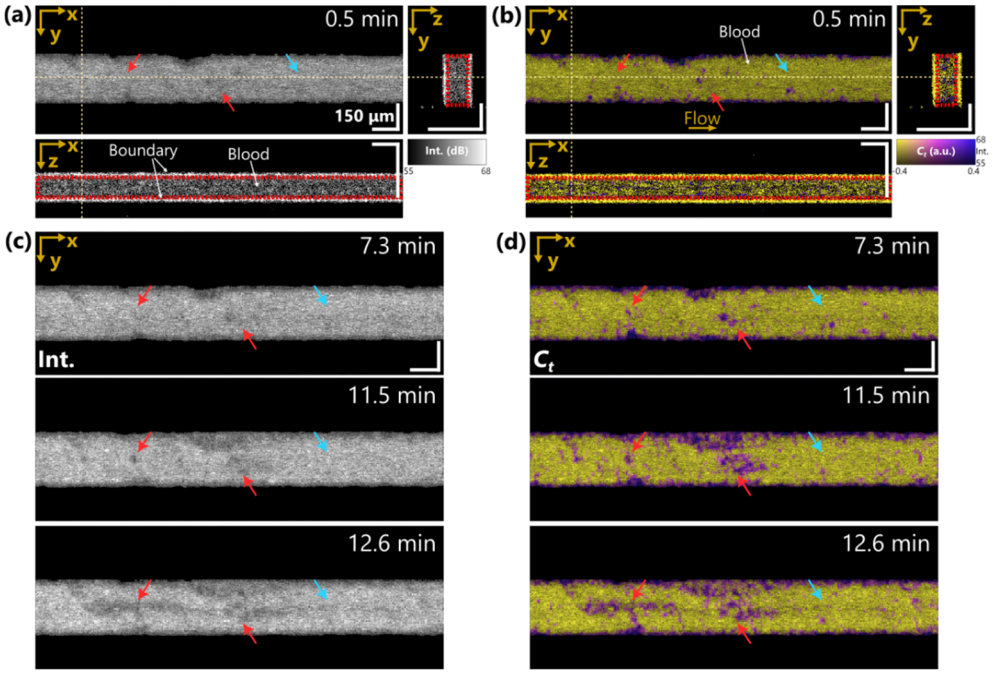

Figure 6-2: OCT intensity and correlation at selected times during the blood perfusion assay. (a) En-face and cross-sectional views of the VoC with flowing blood at the beginning of the blood perfusion assay, the channel boundary is visible in the cross-sectional views. En-face view and cross-sections of the correlation map Ct derived with Eq. (1) from (a) and (b). En-face images in (a) and (b) were produced by averaging the values within the red box indicated in the cross-sections. (c) En-face intensity and (d) correlation as a function of time during the blood perfusion assay. Red arrows indicate the origin of a thrombus. The blue arrow indicates a region without thrombus formation.

6.3.2 Thrombus formation validation

After the blood perfusion assay, the flow channel was flushed with cell culture medium, and an additional OCT scan was performed. Figure 3a shows the OCT intensity of the flushed VoC, where the final thrombi are visible. The cross-sectional views reveal that thrombi can occupy the full height of the channel. In figure 3b, the last correlation map just before flushing displays a significant portion of the chip where the correlation is below the defined threshold of $Ct \geq 0.4$. En-face images in figure 3a and 3b reveal a similar location where thrombi are expected from the correlation and are visible after flushing. The slight shift in the x-axis in 3a is due to the minor movement of the chip after the tip with blood (figure 1b) was removed. Figure 3c shows a direct comparison between the OCT signal and microscopy images taken after the blood perfusion assay at two separate locations in the microfluidic channel, indicated by box I (solid green line) and II (dashed blue line). During the blood perfusion assay, the OCT image shows a high intensity at sites with blood flow

due to the scattering by red blood cells. After the blood perfusion assay, the channels were flushed with cell culture medium and scanned once more. The flushed OCT intensity reveals the presence of thrombi at the suspected locations. This image was used to compare the OCT signal to the microscopy images. Because the blood was pre-stained with the fluorescent markers for fibrin (purple) and platelets (green), thrombi were imaged after the blood perfusion assay. The first and second rows of the regions of interest I and II in figure 3c show a similar shape among the correlation map, the OCT flushed signal and the microscopy images. The overlay image shows activated platelet adherence and fibrin threads at the site of the suspected thrombi. A visual comparison of the thrombus between the brightfield image and the flushed OCT channel reveals a similar pattern. As this pattern is also present in the correlation map, our results suggest the possibility for live image thrombus formation without the necessity of fluorescent markers.

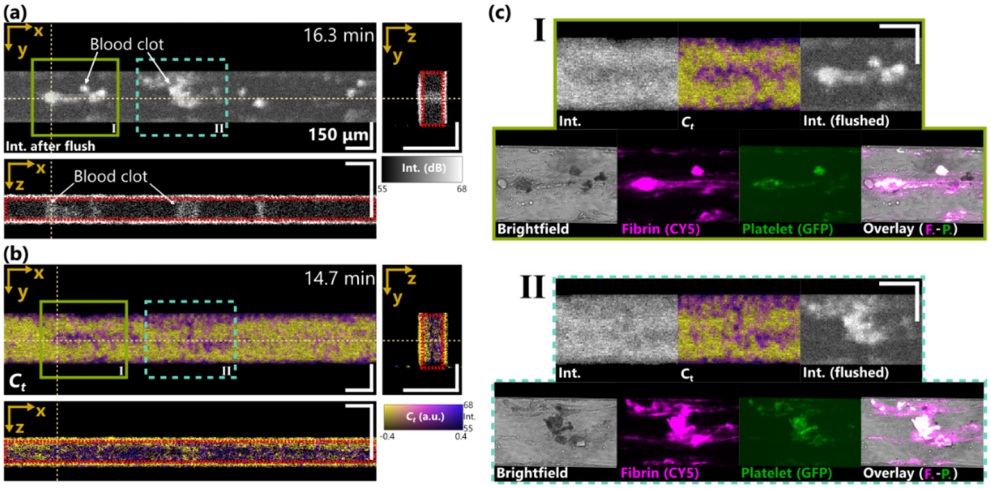

Figure 6-3: Thrombus formation and validation with microscopy images. (a) OCT intensity of the VoC after flushing. (b) Last correlation map before flushing the VoC, exhibiting thrombi presence. (c) OCT images from the regions of interest I and II in (a) and (b), and respective comparison with images obtained in the microscope consisting of brightfield, fibrin and platelets markers, and the corresponding overlay.

6.3.3 Thrombus growth

Finally, we evaluated the thrombus development and the total thrombus covered area over time. Figure 4 presents the evolution of the thrombi in the channel over time. Figure 4a is a color-encoded representation of the locations where $Ct \geq 0.4$ at a given time, where the color represents the moment in time that a pixel complies with the threshold. At the beginning of the assay, small thrombi appear at the

squared edges of the channel that remain in position until the end of the process. The origin of multiple large thrombi is visible short into the assay (~ 5 min) and highlighted with purple arrows in figure 4a. After ~ 10 min, the thrombi have minimally expanded, and the channel allows free blood flow. After ~ 12 minutes, the thrombus indicated by the right purple arrow has grown significantly. Near the end of the assay (~ 15 min), significantly larger thrombi appear. Figure 4b summarizes the dynamic behavior of the thrombus formation. The violin plot (obtained from the area of interest in figure 4a) shows that for most of the process (~ 11 minutes), the thrombus count and size remain constant. However, at the later stages of the process, bigger thrombi emerge and expand. Figure 4c demonstrates that the total area covered by thrombi inside the flow channel increases (figure 4).

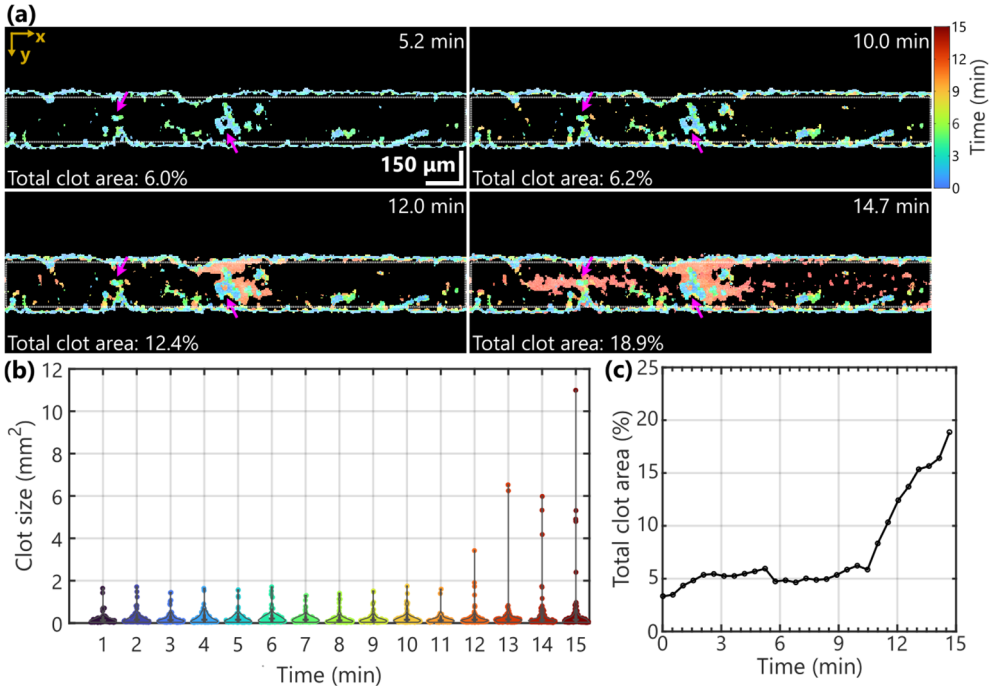

Figure 6-4: Thrombus formation, growth, and evolution over time. (a) Color-coded location of thrombi over time. The color represents the time at which a $Ct \geq 0.4$ was registered. The thrombotic area increases over time as the assay progresses. The purple arrows indicate the presumed origin of two thrombi. (b) Violin plot showing the distribution of thrombi over time within the area of interest (white box) in (a) (excluding the flow channel boundaries). As the assay progresses, bigger thrombi. (c) Total percentage area of the channel covered with thrombi as a function of time.

6.4 Discussion

In this work, we demonstrated that OCT can visualize the thrombus formation without fluorescent markers in flowing blood. We used a microfluidic VoC device to mimic the interaction between human-whole blood and endothelial cells. We combined a vis-OCT system with the VoC to simulate and image thrombi formation. By analyzing the correlation between two consecutive B-scans, we observed thrombus formation by thresholding the increase in correlation due to reduced blood flow in thrombi. We validated our observations with fluorescence microscopy images highlighting fibrin and platelets as thrombus markers. We found similarities between the final thrombi after flushing the VoC compared to the correlation maps at the end of the perfusion assay. Finally, we quantified thrombus formation by measuring the thrombus size and chip thrombus-covered area as a function of time. Our findings may have several applications in OCT imaging of thrombus formation in a VoC. In the remaining discussion, we review relevant aspects of our results and their applicability in different areas.

6.4.1 Thrombus formation monitoring

From the OCT data, we could detect thrombi formation in the VoC. As presented in figure 2, the OCT signal shows thrombi as a lower intensity signal, indicating more scattering and absorption by red blood cells. The presence of thrombi is even more notorious when analyzing the correlation signal. We found that if the size of the high correlation area increases over time (as presented in figure 4), those spots mark the origin of thrombi. However, we recognized that the constant blood flow washed out some of the thrombi. This can occur when a thrombus is formed but lacks proper adherence to the endothelial layer. The zx cross-section in figure 3a shows that the thrombi seem connected to the cell layer. This thrombus-endothelial interaction could not be observed during the blood perfusion assay, due to the constant change in correlation produced by the blood flow. A limitation of the vis-OCT system that was employed in this study, is the low acquisition rate compared to wavelength-swept source OCT (SS-OCT) systems[62,63]. Increasing the sampling rate could reveal thrombus expansion of in three dimensions. However, the availability of SS-OCT systems in the visible wavelength range is limited, and higher resolution (in the order of 5 µm) is beneficial to observe thrombus formation[64].

6.4.2 Correlation mapping as thrombus marker

We noticed that the correlation, thus thrombus formation, increases over time during the blood perfusion assay. We attribute this to the overall change in the

viscoelastic properties of the blood[22]. Thrombi attached to endothelial cells do not undergo the rapid motion of the free-flowing red blood cells, thus increasing the correlation when compared to the rapid change experienced by moving red blood cells. However, as the overall flowing blood is coagulating, the scattering red blood cells are expected to undergo slower motion, increasing the overall correlation value. Therefore, we defined a thrombus as a region where the correlation $Ct \geq 0.4$ in the flowing blood. The thrombus correlation value can vary among OCT systems since the correlation value depends on the camera line rate, the spatial sampling, and the number of B-scans averaged[59,60]. A significant expansion of the thrombi is observed after $\sim$ 10 minutes have elapsed, which can be explained by the exponential growth occurring in thrombus formation.

A limitation of the system is that we do not measure platelets or fibrin aggregation directly, but rather the changes in flow, which could lead to false positives in the data. There is a possibility of a shadow effect presenting before the thrombus due to a limited flow which is not due to an aggregate itself[60]. However, looking at the data after flushing, we have captured the final thrombus reasonably well. The shadow effect is negligible for endpoint measurements.

6.4.3 Validation with microscopy

As presented in figure 3a and figure 3b, visual microscopic thrombus inspection shows correspondence in location, shape, and size compared to the OCT results. However, due to the intermediate flushing step, the exact size and shape of the thrombi before flushing is unknown. Therefore, our OCT-based estimation of the thrombus size and area may be biased compared to the actual size of the thrombus after flushing. Figure 3c exhibits the limitation of conventional OCT intensity to identify thrombi since the contrast is low compared to the flowing blood. The brightfield image and fibrin and platelet markers in figure 3c have a similar appearance to the intensity of the flushed chip in OCT, even though OCT has a lower resolution. These images reveal a high correspondence between Ct at the end of the process and the location of thrombi.

6.4.4 Blood-vessel on a chip device

The VoC consists of rectangular microchannels, which are an abstraction of the actual anatomy of blood vessels *in vivo*. In the VoC, flowing blood components will experience a lower forward velocity in the corners of the channel, leading to higher residence times and exacerbated fibrin deposition. Consequently, we excluded the corner areas layer from the analyses of thrombus formation, as described earlier[39].

Excluding these areas with biological artifacts can affect the data analysis and lead to missing imperative information in the clotting process. Cylindrical VoC models[65–67] could be used to mimic the *in vivo* geometry more closely. The height of these cylindrical models is approximately 250 – 300 µm. With those sizes, OCT could unveil the interaction between endothelial cells and flowing blood in arterioles and venules. In our study, HUVECs were used to line the VoC. Although they are a commonly used cell type in blood vessel modeling, these cells are not patient specific, thereby limiting the applicability of the VoC in disease modeling. Therefore, similar research using OCT and human induced pluripotent stem cells (hiPSC-ECs) could determine patient-specific clotting mechanisms and responses.

6.5 Conclusion

In conclusion, we used vis-OCT to monitor the formation of thrombi in a VoC device. The VoC containing HUVECs simulated the interaction between flowing blood and endothelial cells. The OCT correlation signal provided a marker to observe the evolution of thrombi over time. By thresholding the correlation, we tracked the origin and growth of thrombi. The thrombi detected from the correlation signal were similar in shape and size to the OCT intensity measurements after flushing the chip and with microscopy images. Those microscopy images validated the presence of thrombi. As this pattern is also present in the correlation map, our results suggest the possibility for live image thrombus formation without the necessity of fluorescent markers. Furthermore, we were able to visualize the thrombus formation not only in width and length, but also in height. This dimension could not be determined in real -time using previous fluorescent marker experiments, but only as an end-point measurement using confocal microscopy. Thus, we show a new non-invasive technique to measure thrombus formation in real-time in 3 dimensions. This technique can now be applied in different, more complex, OoC systems to obtain greater understanding of thrombus formation and development and with that personalized drug development.

Acknowledgments

This work was supported by the Netherlands Organ-on-Chip Initiative, an NWO Gravitation project (024.003.001) funded by the Ministry of Education, Culture and Science of the government of the Netherlands.

Disclosures

The authors declare no conflicts of interest related to this work.

References

1. S. Palta, R. Saroe, and A. Palta, "Overview of the coagulation system," Indian J. Anaesth. **58**, 515–523 (2014).
2. M. H. Periayah, A. S. Halim, and A. Z. M. Saad, "Mechanism action of platelets and crucial blood coagulation pathways in hemostasis," Int. J. Hematol. Stem Cell Res. **11**, 319–327 (2017).
3. J. Stone, P. Hangge, H. Albadawi, A. Wallace, F. Shamoun, M. G. Knuttien, S. Naidu, and R. Oklu, "Deep vein thrombosis: pathogenesis, diagnosis, diagnosis, and medicam management," Cardiovasc. Diagn. Ther. **7**, S276–S284 (2017).
4. D. A. Anaya and A. B. Nathens, "Thrombosis and coagulation: Deep vein thrombosis and pulmonary embolism prophylaxis," Surg. Clin. North Am. **85**, 1163–1177 (2005).
5. M. Hepburn-Brown, J. Darvall, and G. Hammerschlag, "Acute pulmonary embolism: a concise review of diagnosis and management," Intern. Med. J. **49**, 15–27 (2019).
6. C. J. Sommer, "Ischemic stroke: experimental models and reality," Acta Neuropathol **133**, 245–261 (2017).
7. S. K. Feske, "Ischemic stroke," The Am. J. Med. **134**, 1457–1464 (2021).
8. A. Siniarski, A. Gasecka, J. A. Borovac, P. E. Papakonstantinou, D. Bongiovanni, H. Ehrlinder, M. Giustozzi, R. A. Guerreiro, and W. A. E. Parker, "Blood coagulation disorders in hearth failure: from basic science to clinical perspectives," J. Cardiac Fail. **29**, 517–526 (2023).
9. L. Lu, M. Liu, R. Sun, Y. Zheng, and P. Zhang, "Myocardial infarction: symptoms and treatments," Cell Biochem. Biophys **72**, 865–867 (2015).
10. M. M. Aria, A. Erten, and O. Yalcin, "Technology advancements in blood coagulation merasurements for point-of-care diagnostic testing," Front. Bioengeneering Biotechnol. **7**, 395 (2019).
11. B. Ramaswamy, Y.-T. T. Yeh, and S.-Y. Zheng, "Microfluidic device and system for point-of-care blood coagulation measurement based on electrical impedance sensing," Sensors Actuators B **180**, 21–27 (2013).
12. H. Berney and J. J. O'Riordan, "Impedance measurement monitors blood coagulation," Analog. Dialogue **42**, 08 (2008).
13. K. F. Lei, K.-H. Chen, P. Tsui, and N.-M. Tsang, "Real-time electrical impedimetric monitoring of blood coagulation process under temperature and hematocrit variations conducted in a microfluidic chip," Plos One **8**, e76243 (2013).
14. M. Liu, K. Zaman, and Y. M. Fortenberry, "Overview of the therapeutic potential of aptamers targeting coagulation factors," Int. J. Mol. Sci. **22**, 3897 (2021).
15. D. Chen, S. Song, J. Ma, Z. Zhang, P. Wang, W. Liu, and Q. Guo, "Micro-electromechanical film bulk acoustic sensor for plasma and whole blood coagulation monitoring," Biosens. Bioelectron. **91**, 465–471 (2017).
16. O. Cakmak, E. Ermek, N. Kiinc, S. Bulut, I. Baris, I. H. Kavakli, G. G. Yaralioglu, and H. Urey, "A cartridge based sensor array platform for multiple coagulation measurements from plasma," Lab Chip **15**, 113 (2015).
17. Z. Chen, J. Lu, C. Zhang, I. Hsia, X. Yu, L. Marecki, E. Marecki, M. Asnani, S. Jain, S. Neelamegham, and R. Zhao, "Microclot array elastometry for integrated measurement of thrombus formation and clot biomechanics under fluid shear," Nat. Commun. **10**, 2051 (2019).
18. A. B. Karpiouk, S. R. Aglyamov, S. Mallidi, J. Shah, W. G. Scott, J. M. Rubin, and S. Y. Emelianov, "Combined ultrasound and photoacoustic imaging to detect and stage deep vein thrombosis: phantom and *ex vivo* studies," J. Biomed. Opt. **13**, 054061 (2008).
19. M. A. Juratli, Y. A. Menyaev, M. Sarimollaoglu, A. V. Melerzanov, D. A. Nedosekin, W. C. Culp, J. Y. Suen, E. I. Galanzha, and V. P. Zharov, "Noninvasive labe-free detection of circulating white and red blood clots in deep vessels with a focused potoacoustic probe," Biomed. Opt. Express **9**, 5667–5677 (2018).
20. M. M. Tripathi, S. Egaw, A. G. Wirth, D. M. Tshikudi, E. M. V. Cott, and S. K. Nadkarni, "Clinical

evaluation of whole blood prothombin time (pt) and international normalized ratio (inr) using a laser speckle rheology sensor," Sci. Reports **7**, 9169 (2017).
21. X. Xu, J. Zhu, and Z. Chen, "Dynamic and quantiative assesment of blood coagulation using optical coherence elastography," Sci. Reports **6**, 24294 (2016).
22. Y. Tang, J. Zhu, L. Zhu, F. Fan, Z. Ma, and F. Zhang, "Blood coagulation monitoring under static and flow conditions with optical coherence tomography autocorrelation analylsis," Appl. Phys. Lett. **120**, 163702 (2022).
23. X. Xu, J. Geng, and X. Teng, "Monitoring the blood coagulation process under various flow conditions with optical coherence tomography," J. Biomed. Opt. **19**, 046021 (2014).
24. X. Xu, J. Lin, and F. Fu, "Optical coherence tomography to investigate optical properties of blood during coagulation," J. Biomed. Opt. **16**, 096002 (2011).
25. M. M. Tripathi, Z. Hajjarian, E. M. V. Cott, and S. K. Nadkarni, "Assessing blood coagulation status with laser speckle rheology," Biomed. Opt. Express **5**, 817–831 (2014).
26. S. P. Chong, C. W. Merkle, C. Leahy, H. Radhakrishnan, and V. J. Srinivasan, "Quantitative microvascular hemoglobin mapping using visible light spectroscopic optical coherence tomography," Biomed. Opt. Express **6**, 1429–1450 (2015).
27. S. Pi, T. T. Hormel, X. Wei, W. Cepurna, B. Wang, J. C. Morrison, and Y. Jia, "Retinal capillary oximetry with visible light optical coherence tomography," Proc Natl Acad Sci U S A **117**, 11658–11666 (2020).
28. X. Xu and X. Teng, "Effect of fibrinogen on blood coagulation detected by optical coherence tomography," Phys. Med. Biol. **60**, 4185–4195 (2015).
29. C. Cuartas-Vélez, C. Veenstra, S. Kruitwagen, W. Petersen, and N. Bosschaart, "Optical density based quantification of total haemoglobin concentrations with spectroscopic optical coherence tomography," Sci. Reports **11**, 8680 (2021).
30. W. Drexler and J. G. Fujimoto, *Optical coherence tomography: Technology and applications* (Springer Reference, 2015).
31. B. R. Branchford, C. J. NG, K. B. Neeves, and J. D. Paola, "Microfluidic technology as an emerging clinical tool to evaluate thrombosis and hemostasis," Thromb. Res. **136**, 13–19 (2015).
32. J. Cable, , P. Arlotta, K. K. Parker, A. J. Hughes, K. Goodwin, C. L. Mummery, R. D. Kamm, S. J. Engle, D. A. Tagle,S. F. Boj, A. E. Stanton, Y. Morishita, M. L. Kemp, D. A. Norfleet, E. E. May, A. Lu, R. Bashir, A. W. Feinberg, S. M. Hull, A. L. Gonzalez, M. R. Blatchley, N. M. Pulido, R. Morizane, T. C. McDevidd, D. Mishra, and A. Mulero-Russe, "Engineering multicellular living systems—a keystone symposia report," Ann. N. Y. Acad. Sci. **1518**, 183–195 (2022).
33. E. Ko and R. D. Kamm, "Neurovascular models for organ-on-a-chips," Vitr. Model. **1**, 125–127 (2022).
34. D. R. Myers and W. A. Lam, "Vascularized microfluidics and their untapped potential for discovery in diseases of the microvasculature," Annu. Rev. Biomed. Eng. **23**, 2021 (407–432).
35. J. Ko, D. Park, S. Lee, B. Gumuscu, and N. L. Jeon, "Engineering organ-on-a-chip to accelerate translational research." Micromachines **13**, 1200 (2022).
36. V. Paloschi, M. Sabater-Lleal, H. Middelkamp, A. Vivas, S. Johansson, A. van der Meer, M. Tenje, and L. Maegdefessel, "Organ-on-a-chip technology: a novel approach to investigate cardiovascular diseases," Cardiovasc. Res. **0**, 1–13 (2021).
37. N. K. R. Pandian, R. G. Mannino, W. A. Lam, and A. Jain, "Thrombosis-on-a-chip: Prospective impact of microphysiological models of vascular thrombosis," Curr. Opin. Biomed. Eng. **5**, 2018 (29–34).
38. H. H. G. Song, R. T. Rumma, C. K. Ozaki, E. R. Edelman, and C. S. Chen, "Vascular tissue engineering: progress, challenges, and clinical promise," Cell Stem Cell **22**, 340–354 (2018).
39. H. J. Albers, R. Passier, A. van den Berg, and A. D. van der Meer, "Automated analysis of platelet aggregation on cultured endothelium in a microfluidic chip perfused with human whole blood," Micromachines **10**, 781 (2019).

40. P. F. Costa, H. J. Albers, J. E. A. Linssen, H. H. T. Middelkamp, L. van der Hout, R. Passier, A. van den Berg, J. Malda, and A. D. van der Meer, "Mimicking arterial thrombosis in a 3d-printed microfluidic: In vitro vascular model based on computed tomography angiography data," Lab Chip **17**, 2785 (2017).
41. A. Hasan, A. Paul, A. Memic, and A. Khademhosseini, "A multilayered microfluidic blood vessel-like structure," Biomed. Microdevices **17**, 88 (2015).
42. L. Jia, F. Han, H. Yang, G. Turnbull, J. WAng, J. Clarke, W. Shu, M. Guo, and B. Li, "Microfluidic fabrication of biomimetic helical hydrogel microfibers for blood-vessel-on-a-chip applications," Adv. Healthc. Mater. **8**, 1900435 (2019).
43. R. G. Mannino, D. R. Myers, B. Ahn, Y. Wang, M. Rollins, H. Gole, A. S. Lin, R. E. Guldberg, D. P. Giddens, L. H. Timmins, and W. A. Lam, "Do-it-yourself in vitro vasculature that recapitulates in vivo geometries for investigating endothelial-blood cell interactions," Sci. Reports **5**, 12401 (2015).
44. M. Tsai, A. Kita, J. Leach, R. Rounsevell, J. N. Huan, J. Moake, R. E. Ware, D. A. Fletcher, and W. A. Lam, "In vitro modeling of the microvascular occlusion and thrombosis that occur in hematologic diseases using microfluidic technology," J. Clin. Invest. **122**, 408–418 (2012).
45. C. G. M. van Dijk, M. M. Brandt, N. Poulis, J. Anten, M. van der Moolen, L. Kramer, E. F. G. Homburg, L. Louzano-Martinez, J. Pei, M. M. Krebber, B. W. M. van Balkom, P. de Graaf, D. J. Duncker, M. C. Verhaar, R. Luttge, and C. Cheng, "A new microfluidic model that allows monitoring of complex vascular structures and cell interactions in a 3d biological matrix," Lab Chip **20**, 1827 (2020).
46. E. Westein, A. D. van der Meer, M. J. E. Kuijpers, J.-P. Frimat, A. van den Berg, and J. W. M. Heemskerk, "Atherosclerotic geometries exacerbate pathological thrombus formation poststenosis in a von willebrand factor- dependent manner," Proc. Natl. Acad. Sci. **110**, 1357–1362 (2013).
47. Y. Zheng, J. Chen, M. Craven, N. W. Choi, S. Totorica, A. Diaz-Santana, P. Kermani, B. Hempstead, C. Fischbach- Teschl, J. A. López, and A. D. Stroock, "In vitro microvessels for the study of angiogenesis and thrombosis," Proc. Natl. Acad. Sci. **109**, 9342–9347 (2012).
48. S. Cai, H. Li, F. Zheng, F. King, M. Dao, G. E. Karniadakis, and S. Suresh, "Artificial intelligence velocimetry and microaneurysm-on-a-chip for three-dimensional analysis of blood flow in physiology and disease," Proc. Natl. Acad. Sci. **118**, e2100697118 (2021).
49. P. Elizondo and A. L. Fogelson, "A mathematical model of venous thrombosis initiation," Biophys. J. **111**, 2722–2734 (2016).
50. Y. C. Zhao, P. Vatankhah, T. Goh, R. Michelis, K. Kyanian, Y. Zhang, Z. Li, and L. A. Ju, "Hemodynamic analysis for stenosis microfluidic model of thrombosis with refined computational fluid dynamics simulation," Sci. Reports **11**, 6875 (2021).
51. P. Balogh and P. Bagchi, "A computational approach to modeling cellular-scale blood flow in complex geometry," J. Comput. Phys. **334**, 280–307 (2017).
52. R. Wagenvoord, P. W. Hekmer, and H. C. Hemker, "The limits of simulation of the clotting system," J. Thromb. Haemost. **4**, 1331–1338 (2006).
53. Y. Chen and L. Ju, "Biomechanical thrombosis: The dark side of force and dawn of mechano-medicine," Stroke Vasc. Neurol. **5**, 185–197 (2020).
54. S. P. Jackson, W. S. Nesbitt, and E. Westein, "Dynamics of platelet thrombus formation," J. Thromb. Haemost. **7**, 17–20 (2009).
55. A. Rana, E. Westein, B. Niego, and C. E. Hagemeyer, "Shear-dependent platelet aggregation: mechanisms and therapeutic opportunities," Front. Cardiovasc. Med. **6**, 141 (2019).
56. J. W. Yau, H. Teoh, and S. Verma, "Endothelial cell control of thrombosis," BMC Cardiovasc. Disord. **15**, 130 (2015).
57. N. Tekkeşin, O. B. Esen, C. Kilinç, and O. Eviyaoğlu, "Discard first tube for coagulation testing," Blood Coagul. Fibrinolysis **23**, 299–303 (2012).

58. C. Veenstra, W. Petersen, I. M. Vellekoop, W. Steenbergen, and N. Bosschaart, "Spatially confined quantification of bilirubin concentrations by spectroscopic visible-light optical coherence tomography," Biomed. Opt. Express **9**, 3581–3589 (2018).
59. A. Zhang, Q. Zhang, C.-L. Chen, and R. K. Wang, "Methods and algorithms for optical coherence tomography-based angiography: a review and comparison," J. Biomed. Opt. **20**, 100901 (2015).
60. J. Enfield, E. Jonathan, and M. Leahy, "*In vivo* imaging of the microcirculaton of the volar forearm using correlation mapping optical coherence tomography (cmoct)," Biomed. Opt. Express **2**, 1184–1193 (2011).
61. W. J. Choi, R. Reif, S. Yousefi, and R. K. Wang, "Improved microcirculaton imaging of human skin *in vivo* using optical microangiography with a correlation mapping mask," J. Biomed. Opt. **19**, 036010 (2014).
62. S. Chen, B. Potsaid, Y. Li, J. Lin, Y. Hwang, E. M. Moult, J. Zhang, D. Huand, and J. G. Fujimoto, "High speed, long range, deep penetration swept source oct for structural and angiographic imaging of the anterior eye," Sci. Reports **12**, 992 (2022).
63. F. L. D. Huang, Z. He, Z. Cheng, C. Shang, and P. K. A. Wai, "400 mhz ultrafast optical coherence tomography," Opt. Lett. **45**, 6675–6678 (2020).
64. J. P. Kolb, T. Pfeiffer, M. Eibl, H. Hakert, and R. Huber, "High-resolution retinal swept source optical coherence tomography with an ultra-wideband fourier-domain mode-locked laser at mhz a-scan rates," Biomed. Opt. Express **9**, 120–130 (2018).
65. L. L. Bischel, S. H. Lee, and D. J. Beebe, "Practical method for patterning lumens through ecm hydrogels via viscous finger patterning," J. Lab. Autom. **17**, 96–103 (2012).
66. A. Herland, A. D. van der Meer, E. A. FitzGerald, T.-E. Park, J. F. Sleeboom, and D. E. Ingber, "Distinct contributions of astrocytes and pericytes to neuroinflammation identified in a 3d human blood-brain barrier on a chip," Plos one **11**, e0150360 (2016).
67. M. N. S. de Graaf, A. Cochrane, F. E. van den Hil, W. Buijsman, A. D. van der Meer, A. van den Berg, C. L. Mummery, and V. V. Orlova, "Scalable microphysiological system to model three-dimensional blood vessels," APL Bioeng. **3**, 026105 (2019).

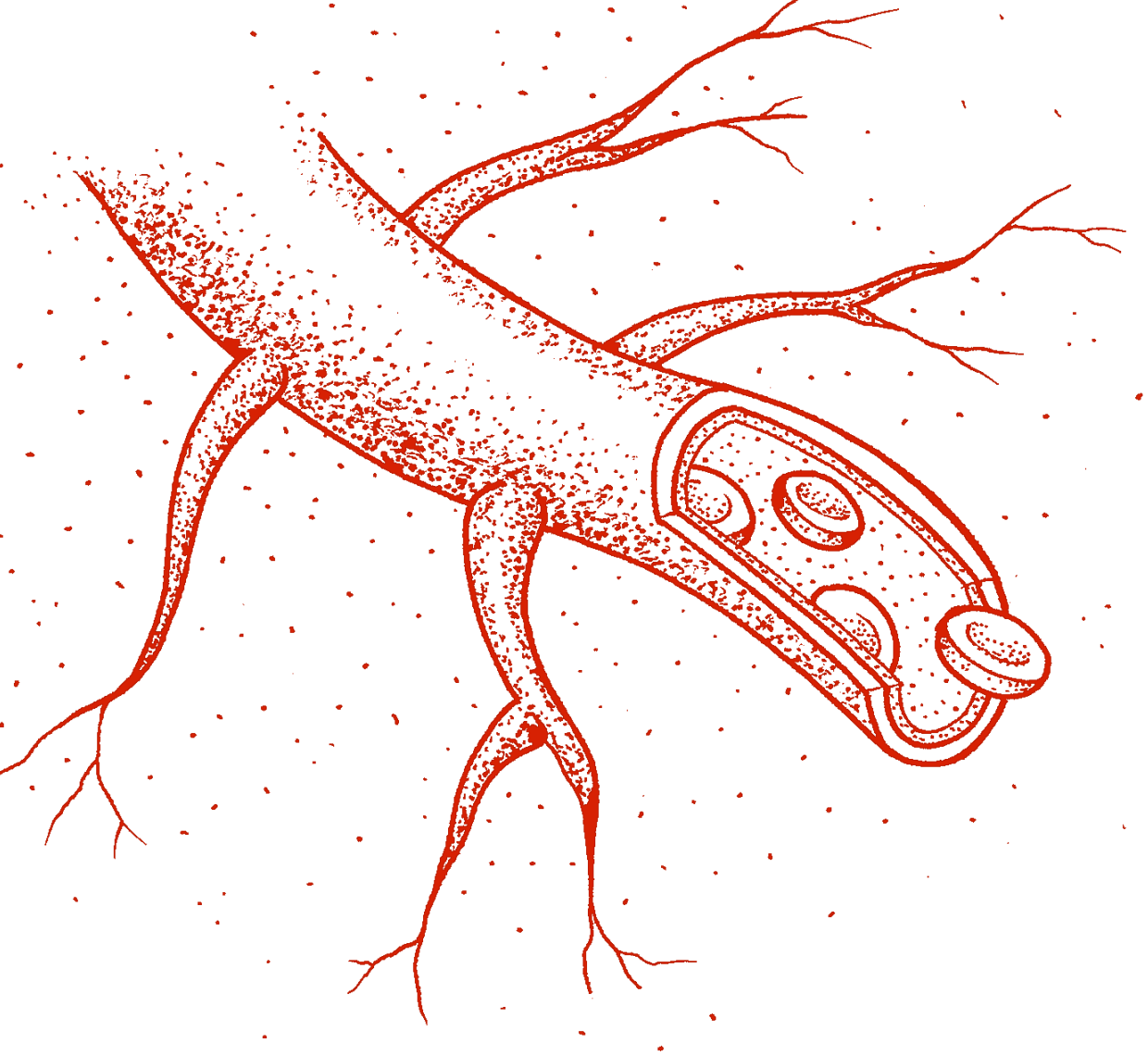

7

Summary and outlook

H.H.T. Middelkamp

7.1 Summary

More than 30% of all deaths worldwide have a vascular cause, which mostly involves heart attack or stroke caused by arterial diseases such as atherosclerosis. The exact mechanisms of early development of atherosclerosis are still unknown and need to be investigated in order to find new strategies for prevention and treatment. Organs-on-chips (OoCs) and specifically blood vessels-on-chips (BVoCs) can assist in investigating vascular diseases, by recapitulating the human vasculature more accurately than other models such as animal models. In this thesis we have developed and presented multiple vessel-on-chip (VoC) models to investigate different types of vascular disease.

A full overview of current VoC chip models is given in **chapter 2**, where we also discuss why it is important to involve all stakeholders in the development of OoC in context of incorporating OoC systems in the drug development process.

In **chapter 3** we present a three-dimensional (3D) BVoC recreate to model endothelial cell training using a monocyte adhesion assay. 3D BVoCs were developed that contain donor-specific human umbilical vein endothelial cells (HUVECs). HUVECs were stimulated once or twice with the well-known inflammatory factor tumor necrosis factor-α (TNF-α) to simulate training *in vivo*. A donor-specific training response was observed as an increase of the number of monocytes adhered to the blood vessel after the second stimulation.

A related BVoC model was used in **chapter 4** to model the early stages of vascular inflammation, plaque development and wound healing. In early stages of vascular inflammation, first responder white blood cells (i.e., monocytes) play a major role as they activate the immune system and often embed underneath the endothelial cell layer and differentiate into macrophages. To investigate the effect of these macrophages on the endothelial cell layer, THP-1 derived macrophages were lipid-laden and embedded underneath a human induced pluripotent derived endothelial cell (hiPSC-EC) layer. After this protocol was systematically set up, a blood perfusion assay was developed to observe a thromboinflammatory effect. An increase in fibrin deposition and therefore thrombus formation could be observed in the channel containing (lipid-laden) macrophages embedded underneath the hiPSC-EC layer. This suggests a higher inflammatory response of endothelial cells, even in early stages of inflammation or plaque formation where these monocytes and macrophages are understood to assist in disposing of inflammatory factors.

To observe cell-cell interaction and the effect of culturing cells in a microfluidic device on gene expression patterns, we have developed a new microfluidic chip in **chapter 5**. This microfluidic chip consists of 2 channels, separated by a porous membrane, with an 'open top' top channel. The top channel was specifically designed for neuronal differentiation, with a bottom channel which is separately accessible for endothelial cell seeding. For the first time, we have performed a complete neuronal differentiation on chip. We performed RNA-sequencing on both cell types to observe transcriptomic differences. Our results show that culturing cells on microfluidic chip instead of the conventional well-plate changes gene expression profiles, for endothelial cells the cell division rate was decreased, and neurons show an increase in maturity.

Optical coherence tomography (OCT) is used in **chapter 6** to non-invasively visualize thrombus formation in BVoCs. OCT is a technique in which light backscattering is measured to visualize objects. HUVECs were seeded in VoC models consisting of straight, rectangular microfluidic channels. After 24 hours blood was perfused through these channels. Using OCT, we show the ability to image thrombus formation and development over time. Using thresholding we were able to identify clots; their size; and growth over time.

7.2 Outlook

Over the last decade OoC systems have been developed towards more mature models and show great potential for improving the drug development process as well as a higher understanding of disease mechanisms.
This thesis has shown the advancements made in VoC development focusing specifically on the development of co-culture systems with quantifiable readouts. Different chip designs can be used for modelling different disease types. From basic squared channel chips to 3D lumen BVoCs, as well as a multilayered chip to model the blood-brain-barrier as well.

7.2.1 Organs on chips

The field of OoCs is still developing and multiple advances are made rapidly. To further improve OoCs however, it is imperative to incorporate more standardization and quantification in these systems. Many OoC devices are now developed by many researchers for their own purposes. As this improves our knowledge regarding organs and organ-specific mechanisms, this can be viewed as an advantage, however, it makes it difficult to compare results. A more standardized method of

setting up OoC systems can bridge this problem and assist in quicker and easier development of new OoC systems.
Furthermore, current OoC systems often consist of only a few channels, with no possibility of easily scaling up and no quantification methods. A possible solution for these problems could be to use a standardized platform such as the translational organ-on-chip platform (TOP)[2,3]. This platform consists of a fluidic circuit board, which is designed to conform to ISO standards, on which separate building blocks or modules can be attached, which can be designed to possess the desired properties.

7.2.2 Blood vessels on chip

Human blood vessels experience high levels of shear stress, due to the constant blood flow. Endothelial cells cultured under standard two-dimensional (2D) conditions usually do not experience any level of stress as they are cultured under static conditions. Endothelial cell culture using flow has been demonstrated to improve endothelial cell specific functions such as barrier properties[4–6]. In this thesis we have made small advances in adding flow to BVoCs. By using a rocking table while culturing cells in microfluidic chips, we were able to have a bidirectional flow in the blood vessel channels. However, bi-directional flow is physiologically irrelevant. Addition of continuous flow has been a main research subject in BVoCs, which can, on a small scale, be achieved using a specific chip design which can be placed on a rocking table or by using a pressure pump and a fluidic circuit board[7–10]. However, long term reperfusion with inclusion of different cell types or even blood, has not been achieved yet. To improve blood vessel models and therefore give more physiological relevance to OoCs, it would be greatly recommended to further develop a 'continuous reperfusion on chip' blood vessel model.
Currently, many blood vessel models are created using either immortalized cell lines or HUVECs[11–18]. Although these cell types are usually easy to handle and can be kept in culture over long periods of time, they do not represent actual human blood vessels. Immortalized cell lines can lose endothelial phenotypical abilities, such as growth inhibition and barrier function, which is an important part in creating an endothelial monolayer[19]. Next to that, HUVECs are often considered a non-representative endothelial cell for modelling organ specific blood vessels, due to the their lack of organ-specific endothelial markers[20,21]. To progress towards a more complex and, equally important, a more personalized model, the use of hiPSC-EC would be advantageous. Using hiPSC-ECs can give insight in gene, patient, and population specific mechanistic responses and responses to specific target therapies[22,23].

As blood vessels are the main organ to transport nutrients and oxygen throughout the body, it is imperative to have proper models to further investigate vessel function in both health and disease. Next to that, blood vessel incorporation will be important in modelling different organs, for instance the brain, lung, and heart. Therefore, it will be important to design models which can incorporate different cell types in a physiological relevant way. Multiple models already incorporate multiple cell types such as discussed in chapter 5[17,18,24–26]. These models do not represent the true human physiology, consisting mostly of a 2D endothelial layer separated from other tissues by a membrane, thus more representative models are desired. Organoids do have a more physiological physiology, have the ability to self-organize, and consist of multiple relevant cell types. However, organization of the different cell types cannot be controlled[27,28]. To improve the OoC models, development can be focused on making a more physiological relevant model, consisting of different cell types that can self-organize, as well as keep the ability to control their organization, by e.g., adding cells in the hydrogel surrounding the endothelial cells and let them self-organize around the blood vessel.

7.2.3 Human body on chip

One step further is to combine multiple OoC systems to model human physiology to an even higher extend. The human body on chip (HBoC) is a concept where multiple organ tissues can be connected[29,30]. These tissues can be connected by sequentially collecting medium at the outlet of one system and adding it as input medium for a second system or by creating a single blood vessel channel, flowing past multiple organ tissues[31–33]. A HBoC model can be beneficial for modelling more complex processes involving multiple organs such as pharmacokinetics and pharmacodynamics (PK/PD)[34,35].

To effectively look at PK/PD responses, however, a gas impermeable chip system needs to be established[36]. Polydimethylsiloxane (PDMS) is a silicon polymer which is currently the most commonly used material to fabricate OoCs as it is an easy and cheap material to use[37,38]. PDMS is very gas permeable and can therefore absorb target molecules. For more complex models it would be preferred to design chips using another material, such as glass, ceramic materials, or thermoplastic polymers[36,39,40].

In conclusion, as vascular diseases are still the main cause of death worldwide, modelling the vasculature is very important in understanding vascular mechanisms and diseases. Furthermore, BVoCs can help interconnect multiple different OoCs. Multiple BVoC models are already in existence and can be used to model different types of vasculature in disease and health. The models presented in this thesis are an addition to the models already in existence and can greatly benefit our understanding of vascular mechanisms, however, improvement and critical observations are always needed to further improve on the existing models. By incorporating the improvements suggested in this chapter, we can move towards a more complex, more personalized model and greatly improve patient-specific treatments and mechanistic disease understanding.

References

1. World Health Organization. Leading causes of death worldwide in 2016 (in millions). Statista. https://www.statista.com/statistics/288839/leading-causes-of-death-worldwide/ (2019).
2. Vollertsen, A. R. *et al.* Facilitating implementation of organs-on-chips by open platform technology. *Biomicrofluidics* **15**, 1ENG (2021).
3. Vollertsen, A. R. *et al.* Highly parallelized human embryonic stem cell differentiation to cardiac mesoderm in nanoliter chambers on a microfluidic chip. *Biomed. Microdevices* **23**, (2021).
4. Winkelman, M. A. *et al.* Interstitial flow enhances the formation, connectivity, and function of 3D brain microvascular networks generated within a microfluidic device. *Lab Chip* **22**, 170–192 (2022).
5. Gordon, E., Schimmel, L. & Frye, M. The Importance of Mechanical Forces for in vitro Endothelial Cell Biology. *Front. Physiol.* **11**, (2020).
6. Mannino, R. G. *et al.* Do-it-yourself in vitro vasculature that recapitulates in vivo geometries for investigating endothelial-blood cell interactions. *Sci. Rep.* **5**, 1–12 (2015).
7. Wang, Y. I. & Shuler, M. L. UniChip enables long-term recirculating unidirectional perfusion with gravity-driven flow for microphysiological systems. *Lab Chip* **18**, 2563–2574 (2018).
8. de Graaf, M. N. S. *et al.* Multiplexed fluidic circuit board for controlled perfusion of 3D blood vessels-on-a-chip. *Lab Chip* **23**, 168–181 (2022).
9. de Graaf, M. N. S., Vivas, A., van der Meer, A. D., Mummery, C. L. & Orlova, V. V. Pressure-Driven Perfusion System to Control, Multiplex and Recirculate Cell Culture Medium for Organs-on-Chips. *Micromachines* **13**, (2022).
10. Schimek, K. *et al.* Integrating biological vasculature into a multi-organ-chip microsystem. *Lab Chip* **13**, 3588–98 (2013).
11. Middelkamp, H. H. T. *et al.* Cell type-specific changes in transcriptomic profiles of endothelial cells, iPSC-derived neurons and astrocytes cultured on microfluidic chips. *Sci. Rep.* **11**, 1–12 (2021).
12. Costa, P. F. *et al.* Mimicking arterial thrombosis in a 3D-printed microfluidic: In vitro vascular model based on computed tomography angiography data. *Lab Chip* (2017) doi:10.1039/c7lc00202e.
13. Song, H. H. G., Rumma, R. T., Ozaki, C. K., Edelman, E. R. & Chen, C. S. Vascular Tissue Engineering: Progress, Challenges, and Clinical Promise. *Cell Stem Cell* **22**, 340–354 (2018).
14. Jain, A. *et al.* Assessment of whole blood thrombosis in a microfluidic device lined by fixed human endothelium. *Biomed. Microdevices* **18**, 1–7 (2016).
15. Jia, L. *et al.* Microfluidic Fabrication of Biomimetic Helical Hydrogel Microfibers for Blood-Vessel-on-a-Chip Applications. **1900435**, 1–10 (2019).
16. Saili, K. S., Zurlinden, T. J. & Knudsen, T. B. *Modeling the Neurovascular Unit In Vitro and In Silico*. *Handbook of Developmental Neurotoxicology* (Elsevier Inc., 2018). doi:10.1016/B978-0-12-809405-1/00011-0.
17. van der Helm, M. W., van der Meer, A. D., Eijkel, J. C. T., van den Berg, A. & Segerink, L. I. Microfluidic organ-on-chip technology for blood-brain barrier research. *Tissue barriers* **4**, e1142493 (2016).
18. Walter, F. R. *et al.* A versatile lab-on-a-chip tool for modeling biological barriers. *Sensors Actuators, B Chem.* **222**, 1209–1219 (2016).
19. Rahman, N. A. *et al.* Immortalized endothelial cell lines for in vitro blood-brain barrier models: A systematic review. *Brain Res.* **1642**, 532–545 (2016).
20. Cao, Y. *et al.* The use of human umbilical vein endothelial cells (HUVECs) as an in vitro model

to assess the toxicity of nanoparticles to endothelium: a review. *J. Appl. Toxicol.* **37**, 1359–1369 (2017).
21. Medina Leyte, D. J., Domínguez Pérez, M., Mercado, I., Villarrreal Molina, M. T. & Jacobo Albavera, L. Use of Human Umbilical Vein Endothelial Cells (HUVEC) as a Model to Study Cardiovascular Disease : A Review. *Appl. Sci.* **10**, (2020).
22. Pflaum, M. *et al.* Towards biohybrid lung: Induced pluripotent stem cell derived endothelial cells as clinically relevant cell source for biologization. *Micromachines* **12**, (2021).
23. Orlova, V. V *et al.* Generation, expansion and functional analysis of endothelial cells and pericytes derived from human pluripotent stem cells. *Nat. Protoc.* **9**, 1514–31 (2014).
24. Pediaditakis, I. *et al.* Modeling alpha-synuclein pathology in a human brain-chip to assess blood-brain barrier disruption. *Nat. Commun.* **12**, 1–17 (2021).
25. Brown, J. A. *et al.* Recreating blood-brain barrier physiology and structure on chip: A novel neurovascular microfluidic bioreactor. *Biomicrofluidics* **9**, (2015).
26. Huh, D. *et al.* Microfabrication of human organs-on-chips. *Nat. Protoc.* **8**, 2135–57 (2013).
27. Hofer, M. & Lutolf, M. P. Engineering organoids. *Nat. Rev. Mater.* **6**, 402–420 (2021).
28. De Souza, N. Organoids. *Nat. Methods* **15**, 23 (2018).
29. Polini, A. *et al.* Organs-on-a-chip: a new tool for drug discovery. *Expert Opin. Drug Discov.* **9**, 335–52 (2014).
30. Ingber, D. E. Is it Time for Reviewer 3 to Request Human Organ Chip Experiments Instead of Animal Validation Studies? *Adv. Sci.* **7**, 1–15 (2020).
31. Ingber, D. E. Human organs-on-chips for disease modelling, drug development and personalized medicine. *Nat. Rev. Genet.* **23**, 467–491 (2022).
32. Low, L. A. & Tagle, D. A. Organs-on-chips: Progress, challenges, and future directions. *Exp. Biol. Med.* **242**, 1573–1578 (2017).
33. Park, D., Lee, J., Chung, J. J., Jung, Y. & Kim, S. H. Integrating Organs-on-Chips : Multiplexing , Scaling , Vascularization , and Innervation. *Trends Biotechnol.* **xx**, 1–14 (2019).
34. Lee, H. *et al.* A pumpless multi-organ-on-a-chip (MOC) combined with a pharmacokinetic–pharmacodynamic (PK–PD) model. *Biotechnol. Bioeng.* **114**, 432–443 (2017).
35. Sung, J. H., Kam, C. & Shuler, M. L. A microfluidic device for a pharmacokinetic-pharmacodynamic (PK-PD) model on a chip. *Lab Chip* **10**, 446–455 (2010).
36. Campbell, S. B. *et al.* Beyond Polydimethylsiloxane: Alternative Materials for Fabrication of Organ-on-a-Chip Devices and Microphysiological Systems. *ACS Biomater. Sci. Eng.* **7**, 2880–2899 (2021).
37. Banik, S. *et al.* The revolution of PDMS microfluidics in cellular biology. *Crit. Rev. Biotechnol.* **43**, 465–483 (2023).
38. Torino, S., Corrado, B., Iodice, M. & Coppola, G. PDMS-Based Microfluidic Devices for Cell Culture. *Inventions* **3**, 1–14 (2018).
39. Cao, U. M. N. *et al.* Microfluidic Organ-on-A-Chip : A Guide to Biomaterial Choice and Fabrication. *Int. J. Mol. Sci. Rev.* **24**, (2023).
40. Leung, C. M. *et al.* A guide to the organ-on-a-chip. *Nat. Rev. Methods Prim.* **2**, (2022).

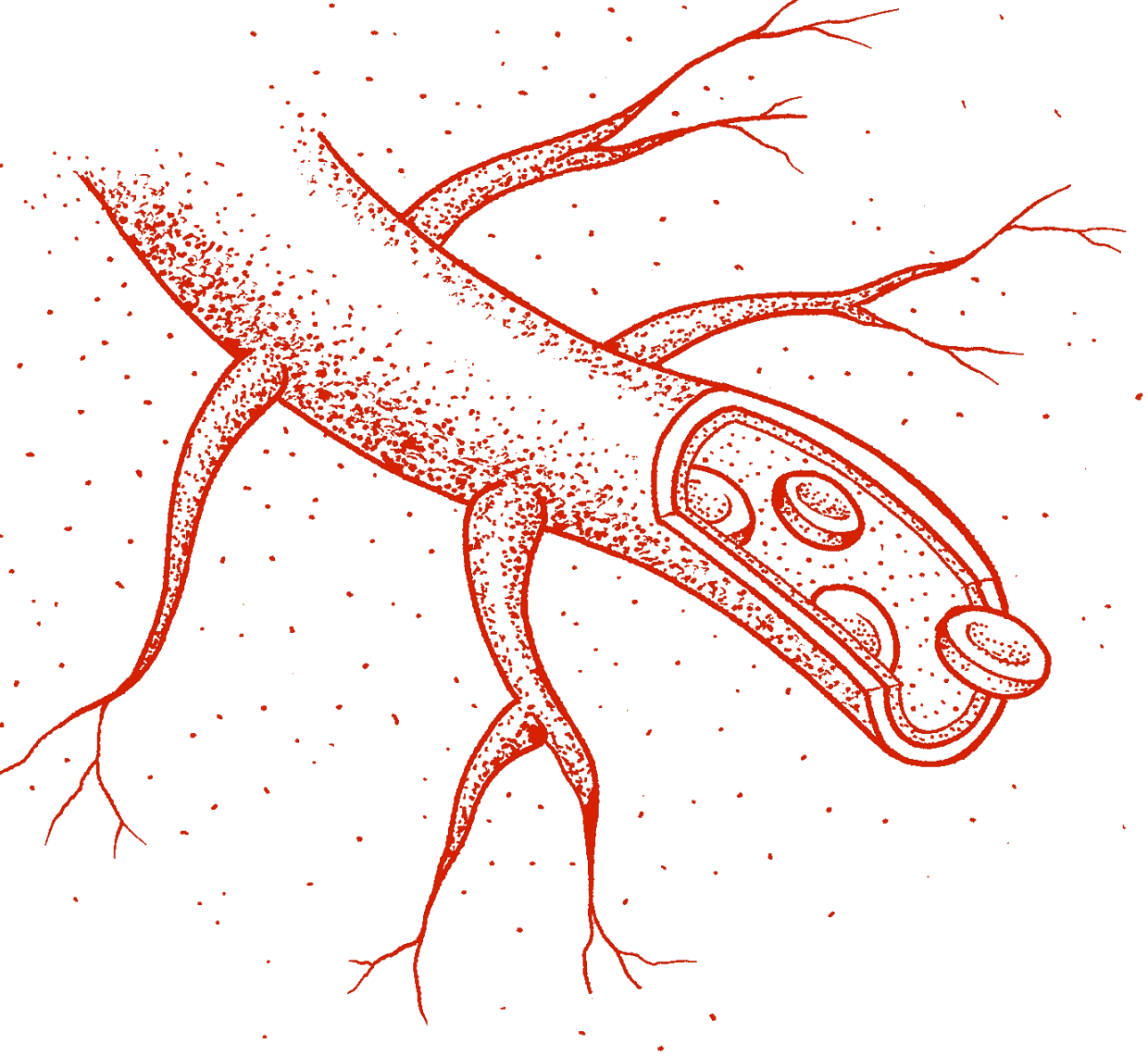

A

Appendix

Samenvatting

Meer dan 30% van alle doden wereldwijd hebben een vasculaire oorzaak waarbij een hartaanval of hersenbloeding, veroorzaakt door vasculaire ziekten zoals atherosclerose, een groot aandeel hebben. Atherosclerose is een vernauwing van de aderen, ook wel plaqueformatie genoemd. Wanneer deze plaque scheurt kan er een trombus ontstaan die de bloedtoevoer naar essentiële organen kan blokkeren. De exacte mechanismen van het ontstaan van vroege atherosclerose zijn tot op heden niet bekend en moeten worden onderzocht om nieuwe strategieën te ontwikkelen om plaqueformatie tegen te gaan of zelfs te genezen. Organen-op-chips (OoCs) zijn microfysiologische systemen die bestaan uit één of meerdere microfluïdische kanalen waarmee menselijke organen en weefsels goed kunnen worden nagebootst. Daarnaast kunnen we patiëntspecifieke cellen gebruiken waardoor resultaten vertaalbaar zijn naar een specifieke patiënt of patiëntengroep en meer representatief zijn dan diermodellen. Bloedvaten-op-chips (BVoCs) kunnen daarom helpen bij het onderzoek naar vasculaire ziektebeelden. In dit proefschrift hebben we verschillende BvoC-modellen ontwikkeld en gepresenteerd om verschillende vasculaire ziektebeelden te kunnen nabootsen en onderzoeken.

Hoofdstuk 2 is een introductiehoofdstuk, waarin een volledig overzicht wordt gegeven van de huidige ontwikkelingen op het gebied van BVoCs. Daarnaast bespreken we waarom het belangrijk is om OoC systemen te implementeren in het medicijnontwikkelingsproces en om belanghebbenden te includeren in het ontwikkelingsproces.

In **hoofdstuk 3** wordt er een model gepresenteerd waarin endotheelceltraining kan worden aangetoond op functioneel niveau met behulp van een monocytenadhesietest. Drie-dimensionele (3D) BVoCs zijn ontwikkeld met het gebruik van menselijke navelstreng-endotheelcellen (HUVECs) van verschillende donoren. HUVECs werden één of twee keer gestimuleerd met de bekende ontstekingsfactor tumor necrosis factor-α (TNF-α) om *in vivo* training te simuleren. Door een verschil in toename van monocyten die adhereerden aan de endotheellaag na de 2^{e} stimulatie kon een donorspecifiek trainingspatroon worden geobserveerd.

Hetzelfde type BvoC-model is gebruikt in **hoofdstuk 4** om de vroege fase van vasculaire ontsteking, plaqueformatie en wondheling te modelleren. In vroege plaque-ontwikkeling, spelen witte bloedcellen (zoals monocyten) een grote rol, omdat ze het immuunsysteem activeren. Daarnaast migreren deze monocyten vaak

onder de endotheellaag, waar ze differentiëren naar macrofagen. Om het trombo-inflammatoire effect te bepalen van deze macrofagen, zijn THP-1-afgeleide macrofagen gevuld met *low-density lipoprotein-cholesterol* (LDL-cholesterol) en geïntegreerd in een laag met van humaan geïnduceerde pluripotente stamcel-afgeleide endotheelcellen (hiPSC-ECs). Nadat er systematisch een protocol is opgezet om deze cellen te integreren is een bloed perfusietest ontwikkeld om te observeren of er een trombo-inflammatoir effect plaatsvindt. Een toename in fibrine uitstoot, en daarmee trombusformatie, werd geobserveerd in de kanalen met geïntegreerde (LDL-cholesterol gevulde) macrofagen onder de hiPSC-EC-laag. Dit suggereert een hogere ontstekingsreactie van endotheelcellen in de vroege fases van vasculaire ontstekingen of plaqueformatie, waar de monocyten en macrofagen zouden moeten ingrijpen en helpen met het afbreken van ontstekingsfactoren.

Om interactie tussen verschillende celtypes en het effect van het kweken van cellen in een microfluïdisch systeem te observeren, hebben we voor **hoofdstuk 5** een nieuwe microfluïdische chip ontwikkeld. Deze chip bestaat uit 2 kanalen die gescheiden worden door een poreus membraan, waarbij het bovenste kanaal een 'open bovenkant' heeft. Het bovenste kanaal is specifiek ontworpen om neurondifferentiatie te kunnen uitvoeren, met een onderkanaal dat afzonderlijk toegankelijk is voor het kweken van endotheelcellen. Voor de eerste keer ooit hebben we een volledige neurondifferentiatie uitgevoerd op een microfluïdische chip. RNA-sequencing is uitgevoerd op beide celtypes om verschillen in transcriptomica te observeren. Onze resultaten laten zien dat het kweken van cellen op een microfluïdische chip, in plaats van de conventionele kweekplaten, resulteert in andere genexpressieprofielen. Voor endotheelcellen ging bijvoorbeeld de celdeling omlaag, terwijl de neuronen een hogere maturatie laten zien.

Optische coherentietomografie (OCT) is gebruikt in **hoofdstuk 6** als niet-invasieve methode om trombusformatie te visualiseren in BVoCs. Bij OCT wordt terugkaatsing van licht gemeten om objecten te visualiseren. HUVECs zijn gekweekt in rechthoekige kanalen en na 24 uur kweken is er een bloedperfusietest uitgevoerd. Door drempelwaardeanalyse waren we in staat om trombussen, het formaat van de trombus, en de ontwikkeling gedurende de bloedperfusietest te meten. Met behulp van OCT laten we zien dat we niet-invasief trombusformatie en ontwikkeling kunnen visualiseren in meer dimensies dan tot nu toe mogelijk was met fluorescentiemicroscopie.

Hoofdstuk 7 geeft naast de Engelstalige samenvatting aanbevelingen voor de verdere ontwikkeling van BvoC-systemen.

Concluderend, gezien de grote impact van vasculaire ziekten, is het erg belangrijk om modellen te ontwikkelen die meer inzicht geven in vasculaire mechanismen en ziekten. De modellen die in dit proefschrift gepresenteerd worden, zijn een toevoeging op de al bestaande modellen en kunnen een grote bijdrage leveren in het begrip van vasculaire mechanismen. Door verdere ontwikkeling van de bestaande technieken kunnen we werken naar gestandaardiseerde, meer complexe, gepersonaliseerde modellen met kwantificeerbare uitleesmogelijkheden van resultaten voor het testen van patiëntspecifieke behandelingen en ziektemechanismen. Hiermee kan worden bijdragen aan het terugdringen van vasculaire ziekten.

Scientific output

Journal papers

V. Paloschi; M. Sabater-Lleal; **H.H.T. Middelkamp**; A.G. De Sá Vivas; S. Johansson; A.D. van der Meer; M. Tenje; L. Maegdefessel. Organ-on-a-chip technology: a novel approach to investigate cardiovascular diseases. Cardiovascular Research, Volume 117, Issue 14, 1 December 2021, Pages 2742–2754, https://doi.org/10.1093/cvr/cvab088

H.H.T. Middelkamp*; A.H.A. Verboven*; A.G. De Sá Vivas; R. Passier; C.A. Albers; N. Nadif Kasri; A.D. van der Meer. Cell type-specific changes in transcriptomic profiles of endothelial cells, iPSC-derived neurons and astrocytes cultured on microfluidic chips. Scientific Reports volume 11, Article number: 2281 (2021)

P.F. Costa; H.J. Albers; J.E.A. Linssen; **H.H.T. Middelkamp**; L. van der Hout; R. Passier; A. van den Berg; J. Malda and A.D. van der Meer. Mimicking Arterial Thrombosis in a 3D-Printed Microfluidic in vitro Vascular Model Based on Computed Tomography Angiography Data. Lab Chip. 2017 Aug 8;17(16):2785-2792. doi: 10.1039/c7lc00202e

H.H.T. Middelkamp*; A.D. van der Meer*; J.M. Hummel; D.F. Stamatialis; C.L. Mummery; R. Passier; M.J. IJzerman. Organs-on-Chips in Drug Development: The Importance of Involving Stake-holders in Early Health Technology Assessment. Applied In Vitro Toxicology, ePub, DOI:10.1089/aivt.2015.0029

*Equal author contribution

Conference contributions

Oral presentations

Invited talk - Brain-on-a-chip: Models of neuronal development and the blood-brain barrier for personalized drug testing. Health Valley 2019

Towards a Neurovascular-Unit-on-a-Chip: differentiating neurons from human induced pluripotent stem cells in an open-top microfluidic chip. Annual hDMT consortium meeting 2019

Poster presentations

H.H.T. Middelkamp, H.J. Weener; T. Gensheimer; K. Vermeul; L.E. de Heus; H.J. Albers; Albert van den Berg, Andries D. van der Meer. The effect of embedded macrophages on intravascular coagulation in 3D vessels-on-chips. MPS World summit 2023.

H.H.T. Middelkamp; K.T.T. Le; A. van den Berg; S. Withoff; V. Kumar; A.D. van der Meer. Blood-vessel-on-chip: trained immunity in endothelial cells, a functional assay. NanoBioTech-Montreux Conference; annual European conference on micro & nanoscale technologies for the biosciences 2022.

K.T.T Le; **H.H.T. Middelkamp**; L. Do, M. Netea; I. Jonkers; V.V. Orlova; S. Withoff; A.D. van der Meer; V. Kumar. A Blood-vessel-on-chip to characterize trained immunity in endothelial cells. The European Organ-on-Chip Society annual meeting 2022.

H.H.T. Middelkamp; A. van den Berg; A.D. van der Meer. 3D blood vessels-on-chip for atherosclerosis modelling. MicroTAS 2021 - 25th International Conference on Miniaturized Systems for Chemistry and Life Sciences

K.T.T Le; **H.H.T. Middelkamp**; L. Do, M. Netea; I. Jonkers; V.V. Orlova; S. Withoff; A.D. van der Meer; V. Kumar. A 'blood vessel-on-chip' to study the role of trained immunity in sepsis. The European Organ-on-Chip Society annual meeting 2021.

H.H.T. Middelkamp; A.H.A. Verboven; A.G. De Sá Vivas; R. Passier; N. Nadif Kasri; C.A. Albers; A.D. van der Meer. Towards a Neurovascular-Unit-on-a-Chip: differentiating neurons from human induced pluripotent stem cells in an open-top microfluidic chip. hDMT International Organ-on-chip Symposium 2018

H.J. Albers; J.P. da Silva Simão; **H.H.T. Middelkamp**; C.L. Mummery; R. Passier; A. van den Berg; V.V. Orlova; A.D. van der Meer. Human induced pluripotent stem cell-derived endothelial cells in thrombosis-on-a-chip devices. 22nd International Conference on Miniaturized Systems for Chemistry and Life Sciences, µTAS 2018

H. J. Albers; J.E.A. Linssen; P. F. Costa; **H. H.T. Middelkamp**; L. van der Hout; J. Malda; R. Passier; A. van den Berg; A. D. van der Meer. Using 3D-printing to fabricate a microfluidic vascular model to mimic arterial thrombosis. 21st International Conference on Miniaturized Systems for Chemistry and Life Sciences, MicroTAS 2017

H.H.T. Middelkamp; J.M. Hummel; M.J. IJzerman; C.L. Mummery; R. Passier; A.D. van der Meer. Early Health Technology Assessment for the development of Thrombosis-on-a-chip. hDMT International Organ-on-Chip Symposium 2016

Prizes

hDMT challenge pitch: 3D blood Vessels-on-a-chip Cultured Under Flow. H.H.T. Middelkamp; M. de Graaf; A.G. De Sá Vivas.

About the author

Heleen was born in Enschede on August 18th, 1985. After she graduated from the MAVO, she pursued an education in middle laboratory sciences, at ROC van Twente. She started her working career and after having worked in a couple of laboratories, she decides to continue her educational journey by studying 'biomedical laboratory research' at hogeschool Saxion in Enschede.

During her bachelor program she started to get more interested in pursuing a scientific carrier and in preparation to this, follows her minor classes at the University of Twente. Her bachelor thesis was performed at the toxicology department of the University of Iowa, where she investigated the toxicity of a new anti-cancer drug in the lab of prof. Larry Robertson and prof. Gabriele Ludewig.

After finishing her bachelor Heleen started her master program 'health sciences' at the University of Twente. Following the 'Health Technology Assessment and Innovation' track, she got in touch with organs on chips and during her master thesis 'Organs-on-chips in drug development: the importance of involving stakeholders in early health technology assessment' she decided to pursue a PhD position in this field. First, she gained hands on experience with organs on chips by working as a researcher for the 'Applied Stem Cell Technologies' group of prof. dr. Robert Passier and prof. dr. Andries van der Meer, focusing mostly on blood vessel models.

In 2018 she started her PhD project at the BIOS lab-on-a-chip group of the University of Twente under the supervision of prof. dr. ir. Albert van den Berg and prof. dr. Andries van der Meer. While being part of the Netherlands Organ on Chip Initiative (NOCI), she started working on modelling blood vessels on chip. The NOCI network, gave her the opportunity to meet other scientists working in the organ on chip field, which lead to many inspiring collaborations and a broad network of close colleagues. Most of the work of the work performed during this NOCI project is described in this thesis, which she will defend on September 8th 2023.

Acknowledgements

Here it is, my thesis. I'm happy that after (almost) 5 years of hard work, I can finally show it to the world. But of course, this would not have been possible without the help and guidance of many people.

First: Albert, thank you for having the faith in me at the beginning of my project. Thank you for the good conversations and discussions regarding my ongoing projects and thesis. You kept me on my toes with your curveball questions, but next to that, you've always had good scientific input that made the chapters in this thesis clearer. Thanks to you, and Trudy as well, for organizing the yearly BIOS mountain bike/BBQ outing. Aside from a broken leg and concussion, I will always have fond memories of these events.
Andries, this journey would have never been possible without you. You decided to hire me for a one year project right after I finished my master thesis. When you couldn't get rid of me after three years, decided to hire me for a PhD position. We've had the best hours-long conversations, even before you hired me, about (starting with) organs-on-chips, but also had a lot of fun during the AST social events, train rides and conferences. Thanks for being a very good advisor (I know you don't like to be called a boss) for the last 8 years! It's been great!

Of course, this defense would not be possible without the defense committee: prof. dr. Maassen van den Brink, prof. dr. van den Maagdenberg, prof. dr. ir. Bosschaart, dr. Bansal. Thank you all for taking the time out of your busy schedules to assess my thesis and be at my defense.

Rolf & Paul, it was not hard to decide on my paranymphs, and I am very happy that you two will be by my side at the defense! Rolf, we were a team from my very first day at AST. The department of Awesome would have been a lot less awesome without you in it. Paul, the same goes to you, you were already very helpful when 'we' AST needed the BIOS PDMS lab. Furthermore, you made my transition going from AST to BIOS very smooth and we had a lot of fun singing along with 'het foute uur' in the BIOSBIOLAB.

Robert, officially you are not part of my PhD thesis, but unofficially you of course are. We met already during my master thesis and hit it off immediately. Thank you for your guidance while I was still at AST and thank you as well for making AST a very nice working environment from the start.

Loes, I've jokingly called you my adoptive PI, but of course it was not completely a joke! I've really appreciated you during my time at BIOS. It was very nice to have someone at the department to go to when something was bothering me, or just for a nice chat.

My time at utwente wouldn't have been the same without my roomies by my side! Kim & Rolf, as part of the now inner circle (see ASTable) and first members of AST we bonded immediately. Kim, thank you for borrowing your coffee card for the first two weeks at work. We wouldn't have survived without you. Thank you both for the amazing times at the office, singing along to Disney songs. But even more important, thank you both for our amazing roomies dinners (& drinks). There were a lot of long nights we spend eating, drinking, and especially talking. Hopefully those can continue for a long time! Thanks for helping me through hard times and thanks for being there during the fun times as well!
During this time, I have quite a couple of roommates, who shouldn't go unmentioned: Yusuf, Wesley, Nienke, Ruben, Edo, Job, Miguel & Laurens. Some of you I've spend a lot of times at the office with, some of you a little, please know that you were all very important to me during this process and I've loved our talks, boardgame nights, scientific discussions, and venting moments.

The work presented in this thesis is often part of collaborations. First, I would like to thank the collaborators from Nijmegen: Anouk, Cees, Nael, Monica, Chantal, Teun & Britt. Second, my collaborators from Groningen Kieu, Sebo & Vinod. And third, you don't always have to go far away for a collaboration. I would like to thank Carlos and Nienke from the University of Twente for our collaboration. You never know what will happen if you turn a Friday afternoon idea into an experiment, but it all came together very well.
Huub, Laura & Tarek, as Andries' PhDs we all bonded, and I am very happy about our fun time inside and outside of the labs. Lots of laughter and lab struggles we went through together.

There were of course students I've supervised during my PhD thesis. Thanks to Johanna, Jet, Yuki, Franca & Meike for helping me develop as an educator and for the nice projects we've worked on together.

Michelle, Yusuf & Wesley, thanks for a lot of coffee breaks, bouldering nights, bouldering days, sushi dates, raki dates, talks, advice, basically just being amazing friends through all this! Hugo & Martijn, thanks for helping me finding my way within

BIOS when I just started and especially the Biolab procedures. **Lisette**, thank you for all the Tuesday morning tea sessions and subway lunches. **Hermine**, thank you for helping me getting settled and helping us organize the NOCI workshops and retreats.

As this thesis would not have been possible without the NOCI grant, I would like to thank all my **NOCI colleagues** who have been there with me throughout the years! We've had great fun during our retreats and workshops. Let's get together soon and drink some apekoppen.
Of course, I would like to thank all my other colleagues at **BIOS** and **AST** for making my time here so much fun! There are too many fond memories to mention in this acknowledgment otherwise it would become too long, but I had a great time during our coffee breaks, workweek, and lab chats. Furthermore, its always nice to have so many people to ask for advice, whether it was regarding science, thesis or even climbing.

Thanks for scheduling our dates in the weekends around my cells' feeding times **Karin**, **Manon**, **Floortje** and **Inger**! Thanks for putting up with my sometimes high stress levels. As if that wasn't enough, I couldn't even answer any of the sciences questions during the pub quizzes.
All my other friends, who I cannot all mention by name, but were there for me during this time! Thanks so much for your support and for being here to celebrate with me as well.
To my **family (in law)**, bedankt voor jullie hulp tijdens dit proces. Bedankt voor het onverwacht oppassen als ik weer eens een experiment had lopen. Bedankt voor het nakijken van teksten. Bedankt voor jullie steun!
Michael, dankjewel voor je geduld en hulp en optimisme de afgelopen jaren. Als het even niet lekker liep dan vond jij altijd dat het wel goed zou komen, en wonder boven wonder was dat ook zo. Het was soms stressvol, iets met baby, verbouwen, verhuizen en proefschrift, maar we hebben het toch maar mooi gedaan.

Lise, een proefschrift schrijven terwijl je een baby hebt is zeker niet de makkelijkste weg, je zit zelfs op schoot terwijl ik dit schrijf, maar wat ben ik blij dat we dat toch hebben gedaan. Lieve Lise, deze is voor jou!

ISBN 978-90-365-5723-8